Doctoral School in Neuroscience
Course in "Neuroscience and Neurotechnologies"
Cycle XXXIII

Advanced microstructured platforms for neuroscience: from lab-on-chips for circadian clock studies to next generation bionic 3D brain tissue models

Author: Lidia Giantomasi

Supervisor: Dr. Luca Berdondini

ISTITUTO ITALIANO
DI TECNOLOGIA

Table of Contents

1. General Introduction

The human brain is the most fascinating and complex organ that we know. A conservative estimate of the number of neurons in the brain is 80 billion, more than 10 times the population of the world; the number of possible connections among those neurons is at least 100 trillion, many thousands of times the number of stars in our galaxy. It controls all functions of the body, interprets information from the outside world, and embodies the essence of the mind and soul. Intelligence, creativity, emotion, and memory are a few of the many things governed by the brain.

Not very long time ago, the feasibility of mapping the distinguishable regions of the human brain in relation to their functional roles seemed remote. With the tremendous advances in neuroscience and neurotechnologies undertaken over the past two decades, however, the opportunity now exists. This allows to approach experimental, computational and theoretical studies to gain an integrated understanding of the brain structure and its functioning, as necessary to clarify the neurobiological basis of human thought and emotion and to discern mechanisms that underlie sensory perception and locomotor functions. Indeed, many of the intricate anatomical connections of the brain are being defined in great detail. New capabilities have emerged to identify and describe the biochemical, molecular, and genetic mechanisms that determine brain structure and functions, and the overall activity of the human brain during mental activity can be measured and visualized. Using new generations of implantable silicon probes, it is even becoming possible to monitor simultaneously the activity of many neurons within complex neural networks during discrete behaviors.

Although all these progresses, our current understanding of the brain is still primitive and discovering its secrets continues to be a challenging goal in neuroscience. Given the complexity of signaling and interactions occurring in the brain at multiple scales, advances in neuroscience is intimately related to advances in neurotechnologies capable of monitoring and manipulating such a signaling diversity across scales, ranging from nanometers (biomolecules) to centimeters (entire organisms), but also to the availability of relevant models of brain circuits. The development of biological models enabling to dig into the fine details of the cellular complexity of the brain, inaccessible in human subjects, is crucial for gaining a better understanding of brain functions, of its development and of human brain diseases. In particular, as we know, the brain is not only composed by neurons. Neurons remain the major subject of study for neuroscience, but research on glia cells and neuro-glia interactions has radically increased over the last twenty years. Neurons and glia in the brain exchange (bio)chemical, electrical, and

mechanical cues. This symphony of signals originates at the nanoscale, where molecular machinery coordinates chemical reactions and conformation changes, e.g., ion channel opening. Combined, these events govern cellular function at the microscale, such as for tuning action potential firing. Coordination at the microscale then translates into the emergence of macroscale neural circuits, which drive behavior.

Driven by with my deep interest in the neurobiology of neuro-glia interactions, and motivation to contribute in advancing our current understandings of neurobiological processes in health and disease, in this PhD thesis I focused on the opportunity to study that apply new microtechnology platforms for investigating neurobiological questions in *in vitro* neuronal models. In particular, my work focused on two major projects that are reported in this thesis. While in the first I focused on the use of a more conventional technology (i.e. microfluidics) to dig into specific neurobiological questions, in the second I contributed to the development of a radically new technology to interface brain organoids that is currently under study at IIT.

In the first project, I focused on a microfluidic device that allows me to experimentally investigate the synchronization process of clock genes among distant neuronal populations through neuro-glia interactions. As it will be described, the *in vitro* approach that I developed allowed me to dissect different signaling channels that cannot be easily addressed *in vivo* due to the high cellular density and connectivity complexity of the brain.

In the second project, I investigated the effects of surface functionalization of silicon (Si) microchips (100 x 100 x 50 μm^3) in driving their three-dimensional (3D) assembling with cortical cells and in spatially tuning their 3D incorporation inside neurospheroids. This work is part of a larger project of my laboratory aimed at developing a new generation of "bionic organoids" with built-in wireless transducers that may enable to advance in the exploitation of brain organoids as model systems of the human brain for dissecting cellular and molecular mechanisms of human brain diseases and for the identification and study of therapeutic strategies.

2. Lab-on-a-chip investigation of molecular clock synchronization among segregated neural populations

2.1 Abstract

In mammals, the suprachiasmatic nucleus (SCN) of the hypothalamus is considered the master circadian pacemaker which coordinates circadian rhythms in the central nervous system (CNS) and across the entire body. The SCN receives light input from the eyes through the retinohypothalamic tract and then it synchronizes other clocks in the CNS and periphery, thus orchestrating rhythms throughout the body. However, little is known about how so many cellular clocks within and across brain circuits can be effectively synchronized to entrain the coordinated expression of clock genes in cells distributed all over the brain.

In this work I investigated the possible implication of two possible pathways: i) paracrine factors-mediated synchronization and ii) astrocytes-mediated synchronization. To study these pathways, I adopted an *in vitro* research model that I developed based on a lab-on-a-chip microfluidic device designed and realized in our laboratory. This device allows growing and compartmentalizing distinct neural populations connected through a network of astrocytes or through a cell-free channel in which the diffusion of paracrine factors is allowed. By taking advantage of this device, upon its validation, I synchronized neural clocks in one compartment and analyzed, in different experimental conditions, the induced expression of clock genes in a distant neural network grown in the second compartment.

Results show that both pathways can be involved, but might have different roles. Neurons release factors that can diffuse to synchronize a neuronal population. The same factors can also synchronize astrocytes that, in turn, can transmit astrocyte-mediated molecular clocks to more distant neuronal populations. This is supported by experimental data obtained using microfluidic devices featuring different channel lengths. I found that paracrine factors-mediated synchronization occurs only in the case of a short distance between neuronal populations. On the contrary, interconnecting astrocytes define an active channel that can transfer molecular clocks to neural populations also at long distances. The study of possibly involved signaling

factors indicate that paracrine factors-mediated synchronization occurs through GABA signaling, while astrocytes-mediated synchronization involves both GABA and glutamate.
These findings strength the importance of the synergic regulation of clock genes among neurons and astrocytes, and identify a previously unknown role of astrocytes as active cells in distributing signals to regulate the expression of clock genes in the brain. Preliminary results also show a correlation between astrocyte reactivity and local alterations in neuronal synchronization, thus opening a new scenario for future studies in which disease-induced astrocyte reactivity might be linked to alterations in clock gene expression.

2.2 Introduction

A key feature of life on Earth is its capacity to adapt to the environment. Different geographical locations have different environments and thus organisms adapt to the conditions that are prevalent at their location to enhance their survival. However, at any given location, profound changes in environmental light and temperature occur daily because of the rotation of the Earth on its axis. To adapt to such changes, most organisms have evolved an internal biological clock that anticipates day/night cycles and helps them to optimize their physiology and behavior (Young and Kay, 2001) (Figure 1). This internally generated day-night rhythm is known as "circadian rhythm" and has a period of approximately 24 h (Dunlap et al., 2004), thus the name circadian, from the Latin words "circa" (about) and "dies" (day), coined by Franz Halberg in 1959.

Circadian rhythms are ancient and conserved throughout evolution. They are known to exist in life forms from unicellular cyanobacteria and protozoans to all multicellular organisms, including fungi, plants, insects, rodents and humans (Dunlap, 1999). Driven by cellular 'clocks' distributed across the body, these rhythms adjust us to the world by preparing the brain, as well as other tissues and organs, to perform very different, often incompatible, functions appropriate to the anticipated day or the anticipated night. For example, in diurnal species, such as humans, neural mechanisms that maintain attention and cognitive capacity are upregulated in daytime, whereas preparation for night involves the activation of pathways that are essential for sleep-dependent memory consolidation (and reconsolidation) and synaptic scaling. On the contrary, nocturnally active species, such as mice, exhibit equally robust daily changes, but they are oppositely phased to light and dark cycles (Hastings et al., 2018). Furthermore, circadian rhythms regulate a large number of physiological and behavioral functions, such as hormone secretion, body temperature, metabolism and immune responses (Stratmann and Schibler, 2006). Therefore, it is not surprising that disruption of the circadian clock is associated with several pathogenesis, such as obesity, cardiovascular diseases, sleep disorder, depression, cognitive function, memory formation, some neurological diseases and even cancer (Gerstner and Yin, 2010; Yu and Weaver, 2011; Karatsoreos et al., 2001).

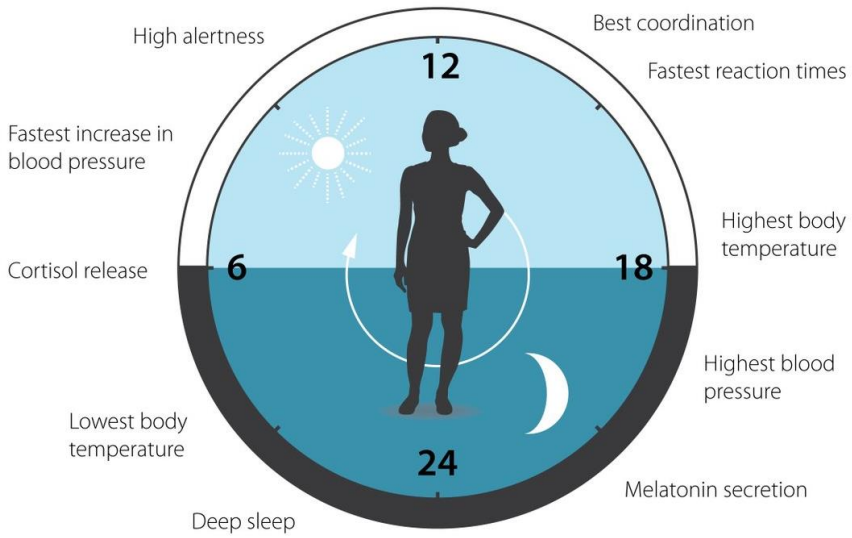

Figure 1: Circadian rhythms in mammals. Mammals biological clock anticipates and adapts physiological and behavioral functions to the different phases of the day. This figure was adopted from The Nobel Committee for Physiology or Medicine.

Observations that organisms adapt their physiology and behavior to the time of the day in a circadian fashion have been documented for a long time and are commonly agreed to have begun with the observation of leaf and flower movements in plants (McClung, 2006). In 1729, the French astronomer Jean Jacques d'Ortous de Mairan noticed that leaves of a heliotrope plant moved rhythmically throughout the day (de Mairan, 1729). To test if this movement was independent of diurnal signals, Jean Jacques d'Ortous de Mairan moved the plants to a dark cellar and observed that, even in the absence of light cues, the leaf movement persisted. This observation suggested an endogenous origin of the daily rhythm. Following this first experiment, a number of scientists repeated and expanded these observations through the 19th and early 20th centuries, in each case exploiting plant leaf movements.

Animal circadian rhythms were not scientifically described until much later, with pigment rhythms in arthropods (Kiesel, 1894) and daily activity in rats (Richter, 1922) being among the first reported in the literature. Nowadays, in mammals the circadian system is considered to be organized in a hierarchy of multiple oscillators at organism and cellular level. At organism level, the suprachiasmatic nucleus (SCN) of the hypothalamus is the central pacemaker at the top of the hierarchy. At cellular level, the circadian clock consists in the transcription- and translation-based interconnected feedback loops, in which the transcription factors BMAL1 and CLOCK drive the expression of *Per* and *Cry* genes, whose products lead to the inhibition of their own transcription (Dunlap, 1999). This process oscillates with a 24 h period, producing the 'ticking' of the biological clock.

2.2.1 Circadian timekeeping at molecular level

A series of biochemical and genetic approaches made it possible to define the core transcriptional components of the oscillatory mechanism. The discoveries of such molecular mechanisms are due to Jeffrey C. Hall, Michael Rosbash and Michael W. Young, winners of the 2017 Nobel Prize in Physiology or Medicine (Callaway and Ledford, 2017).

The recurrent motif of the oscillatory mechanism is one in which positive transcription factors drive the expression of genes encoding negative factors that, following a suitable delay, inhibit the initial activation. This closure of the negative feedback loop completes the first half of the circadian cycle, whilst the second half involves the progressive degradation of the negative factors to facilitate the re-initiation of a new transcriptional phase. Thus, the molecular basis to the oscillation can be viewed as a transcriptional/post-translational feedback loop (TTFL) (Hastings et al., 2019) as it is schematically illustrated in Figure 2.

The mammalian oscillator has clearly taken its cues from its position in the evolutionary tree; it is gratifyingly similar to its closet well-studied relatives, the insects, and contains aspects of logic and protein structure clearly conserved in fungi and perhaps beyond (Dunlap, 1999). The positive factors are Circadian Locomoter Output Cycles Protein Kaput (CLOCK) and Brain and muscle ARNT-like 1 (BMAL1, also known as ARNTL), which are basic helix-loop-helix transcription factors that heterodimerise via so-called PAS domains to bind DNA at Enhancer boxes (E-boxes) and thereby drive transcription. The negative factors are Period (PER1, PER2) and Cryptochromes (CRY1, CRY2) (Takahashi et al., 2017). All these genes involved in the TTFL are commonly named "clock genes".

Briefly, beginning at Circadian Time (CT) 0, heterodimers of CLOCK and BMAL1 drive the expression of PER and CRY proteins. By the end of the circadian day (CT12), PER–CRY complexes have accumulated in the nucleus and start to repress their own expression. Therefore, over the course of the ensuing circadian night (CT12–CT24 (CT0)), *PER* and *CRY* mRNA levels fall and the existing PER–CRY complexes are degraded. This degradation allows the cycle to reinitiate approximately 24 solar hours after the previous transcriptional initiation (Hastings et al., 2018). The cycle is stabilized by accessory loops in which CLOCK and BMAL1 drive E-box-mediated circadian expression of the nuclear receptors RORα, REV-ERBα (also known as NR1D1) and REV-ERBβ (also known as NR1D2), which in turn act via REV response element (RRE) sequences to activate and suppress *BMAL1* transcription, respectively (Preitner et al., 2002; Cho et al., 2012).

The time cues defined by the changing molecular status of these interlocked feedback loops are transmitted to the rest of the cell to coordinate its activities. Indeed, a large number of circadian

transcription factors not only regulate their own transcription, but also the expression of numerous other "clock-controlled genes" (CCGs) (Dunlap, 1999) whose protein products are not essential for the core clock mechanism itself. Among these CCGs there are genes regulating various enzymes, like phosphoenolpyruvate carboxykinase, glycogen phosphoylase, and glucose-6-phosphatase (Panda et al., 2002); various voltage-gated calcium and potassium channels (Ko et al., 2009); peptides, such as Arginine-Vasopressin (AVP; Jin et al., 1999) and albumin site D-Binding Protein (DBP; Lopez-Molina et al., 1996).

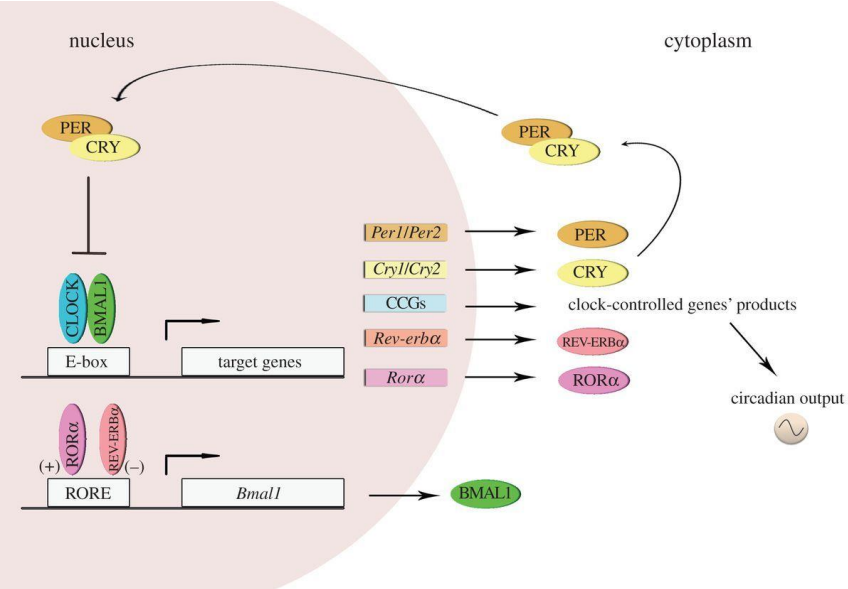

Figure 2: The molecular circadian clock in mammalian cells. The molecular mechanisms of circadian rhythms can be illustrated by the transcription of the *Period* (*Per1* and *Per2*) and *Cryptochrome* (*Cry1* and *Cry2*) genes that are activated by heteromeric complexes containing CLOCK and BMAL1 proteins that act through the E-box regulatory sequences of their target genes. In turn, PER and CRY proteins inhibit BMAL1–CLOCK activity, and therefore, their own transcription. This core oscillation is augmented and stabilized by a secondary loop involving two orphan nuclear receptor proteins, REV-ERBα and RORα, which affect *Bmal1* expression. Importantly, the CLOCK–BMAL1 heterodimer regulates the transcription of many CCGs, which in turn influence a wide array of physiological functions external to the oscillatory mechanism. This figure was adopted from Golombek et al., 2014.

2.2.2 Circadian timekeeping at the organism level: the suprachiasmatic nucleus

Mammals circadian system is a body-wide hierarchy of interlocked circadian oscillators present in cells of major organs. For proper functioning of the circadian timing system, all the circadian clocks in the body must be kept synchronized with one another and to the 24 h day. This is the function of the suprachiasmatic nucleus (SCN) of the hypothalamus, the master circadian pacemaker (Klein et al., 1991; Welsh et al., 2010).

Like other cells, SCN neurons can express self-sustained circadian rhythms (Welsh et al., 1995) but, unlike them, they are special in several important aspects. First, SCN neurons receive direct inputs from the environment, which allow them to synchronize to the day/night cycle. Light is the principal stimulus for external synchronization of circadian clocks, and in the context of mammals this is mediated via the direct retinal innervation of the SCN derived from the retinohypothalamic tract (RHT) (Abrahamson and Moore, 2001). Second, they have distinct, topographically organized coupling mechanisms which allow them to remain synchronized to one another even in constant darkness (Aton and Herzog, 2005). Third, through output pathways, they are able to synchronize other clocks in the central nervous system and periphery, orchestrating rhythms throughout the body (Gachon et al., 2004). Interestingly, these extra-SCN regions are characterized by a variation in phase and amplitude of rhythmic clock gene expression (Kalsbeek et al., 2006; Harbour et al., 2014; Chun et al., 2015).

Thus, the SCN master pacemaker synchronizes ("entrains") to the light/dark cycle, and in turn synchronizes other oscillators throughout the brain and peripheral tissues (Figure 3). However, to date, the process (or processes) by which the SCN synchronizes all the others clocks, as well as a neuronal population synchronizes another neuronal population, is poorly understood.

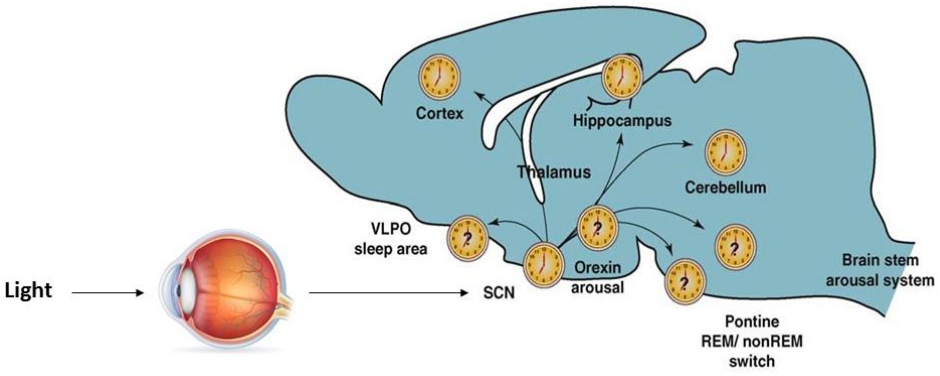

Figure 3: Schematic representation of clocks distributed throughout the brain. The SCN receives light input from the eyes through the retinohypothalamic tract and then it synchronizes other clocks in the CNS and periphery, thus orchestrating rhythms throughout the body. This image was adapted from Kyriacou and Hastings, 2010.

The discovery of the SCN as the master circadian pacemaker dates back to the 70s. Although ablation studies had indicated a hypothalamic site for the circadian clock, the SCN only came to attention once autoradiographic tracing methods revealed it as the principal termination site of the retinohypothalamic tract. Subsequent studies showed that behavioral, endocrine and seasonal rhythms were compromised in damaged SCN. In addition, electrophysiological studies showed that activity in the SCN was rhythmic *in vivo* and that, using slices, the electrical

circadian rhythms were sustained *in vitro*, even when disconnected from the rest of the brain. The potency of this clock function was shown by intracerebral grafting, *in vivo*, of fetal SCN into the brain of mutant animals with abnormally short or long circadian periods. These grafts restored circadian patterning to the arrhythmic activity/rest behaviors, with a period determined by the genotype of the grafted tissue. This showed, definitively, that the SCN was necessary and sufficient to sustain circadian behaviors (Weaver, 1998; Herzog et al., 2017).

2.2.2.1 Cellular organization of the SCN

The SCN is a paired neuronal structure located in the anteroventral hypothalamus, on either side of the third ventricle, just above the optic chiasm (Klein et al., 1991). Each unilateral SCN contains ~10,000 neurons as well as a large number of neuroglia. Axons of SCN neurons terminate mainly within the nucleus itself, thus forming local circuit connections. A small amount of neurons send out projections from the SCN to distal targets, which are predominantly in the hypothalamus, midline thalamus and brain stem (Hastings et al., 2018). Nearly all SCN neurons produce γ-aminobutyric acid (GABA), although there are evidences that a subpopulation is glutamatergic (Csáki et al., 2000).

Conventionally, the SCN is divided in two anatomic sub-divisions: a ventral "core" region which abuts the optic chiasm and receives direct input from the retina, and a dorsal "shell" region which partially envelops and receives input from the core. The core projects densely to the shell, which projects only sparsely back to the core (Welsh et al., 2010). Neurons in core and shell sub-regions are distinguished by neurochemical content. The core contains cells that express vasoactive intestinal peptide (VIP) or gastrin-releasing peptide (GRP), whereas the shell contains a dense population of neurons that express arginine vasopressin (AVP). A number of other neuropeptides, such as neurotensin, somatostatin and prokineticin2 (Prok2), are expressed in cells across the SCN, respecting or straddling these sub-divisions (Hastings et al., 2019).

To date, however, little is known about the mechanisms that mediate the entrainment of cells within the SCN. The major hypotheses in the field are two:

ì) there are "non-rhythmic" SCN cells in the ventral core that respond directly to light inputs, as well as intrinsically "rhythmic" SCN clock cells in the dorsal shell that do not. Consequently, this hypothesis suggests that a light-induced phase shift occurs when non-rhythmic cells in the ventral core communicate the lighting signal to the oscillator in the dorsal shell.

ìì) there are rhythmic neurons in the ventral core that directly or indirectly respond to light. Interactions between the oscillators in the ventral core and dorsal shell are responsible for light-induced phase shifts (Albers et al., 2017).

2.2.2.2 SCN coupling mechanisms

The most prominent network property of the SCN is the remarkable coupling of its constituent cellular oscillators to produce a coherent circadian oscillation at the tissue level. In striking contrast to the independent oscillations of dissociated cells, neurons within SCN tissue adopt identical circadian periods and similar phases, thus indicating a strong communication among these cells. How neurons communicate within the SCN, however, is not completely understood and much remains to be learned. There are a number of different types of signaling processes that may be responsible for communication among SCN cells.

First of all, synaptic activity is an important form of communication among SCN neurons. Synaptic activity is essential for the expression of overt circadian rhythmicity and for the entrainment of the pacemaker with the Light-Dark (LD) cycle (Albers et al., 2017). An important role of synaptic signaling is based on observations that SCN neurons desynchronize when cultured with tetrodotoxin (TTX) to block Na^+-dependent action potentials (Yamaguchi et al., 2003). However, there is also evidence that the SCN network can use other forms of coupling that do not depend on synaptic communication. In a study of 2011, Maywood and colleagues showed that co-cultured SCN slices are able to influence the rhythmic properties of one another even though they are unable to establish cross-slice synaptic connections, thus suggesting the presence of a paracrine signaling (Maywood et al., 2011). Consequently, the study of neurochemical signaling outside of classical synapses has become increasingly recognized as a significant form of inter-neuronal communication in the SCN. Inter-dendritic and inter-somatic appositions within the SCN have the potential to mediate non-synaptic interactions, and neurochemical signals can be released in non-synaptic regions of SCN neurons.

Although it remains a challenge to fully map the neurochemical, temporal, and spatial properties of SCN circuits, different studies were performed to investigate the nature of the neurochemical signaling among SCN neurons.

Within the core, VIP is the most prevalent neuropeptide transmitter, and recent studies have identified VIP in SCN coupling. VIP is released rhythmically from the core and acts through VPAC2 receptors in both core and shell. In mice lacking VIP, or its receptor, SCN cells are hyperpolarized and have low levels of *Per1* and *Per2* expression. These mice also have weak

behavioral rhythms. Daily application of a VIP agonist to mutant SCN cultures restores synchrony. Finally, VIP application to synchronized wild type SCN *in vivo* or *in vitro* produces phase-specific phase shifts similar to those of light. Thus, the synchronizing function of the SCN core requires VIP release from synaptic terminals at target neurons throughout the SCN (Nielsen et al., 2002; Harmar et al., 2002; Colwell et al., 2003; Welsh et al., 2010).

Since it was reported that nearly all SCN neurons express GABA, this neurotransmitter was indicated as a potential regulator of SCN communication. In 2000, Liu and Reppert showed that GABA, acting through A-type receptors, can induce phase shifts in single clock cells in culture, and the amplitude and direction of the phase shifts is determined by the phase of clock cells at the time of the treatment. Furthermore, daily treatments with GABA can synchronize cultured clock cells (Liu and Reppert, 2000). On the other hand, neurons in SCN slices remain synchronized in the presence of $GABA_A$ and $GABA_B$ antagonists (Aton et al., 2006), thus indicating that GABA is sufficient but not necessary for the SCN coupling. In summary, VIP is necessary for SCN coupling, but other neurotransmitters, including GABA, can also contribute or play a modulatory role.

It is also important to highlight that coupling mechanisms do not involve only neurons within SCN. It is demonstrated that various brain regions, including the prefrontal cortex, hippocampus, amygdala and dentate gyrus, exhibit circadian modulations in molecular expressions. When isolated from the SCN *in vivo*, either by ablating the SCN or by encircling it with a knife cut, the periodicity in extra-SCN regions is abolished, thus suggesting that the central pacemaker within the SCN is responsible for driving near 24h rhythmicity in other regions of the brain (Abe et al., 2002). Interestingly, the phase and amplitude of the rhythms of clock genes vary across regions (Harbour et al., 2014; Chun et al., 2015). This reveals the presence of important regional differences in the temporal dynamics underlying local daily rhythm generation in the mammalian forebrain. This observation also underscores the complex temporal organization of subordinate circadian oscillators in the forebrain and raises interesting questions about the connection of these oscillators with the master SCN clock. To date, in fact, it remains unknown how specific circadian cues are conveyed from the SCN to most downstream targets to control physiology and behavior.

2.2.3 The role of astrocytes

The central and peripheral nervous system is characterize by the presence of non-neuronal cells, known as glia. Astrocytes, also known collectively as astroglia, are characteristic star-shaped glial cells and represent the largest population of the glial subtype in the brain. Thanks to its

shape, in humans a single astrocyte cell can interact with up to 2 million neurons at a time (Fields et al., 2014).

Astrocytes perform many functions in the brain, including biochemical support of endothelial cells that form the blood–brain barrier, provision of nutrients to the nervous tissue, and a role in the repair and scarring process of the brain following traumatic injuries. Furthermore, they exert essential functions in maintaining the fluid, ion, pH, and transmitter homeostasis of the synaptic interstitial fluid in a manner that is critical for healthy synaptic transmission. Astrocyte processes at synapses also play essential roles in transmitter homeostasis by expressing high levels of transporters for neurotransmitters such as glutamate, GABA, and glycine that serve to clear the neurotransmitters from the synaptic space. After uptake into astrocytes, the transmitters are converted by enzymes such as glutamine synthetase into precursors such as glutamine and recycled back to synapses for reconversion into active transmitters (Sofroniew and Vinters, 2010). There is now steadily accumulating evidence that astrocytes play direct roles in synaptic transmission through the regulated release of synaptically active molecules including glutamate, purines (ATP and adenosine), GABA, and D-serine. Such evidence has given rise to the 'tripartite synapse' hypothesis, which posits that astrocytes play direct and interactive roles with neurons during synaptic activity in a manner that is essential for information processing by neural circuits (Halassa et al., 2007; Perea et al., 2009).

Unlike neurons, astrocytes do not 'fire' or propagate action potentials along their processes. However, this does not mean that they are physiologically 'silent'. Astrocytes, in fact, express potassium and sodium channels and can exhibit evoked inward currents. Moreover, they exhibit regulated increases in intracellular calcium concentration $[Ca^{2+}]_i$ that are of functional significance in astrocyte–astrocyte as well as in astrocyte–neuron intercellular communication. Astrocyte $[Ca^{2+}]_i$ elevations can (1) occur as intrinsic oscillations resulting from Ca^{2+} released from intracellular stores, (2) be triggered by transmitters (including glutamate and purines) released during neuronal activity, (3) elicit the release from astrocytes of transmitters such as glutamate into the extracellular space and thereby trigger receptor mediated currents in neurons, and (4) be propagated to neighboring astrocytes (Sofroniew and Vinters, 2010). It is also noteworthy that astrocytes can couple to neighboring astrocytes through gap junctions formed by connexins and creating the so called "syncytium". An increase in intracellular calcium concentration can propagate outwards through this functional syncytium, generating calcium waves propagating through the network of astrocytes. Mechanisms of calcium wave propagation include diffusion of calcium ions and IP3 through gap junctions and extracellular ATP signaling (Newman, 2001). Calcium elevations are the primary known axis of activation

in astrocytes, and are necessary and sufficient for some types of astrocytic glutamate release (Parpura and Haydon, 2000). Importantly, because of this ability of astrocytes to communicate with their neighbors, changes in the activity of one astrocyte can have repercussions on the activity of others cells that are quite distant from the source astrocyte.

2.2.3.1 Astrocytes as clock cells

In 2005 Prolo and colleagues, using rat and mouse astroglia obtained from transgenic animals expressing a *per-luciferase* (*per-luc*) reporter, demonstrated for the first time that astrocytes fulfill the criteria of circadian oscillators: they have intrinsic circadian clocks with a genetically defined, temperature-compensated period that can be entrained to daily environmental cycles (Prolo et al., 2005). It was shown that astrocytes exhibit circadian rhythms of clock gene expression, with the consequence of a remarkable circadian variation in morphology. Astrocytes, in fact, express high levels of glial fibrillary acidic protein (GFAP), which exhibits 24 h oscillations in its distribution, both in light-dark conditions and in constant darkness (Lavialle and Servie` re, 1993; Santos et al., 2005). Furthermore, astrocytes exhibit a strong circadian cycle of intracellular calcium ($[Ca^{2+}]i$): they are circadian cells just as neurons are, but the peak of the $[Ca^{2+}]i$ rhythm in astrocytes is much broader than the sharp peak of neurons. More importantly, it phases to circadian night (at about CT18), indicating that the activity cycle of astrocytes in the SCN runs in anti-phase to that of SCN neurons (Brancaccio et al., 2017). This differential phasing between neurons and astrocytes was demonstrated also at the TTFL level, with Cry1-luciferase in astrocytes peaking in circadian night. Surprisingly, therefore, the SCN circadian network incorporates two functionally distinct cellular populations: day-active neurons and night-active astrocytes harnessing a differentially phased TTFL (Brancaccio et al., 2019).

Unlike the sustained oscillations observed in neurons (Welsh et al., 1995), rhythms in cortical glia damps after several cycles *in vitro*. Damping may reflect a gradual desynchronization among a population of sustained oscillators or a loss of rhythmicity in individual cells, suggesting an essential difference in molecular rhythm generation between neurons and cortical glia. Importantly, circadian rhythms in astrocytes can be phase shifted and entrained to a physiologically relevant cycle, suggesting that, *in vivo*, glia continue to oscillate as a result of periodic signaling. In cell cultures, rhythms can be reinitiated by culture medium replacement or treatments with the calcium ionophore Calcimycin or the adenylate cyclase agonist Forskolin. It was suggested that all these stimuli may be acting on the molecular clock through a common mechanism, such as the elevation of intracellular Ca^{2+} levels (Jackson, 2011).

2.2.3.2 Astrocytes control molecular and behavioral rhythms: the astrocyte-neuron communication

Astrocytes are not passive clock cells. Pharmacological inhibitors of glial activity affect the rhythms of SCN neuronal firing and diurnal behavioral rhythms, thereby suggesting that glial cells could play a role as synchronizers of circadian networks within the SCN (Prosser et al., 1994). In support of this notion, a series of recent studies have demonstrated that astrocytes play an important role in circadian timekeeping and behavior as any neuronal cell. Tso et al. have shown that loss of rhythms in SCN astrocytes through *Bmal1* deletion leads to a lengthened circadian period of rest-activity rhythms (Tso et al., 2017). By an alternative astrocyte-targeting strategy, in our laboratory and in collaboration with Davide De Pietri Tonelli, Barca-Mayo et al. have shown that *Bmal1* deletion dysregulates PER2 and VIP expression in the SCN and alters daily locomotor activity and cognitive functions (Barca-Mayo et al., 2017). Successively, Brancaccio et al. have shown that SCN astrocyte-specific deletion of the mutant version of the clock kinase $Csnk1e_{Tau}$ lengthened the period of behavioral rhythms from 20 to 24h (Brancaccio et al., 2017). These phenotypes strengthen the importance of astrocytes as potent regulators of molecular and behavioral rhythms. All together, these results revealed that astrocytes are not only embedded in the clock circuit, but they also are major determinants of its period length. In addition, a recent study reveals the crucial contribution of astrocytic clock in the circadian regulation of metabolism and lifespan (Barca-Mayo et al., 2020). The results highlighted by these studies imply the importance of reciprocal interactions between astrocytes and neurons in the context of circadian circuitry.

There are different signaling pathways involved in the astrocytic control of SCN function. As a GABAergic circuit, the SCN is sensitive to extracellular GABA concentrations, which are in part controlled by GABA transporters that are expressed on SCN astrocytes. Blockade of these transporters in astrocytes not only affects tonic and synaptic $GABA_A$ receptor currents in SCN neurons but also shortens the period of the TTFL (Moldavan et al., 2017). Moreover, *in vitro* co-culture experiments showed that synchronous astrocytes are able to entrain rhythmicity in neurons with a mechanism that is mediated by GABA and $GABA_A$ receptor signaling (Barca-Mayo et al., 2017).

In addition, astrocytes can also exert more direct effects on neurons via the release of gliotransmitters. In the specific context of the SCN, astrocytes have been implicated in modulating the response of the neuronal clock to pro-inflammatory cytokines, and several candidate gliotransmitters, including extracellular ATP, are regulated in a circadian manner in

cultured astrocytes and cultures of the SCN2.2 cell line (derived by adenoviral immortalization of rat SCN cells) (Hastings et al., 2018). In addition, glutamate, a major gliotransmitter in the SCN, also shows daily oscillations. When detected with fluorescence live imaging, its extracellular concentration was shown to be directly in phase with astrocytic $[Ca^{2+}]i$ and to share a similar waveform. This suggests that glutamate contributes to astrocytic circadian signaling. Furthermore, as shown by two independent pharmacological approaches, i.e. interference with glutamate release by astrocytes (via Cx43 inhibition) and with neuronal glutamate sensing (via NMDAR2C antagonism), glutamate is a necessary mediator of astrocytic control of circadian function in the SCN (Brancaccio et al., 2017; Brancaccio et al., 2019).

Although the role of GABA and glutamate in the circadian field is still not completely clear and rather controversial, these two transmitters may act together as powerful circadian synchronizers to combine the effects of their activities in both the astrocytic and neuronal compartments of the SCN circuit.

2.2.4 Microfluidics for cell-cell communication studies

The study of cell-cell communication, or cell-cell signaling, is important in many biological fields, including neuroscience, genetics, cancer, immunology, and more. How two or more cells talk and interact has drastic effects on proliferation, differentiation, migration, and stimulation, while defects in cellular communication can lead to diseases. Some examples of cellular communication include immune-tumor cell interactions, both at the immunological synapses and through secretion of cytokines and growth factors, communication within neural networks, neural and optical synapse formation, and signal propagation. Therefore, the study of cell-cell communication is necessary for both understanding diseases and for creating novel biomedical technologies.

The best method for studying intercellular communication is by using *in vitro* tools that facilitate isolation and control of the microenvironment (Vu et al., 2017). Although there is a clear need to advance in understanding cell-cell communication, these studies remain challenging and prevent scientists' ability to conduct these studies. One of these challenges is the involvement of different mechanisms in cell-cell communications and, consequently, the need of different and specific techniques to specifically study the multiple types of communication pathways, including gap junction signaling, paracrine signaling, endocrine signaling and synaptic/direct signaling (Nahavandi et al., 2014). To date there exists no general platform that can lever all these requirements for studying every pathway in cell-cell

communication. To better study all of these individual phenomena for a variety of scenarios, specific tools designed for each application need to be available to researchers.

The most common tools and techniques that have been used to study cell-cell communication are transwell systems and co-culture systems (Goers et al., 2014). Transwell inserts are one of the oldest technology for co-culture and consist in two separate compartments with multiple surfaces to culture. They are used for communication studies like secretion, differentiation, and migration. However, there are some limits in using the transwell system, such as the lack of physiological relevance, flow, difficulty for imaging, and limited spatial control. Co-culture systems can include heterogeneous cell cultures on Petri dishes, co-culture in gels, or bioreactors. These methods, however, lack of the ability to be easily customized and versatile for many different scenarios, such as gradient culture, different cell sizes, spatial control, and more. To overcome these issues and enhance biological studies, microfluidic technology and the development of microfluidic cell culture devices was proposed and increasingly used in the past two decades.

Microfluidics allows to realize devices known as micro total analysis systems (μTAS), or lab-on-a-chip systems. It converges the science and technology of systems that process or manipulate small amounts of fluids, using channels with dimensions of tens to hundreds of micrometers. It originated from the miniaturization of analytical chemistry and biomedical applications on a chip in the early 1990s and, since then, research on microfluidics has grown to a large community and let to different applications (Zhong et al., 2019), including commercially available products.

According to the different experimental needs, cell culture conditions are usually divided into two major classes that can be distinguished as in a "static state" or a "dynamic state". The "static state" is characterized by a sufficient medium supply for the maintenance of on-chip cells without the use of any perfusion system. The chip is always placed into an incubator and the cell culture medium is typically exchanged daily or even after longer time, a condition that may help to observe the natural performance of cells. The "dynamic state" usually includes the use of some extra auxiliary equipment, such as a micropump, to change medium or even separate cells. This approach provides opportunities for cell manipulation and to precisely control the delivery of pharmacological stimuli (Li et al., 2016). Both static or dynamic cell culture conditions can be realized with microfluidic devices.

The most common material for realizing cell culture microfluidic devices is polydimethylsiloxane (PDMS), an elastomeric material which is featured by air permeability, flexibility and biocompatibility. Microfluidic systems based on PDMS can be realized via

photolithography, as proposed in 1998. Photolithography offers procedures for fabricating networks of channels (typically >20 μm width) rapidly and at low cost. To do so, PDMS microfluidic devices are replicated from photolithographically fabricated masters (such as silicon microstructured wafers). These devices support a wide variety of applications because of their good biocompatibility, optical transparency, and flexibility (Zhong et al., 2019).

Various types of cells, like adherent and non-adherent cells, have been cultured in microfluidic platforms (Yamazoe et al., 2016) that met the strict requirement of defining stable cellular microenvironments. Several novel discoveries on cell structures, characteristics and behaviors, obtained with the support of microfluidic platforms are reported in the literature (Kim et al., 2008; Tazawa et al., 2015). Hence, microfluidic systems are increasingly used in biology and pahramcology as versatile tools and viable alternatives to traditional approaches for several specific applications, such as: single-cell studies, cell trapping, filtration, cell rolling and investigations, detection of biomarkers, drug screening and discovery, cryopreservation of cells (Coluccio et al., 2019).

Recently, microfluidic devices have been coupled with microsystems engineering, tissue engineering, biomimetic principles and cell biology to develop organ-on-a-chip systems. Such organ-on-a-chip usually involve a scaffold, suitable cellular microenvironments, and artificial organ-level stimuli for the formation of viable tissues and organ models. Microfluidics is capable of the precise control of dynamic fluids and pressures at a micrometer scale. Therefore, in combination with microfabrication technologies, it can provide 3D scaffolds and precisely controlled microenvironments with suitable biochemical and physicochemical stimuli. These novel systems are now being utilized to establish physiologically relevant, functional, single- or multi-organ models on a single chip, and are becoming increasingly used tools for physiological and pathological studies, and pharmaceutical applications (Zhong et al., 2019; Park et al., 2019). Even cell-cell communication studies can be greatly enhanced by microfluidic technology. One of the advantages of microfluidics is the ability to spatially manipulate cells with a precision unmet by traditional cell culture technologies. For instance, this allows to spatially control cells individually or collectively. Another advantage is the ease of introducing flow and gradient control capabilities. All these features can be combined with the uniqueness of microfluidics to implement devices for both population-based and single cell studies (Mao et al., 2013; Vu et al., 2017).

Unsurprisingly, a wide range of microfluidic devices were developed for studying interactions between cells in the central nervous system (Rothbauer et al., 2018) (Figure 4). Notably, Taylor et al. studied the effect of chemical injuries between two spatially resolved neural cell culture

compartments (Taylor et al., 2010). Higashimori et al. combined a microfluidic co-culture system with imaging instrumentation to examine cell-to-cell interactions between axonal/dendritic and glial cells (Higashimori and Yang, 2012). For the precise control over CNS injuries and lesions, Kim et al. introduced a microfluidic platform that was capable of controlling axonal growth by surface modification, as well as controlling soluble factors (Park et al., 2006; Kim et al., 2012), and Park et al. established a complex microfluidic 3D platform for studying axon-glia interactions during drug and biomolecule treatment on multiple co-cultures (Park et al., 2012). Another technological advance in chip-based neurobiology includes the possibility of exploiting the integration of microvalves for opening and closing connecting conduits between neighboring cell culture compartments. This allows, for instance, to study interactions between spatially resolved neurons and glial cells (Gao et al., 2011; Majumdar et al., 2011).

Overall, although microfluidic devices emerged a century ago but their development and application did not reached a saturation yet. This field is regularly progressing by targeting diverse and distinct requisites of real lab practice, and advanced experimental research applications.

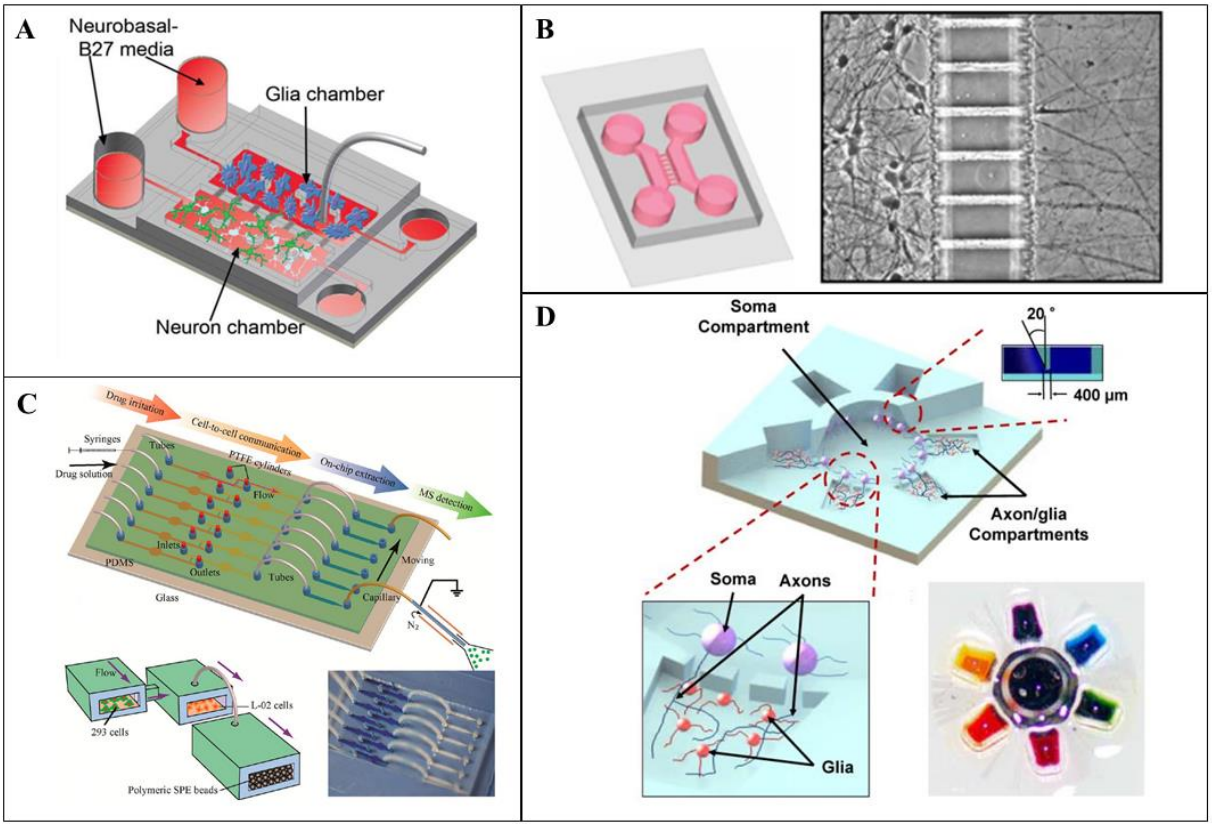

Figure 4: Examples of microfluidic devices for cell-to-cell communication studies. A) Co-culture of neurons and glia in the microfluidic platform (Majumdar et al., 2011). B) Schematic representation of a

microfluidic device (left) and phase-contrast micrographs of axons (right) for investigating injury and regeneration of CNS axons (Park et al., 2006; Kim et al., 2012). C) Microfluidic device for cell-to-cell communication study (Mao et al., 2012). D) 3D illustration of the multi-compartment neuron-glia co-culture microsystem capable of carrying out multiple localized axon treatments in parallel (Park et al., 2012).

2.3 Aims

Since the circadian clock plays a fundamental role in the maintenance of circadian-dependent processes, understanding its regulatory mechanism among neuronal populations is vitally important. In mammals, the suprachiasmatic nucleus (SCN) of the hypothalamus is the master circadian pacemaker which coordinates circadian rhythms in the central nervous system (CNS) and across the entire body. Interestingly, the phase and amplitude of the rhythms of clock genes vary across brain regions (Harbour et al., 2014; Chun et al., 2015). This underscores the complex temporal organization of subordinate circadian oscillators in the forebrain and raises interesting questions about the connection of these oscillators. In particular, an important aspect that remains unclear is how so many and distant neural clocks in the nervous system can be effectively synchronized. About this, it is important to remember that SCN neurons do not project to long distances in the brain (Watts et al., 1987). Therefore, distant cells need other channels of communication in order to be able to synchronize distant clocks.

An unspoken tenet in the circadian field is that neurons, and in particular SCN neurons, do the lion's share of this work. A series of recent studies, however, challenged this view by demonstrating important roles for astrocytes in entraining rhythmicity in neurons (Tso et al., 2017; Barca-Mayo et al., 2017; Brancaccio et al., 2017; Brancaccio et al., 2019).

In light of these recent findings, the working hypothesis that I investigated in this work is whether astrocytes and/or paracrine factors released by neurons may define long-range communication channels to synchronize molecular clocks among distant and segregated neuronal populations. Consequently, by exploiting a microfluidic platform specifically developed for this study, the specific aims of my PhD were to study in an *in vitro* model:

i) whether paracrine factors, released by a synchronous neuronal population, or astrocyte networks can transfer neural circadian information among distant neuronal populations,

ii) how this signaling might occur and, ultimately,

iii) whether these two pathways occur regardless of the distance between the two neuronal populations.

Knowing that an alteration in the astrocyte intercellular communication or of astrocytic clock genes might contribute to the impairment of the neurobehavioral outputs or to disorders associated with the timekeeping system (McKee et al., 2020), in the last period of my PhD I also started to investigate effects related to reactive astrocytes and their implications to synchronize a neuronal population or to transfer molecular clocks among distant neuronal populations.

2.4 Materials and methods

2.4.1 Microfluidic device design and fabrication

In this part of my work I contributed to the development of a two-compartment microfluidic device that was realized to experimentally investigate our hypothesis and, specifically, the involvement of astrocytes and/or paracrine factors to synchronize molecular clocks among distant and segregated neuronal populations.

The realization of the microfluidic device consists in mounting on a 4'' glass wafer a micro-structured polydimethylsiloxane (PDMS) (Sylgard 184, Sigma-Aldrich) layer. This layer defines the microfluidic circuitry and it was obtained as replicas from a Si master by using the so-called micromolding technique (Figure 5). Positive structures on the Si master were obtained by patterning a Cr layer with optical lithography and dry etching the Si substrate using DRIE (Deep Reactive Ion Etching). To do so, 4" p-type Si wafers were first cleaned by subsequent acetone, isopropyl-alcohol and deionized water (DI) washing. Next, positive tone photoresist (MEGAPOSIT SPR 200, MicroChem) was deposited by spin coating (4000 rpm) onto the Si wafer and baked at 115 °C for 2 min. The microfluidic circuitry was patterned by exposing the photoresist to UV light (MA-6, SUSS MicroTec mask align) through a laser written lithography mask and developed for 1 min in Microposit MF-319 developer. Successively, a 200 nm thick Cr layer was deposited by DC sputtering (Kenosistec KS500 Confocal) at 1 Å/s deposition rate and unwanted Cr remaining on the photoresist was lifted-off in acetone (overnight). The Cr patterned layer was then used as mask for dry-etching process. A DRIE Bosh process (SENTECH SI500, ICP-RIE) was employed to etch the Si for 80 μm and the depth measured by mechanical profilometer (Dektak 150). This thickness defines the final depth of the microfluidic channel between the two wells in the PDMS replicas.

The processed Si wafer was then cleaned by O_2 plasma (100 W, 300 s) and the Cr layer removed in a Cr etchant solution. Finally, a fluorosilane anti-sticking layer was deposited onto the Si wafer to facilitate PDMS removal in the molding process. To do so, a 250 μl of Perfluorooctyltriethoxysilane (POTS, Alfa Aesar L16606) were dispensed onto a glass slide and placed under vacuum with the Si wafer for 1 hour. The wafer was then baked on a hot plate at 80°C for 5 min.

PDMS was prepared by mixing the curing agent and PDMS monomers in a ratio 1:10. After degassing under vacuum, it was deposited onto the structured Si mold (approximately 4 mm in height) and cured at 65 °C in oven for 2 hours. Then, the cured PDMS was peeled-off from the Si mold, thus obtaining negative microfluidic structures, i.e. replica of the positive structures

defined onto the Si wafer. A hole punch of 8 mm in diameter was used to realize the two wells through the PDMS layer, while a 1 mm in diameter hole punch was used to make the holes for the input microfluidics used to compartmentalize the cultures. Next, this PDMS structured layer was mounted on a glass wafer, previously cleaned by subsequent acetone, isopropyl-alcohol and DI water washing. To allow the fixing of the PDMS on the glass wafer, the surfaces of both the substrate and the PDMS were treated in O_2 plasma (20 W, 30 s). Finally, glass cylinders (15 mm in diameter, 10 mm in height) were fixed on the PDMS device to create the cell culture wells. As PDMS is hydrophobic, it is necessary to make it hydrophilic to allow cell growth. To do so, the device was treated in O_2 plasma (100 W, 120 s).

The realized PDMS microfluidic devices consist of two chambers communicating through a 3, 10 or 17 mm long microfluidic channel (80 µm in height, 300 µm in width). Additional microfluidic channels, perpendicular to the interconnecting one, are used to continuously perfuse media in order to compartmentalize in a fluidic manner the two cell culture wells.

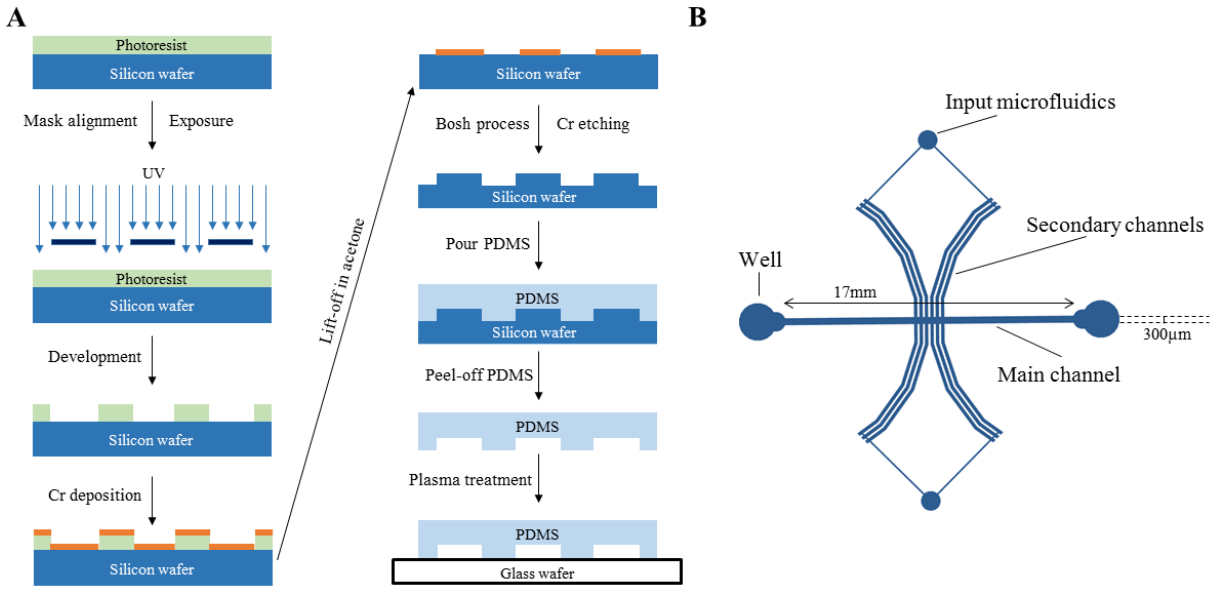

Figure 5: Microfluidic device fabrication. A) Schematic illustration of the fabrication process of the PDMS microfluidic device. B) Illustration of the microfluidic circuitry.

2.4.2 Microfluidic device validation

Microfluidic testing of the functionality of the vertical fluidics developed to compartmentalize the two cell culture wells was performed by applying a Coomassie Brilliant Blue dye (Sigma 27815) in one of the wells, both with/without vertical perfusion. Such perfusion was performed using Milli-Q water.

2.4.3 Primary astrocyte culture

All animal procedures carried out in this work were approved by the institutional IIT Ethics Committee and by the Italian Ministry of Health and Animal Care (Authorization No. 110/2014-PR of the 19th of December 2014).

Primary monolayer cultures of astrocytes were established from cerebral cortices of neonatal (P1–P3) Sprague–Dawley rats and maintained at 37°C in a humidified atmosphere of 5% CO_2. The following solutions and media were used: Hanks Balanced Salt Solution (HBSS) (Sigma H6648); digestion solution − Dispase II 2mg/ml (Roche 04942078001) in Phosphate-Buffered Saline (PBS) (Thermo Fisher Scientific 10010056) + DNAse I 25µg/ml (Sigma D5025) in PBS; complete medium − DMEM/F-12 (Sigma D6421) supplemented with 1% Glutamax (Thermo Fisher Scientific 35050038), 1% Penicillin/Streptomycin (Sigma P4333) and 10% FBS (Sigma F7524). Briefly, pups were removed and decapitated, and the brains were extracted from the skulls and placed in cold HBSS. After dissection, cortices were disaggregated by pipetting, placed in the digestion solution and incubate in water bath at 37°C for 30 min. Cell solution was centrifuged at 900 rpm for 5 min, and the supernatant was removed. The cell pellet was resuspended in complete medium (considering 10ml per pup). The solution was filtered with a cell strainer (Biologix 15-1040, 40 µm pore size), and cells were plated in flasks (considering 1 flask per pup). The day after plating, the medium was changed to remove dead cells. The cultures were maintained at 37°C in a humidified atmosphere of 5% CO_2 for 1 week and thereafter cells were trypsinized and subcultured for the different experiments.

2.4.4 Primary neuronal culture

Primary neuronal cultures were established from cerebral cortices of embryonic day 18 (E18) Sprague–Dawley rats and maintained at 37°C in a humidified atmosphere of 5% CO_2. The following solutions and media were used: Hanks Balanced Salt Solution (HBSS) (Sigma H6648); digestion solution − Trypsin 0,125% (Thermo Fisher Scientific 25050014) in HBSS + DNAse 0,25 mg/ml (Sigma D5025) in HBSS 5mM $CaCl_2$; complete Neurobasal − Neurobasal medium (Thermo Fisher Scientific 21103049) supplemented with 2% B27 (Thermo Fisher Scientific 17504044), 1% Glutamax (Thermo Fisher Scientific 35050038) and 1% Penicillin/Streptomycin (Sigma P4333); FBS (Sigma F7524).

Briefly, embryos were removed and decapitated, and the brains were extracted from the skulls and placed in cold HBSS. After dissection, cortices were placed in the digestion solution and incubate in water bath at 37°C for 30 min. Few ml of complete Neurobasal + 10% FBS were added to the cell solution. It was centrifuged at 1200 rpm for 5 min, and the supernatant was

removed. The cell pellet was resuspended in fresh complete Neurobasal + 10% FBS and gently pipetted for not more than 10 times with P1000 pipette. The solution was filtered with a cell strainer (Biologix 15-1040, 40µm pore size), centrifuged at 700 rpm for 7 min, and the supernatant was removed. The cell pellet was resuspended in complete Neurobasal. Cell viability at the time of isolation was determined by a Trypan Blue Exclusion Assay (Sigma T8154). Cells were plated at a density of 90,000 cells/well onto coverslips coated with poly-D-lysine (PDL) 0.1 mg/ml (Sigma P6407) in 24-well dishes. Five days after plating, half of the medium was added, and subsequently every 4–5 days half of the medium was changed. Neuronal cultures were maintained for up to 3 weeks *in vitro* before being used for the different experiments.

2.4.5 Microfluidic device experiments and treatments

In experiments, the microfluidic device was used either with astrocytes interconnecting the two, wells in which neuronal populations are placed, or without astrocytes to study the effect of released paracrine factors.

In the first experimental condition, cortical astrocytes were plated in the microchannel and in the two wells of the microfluidic device. Once confluent (3-4 DIVs) the medium in the device was replaced with 50% complete Neurobasal + 50% conditioned Neurobasal. The day after, the fluidic connectivity between the two chambers of the microfluidic device with cultured astrocytes was blocked by perfusing 50% complete Neurobasal + 50% conditioned Neurobasal. Then, neurons at 22-24 DIVs that were grown separately on coverslips, were synchronized with Dexamethasone 100nM (Sigma D4902) for 2h and successively placed upside-down in one well of the device (N1). An untreated asynchronous neuronal culture (N2) grown in the same conditions of N1 was placed in the other well of the device. In the second experimental condition, i.e. without astrocytes, experiments were performed by placing neuronal cultures grown on coverslips in the two wells. For experiments with pharmacological compounds such as inhibitors, compounds were added directly in the well, just before placing N2.

All cellular populations in the two wells (i.e. N1, A1 and N2, A2) were harvested at different time points for subsequent qPCR analysis, and all experiments were performed in triplicate by exploiting the integration of multiple distinct microfluidic devices on the same PDMS layer. For the different experimental conditions detailed in the results section, the following compounds were used: DQP1105 50µM (Tocris Bioscience 380560-89-4), Bicuculline 30µM (Sigma B7561), Glutamate 400µM (Sigma 49449), GABA 100µM (Sigma A2129), CNQX

10µM (Tocris Bioscience 479347-85-8), Gap26 100µM (AnaSpec AS-62644), 2-APB 100µM (Tocris Bioscience 524-95-8), TNFα 200ng/ml (PeproTech 315-01A).

2.4.6 Immunofluorescence imaging of astrocytes

Cortical astrocytes were plated on coverslips coated with PDL 0.01 mg/ml in 24-well dishes. Once astrocytes were confluent, some of them were treated with TNFα 200ng/ml (2h). 24h after the treatment, treated astrocytes and control (not treated) astrocytes were washed with PBS and fixed with PFA 4% for 15 min. For the immunostaining, fixed astrocytes were treated with PBS + Triton 0.1% (PBST) for 20 min at room temperature (RT), blocked with PBST + 10% normal goat serum (NGS) for 1h at RT, and subsequently incubated in primary antibodies (rabbit anti-cleaved caspase3, Cell signaling 9664, 1:400) diluted in PBST + 5% NGS overnight at 4°C. The day after, astrocytes underwent 3 washes with PBST and subsequently were incubated with secondary antibodies (Alexa488 goat anti-rabbit, Invitrogen A11034, 1:1000) diluted in PBST + 5% NGS for 45 min at RT. Astrocytes underwent 3 washes in PBST, followed by 1 in PBS. Nuclei were counterstained with DAPI. All images were acquired with 40x objective lenses using a Leica SP5 inverted confocal microscope (Leica Microsystems).

2.4.7 RNA isolation and quantitative real-time PCR (qPCR)

Cells were harvested at the appropriate time points and at a time interval of 6 hours. Total RNA was extracted using TRIzol reagent (Invitrogen 15596018) following the manufacturer's instructions. RNA was further cleaned using a DNase I Kit (Sigma AMPD1). Complementary DNA (cDNA) was obtained by reverse transcription of 300 ng of total mRNA using the M-MuLV-RH First Strand cDNA Synthesis Kit (Experteam R01-500) following the manufacturer's instructions. Real-time reverse transcriptase–PCR was done using the 7900HT Fast Real-Time PCR System (Applied Biosystems). For a 10 ml reaction, 9 ng of cDNA template was mixed with the primers (final concentration: 400nM each primer) and with 5 µl of 2x iTaq Universal SYBR Green Supermix (Biorad 172-5124). The reactions were done in duplicates using the following conditions: 30 s at 95°C followed by 40 cycles of 15 s at 95°C and 60 s at 60°C. The primers used are listed in Table 1. Relative quantification was used to detect changes in the expression of the genes of interest relative to a reference gene (Gapdh). The relative expression was calculated by means of $2^{-\Delta\Delta Ct}$ algorithm.

GENE	SEQUENCE 5'-3'
Gapdh - Forward	TGTGTCCGTCGTGGATCTGA
Gapdh - Reverse	CCTGCTTCACCACCTTCTTGA
Bmal1 - Forward	CCGATGACGAACTGAAACACCT
Bmal1 - Reverse	TGCAGTGTCCGAGGAAGATAGC
Per2 - Forward	CACCCTGAAAAGAAAGTGCGA
Per2 - Reverse	CAACGCCAAGGAGCTCAAGT
Dbp - Forward	CCTTTGAACCTGATCCGGCT
Dbp - Reverse	TGCCTTCATGATTGGCTG
Clock - Forward	TCTCTTCCAAACCAGACGCC
Clock - Reverse	TGCGGCATACTGGATGGAAT
Cx43 - Forward	ACAGCTGTTGAGTCAGCTTG
Cx43 - Reverse	GAGAGATGGGGAAGGACTTGT
GFAP - Forward	ACCAGCTTACTACCAACAG
GFAP- Reverse	CCAGCGACTCAACCTTCCTCT
Serpina3n - Forward	CCTGGAGGACGTCCTTCCA
Serpina3n - Reverse	TCATCAGGAAAGGCCGGTCG
Lcn2 - Forward	CTGGCAGCGAATGCGGTCCA
Lcn2 - Reverse	TGTTCTGATCCAGTAGCGAC

Table 1: Primers used in this work for qPCR (Gapdh transcript as control).

2.4.8 Statistical analysis

Data are presented as mean±s.e.m. and were analyzed and graphed using Prism 5 (GraphPad, San Jose, CA, USA). Statistical significance of the rhythmic expression was determined by Cosinor analysis (expression data was fit by a nonlinear least-squares regression with the following equation: $y = a + b \times \cos [2\pi (t - c)]$, where a is the rhythm-adjusted mean, b is the amplitude of the rhythm, c is the phase given in circadian time representing the time of peak expression and t is the circadian time). $P<0.05$ was considered as statistically significant and the significance is marked by *$P<0.05$, **$P<0.01$ and ***$P<0.001$.

2.5 Results and discussion

In order to study the synergic regulation of clock genes among neurons and astrocytes, and to evaluate the possible pathways involved in the transmission of circadian information among distant neural populations, this work was developed using an *in vitro* model based on a lab-on-a-chip microfluidic device developed in our laboratory. This device allows growing and compartmentalizing distinct neural populations, connected (or not) through a network of astrocytes, to manipulate their clocks and to use real-time quantitative polymerase chain reaction (qPCR) to profile clock genes expression over time.

2.5.1 Specifications and performance of the realized microfluidic device

The lab-on-a-chip device was designed with two distant wells interconnected by a long microfluidic channel (80 μm in height, 300 μm in width and, if not specified differently, 3 mm in length). Six additional microfluidic channels, perpendicular to the interconnecting one, are used to continuously perfuse media in order to compartmentalize in a fluidic manner the two cell culture wells. This was developed by considering enabling to *i*) seed and grow a network of astrocytes covering both wells as well as the interconnecting channel when investigating the astrocytes-mediated neuronal synchronization; *ii*) place neural cultures grown on glass cover-slips in each well, leaving the channel without cells (i.e. "empty" and with only cell culture medium) when investigating paracrine factors-mediated neuronal synchronization and *iii*) use microfluidics to segregate each well, thus avoiding extracellular signaling between the populations in the two wells and leaving only the astrocyte network interconnecting through cell-to-cell interactions the two neural populations.

The fabrication process of these microfluidic devices is depicted in Figure 5A and detailed in the "Materials and Methods" section. It consists in mounting on a 4'' glass wafer a micro-structured Polydimethylsiloxane (PDMS) layer. This layer defines the microfluidic circuitry and it was obtained as replicas from a Si-master by using the so-called "micromolding technique" (Figure 6A). Each device provides 4 pairs of interconnected wells (Figure 6B).

Microfluidic testing of the functionality of the vertical fluidics developed to compartmentalize the two cell culture wells was performed by applying a Coomassie Brilliant Blue dye in one of the wells, both with/without vertical perfusion (Figure 6C). As shown, without the vertical perfusion the dye can flow from one well to the other one. Only when applying the vertical perfusion, the dye remains confined in the first well, resulting in a complete separation of the two chambers. Therefore, these results show that this device can be used: *i*) without vertical

perfusion, to investigate whether paracrine factors released from a synchronous neuronal population can diffuse to synchronize an asynchronous neural population and *ii*) with vertical perfusion, to compartmentalize the cell culture wells and investigate the astrocytes-mediated propagation of circadian rhythms among neural populations located in the wells.

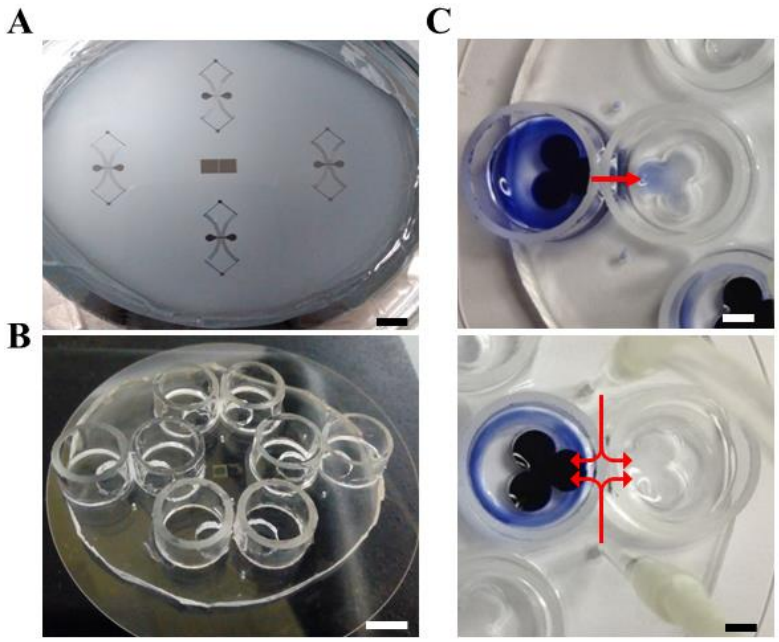

Figure 6: Microfluidic device, its fabrication and compartmentalization testing. A) View of a Si mold. Scale bar: 1 cm. B) View of a PDMS microfluidic device on a glass substrate. Each device is realized on a 4'' wafer and provides 4 pairs of interconnected wells. Scale bar: 1 cm. C) Compartmentalization testing by using a Coomassie Brilliant Blue dye. Case without vertical perfusion (upper panel): as shown the blue dye in the left well can flow in the right well. Case with vertical perfusion (lower panel): as shown the blue dye remains confined in the left well. Scale bar: 0.5 cm.

2.5.2 Paracrine factors-mediated neurons (N1)-to-neurons (N2) synchronization

A possible way for the synchronization between neuronal populations relies on the release and diffusion of paracrine factors. In this case, a synchronous neuronal population may release paracrine factors that diffuse to the asynchronous neural population and synchronize it. To investigate this hypothesis, I used the microfluidic device without applying a vertical perfusion in the interconnecting channel, thus allowing a fluidic connectivity between the two wells and the diffusion of factors among the two neuronal populations.

For these experiments, rat cortical neurons were plated on coverslips and cultured in 24-well dishes for 22-24 days *in vitro* (DIVs). As neurons in culture are asynchronous (Welsh et al., 1995), they were synchronized with 100nM of Dexamethasone (Dexa) for 2h and placed

upside-down in one well of the device (N1), while coverslips with asynchronous neurons (N2) were placed in the other well of the device (Figure 7A). Both neuronal cultures were harvested at different time points, from 6 to 54 h after Dexa treatment, and the expression of the clock gene *Bmal1* was analyzed by qPCR (Figure 7B). As expected, N1 is synchronous. Interestingly, results show that also N2 synchronizes, thus suggesting that paracrine factors released by a synchronous neural population are able to synchronize an asynchronous neural population.

To confirm this result, I performed the same experiment but by blocking the fluidic connectivity between the wells. Having noted that a time window of 36 hours is enough to verify if a cell population is synchronous or not, this and next experiments were performed on an optimized time-window ranging from 6 to 36 h after Dexa treatment. As shown in Figure 7C, N1 is synchronous, with an increase in the amplitude compared with the previous experiment. This could be an effect induced by the continuous supply of medium used for the perfusion. Interestingly, under this condition N2 remains asynchronous, thus suggesting that paracrine factors released by N1 are necessary for its synchronization. Furthermore, this result further proofs that the microfluidic device works properly, and that the vertical perfusion is able to effectively compartmentalize the two chambers.

In order to investigate what are the paracrine factors involved, I decided to start from the main neurotransmitters, i.e. glutamate and GABA. Two different experiments were performed, with a synchronous neural population (N1) in one chamber and an asynchronous neural population (N2) in the other one, in a condition of fluidic connectivity between the two chambers. In the first case, N2 was incubated with the NMDA receptor antagonist DQP1105 (50μM) (Figure 7D); in the second case, N2 was incubated with the $GABA_A$ receptor antagonist Bicuculline (30μM) (Figure 7E). Results show that N2 synchronizes in presence of NMDA receptor antagonist, even if with a different amplitude, while it does not synchronize in presence of $GABA_A$ receptor antagonist, suggesting that for the paracrine factors-mediated synchronization between distant and segregated neuronal populations GABA but not glutamate is necessary. Under this condition, glutamate could have a role in determining the amplitude of the clock genes expression.

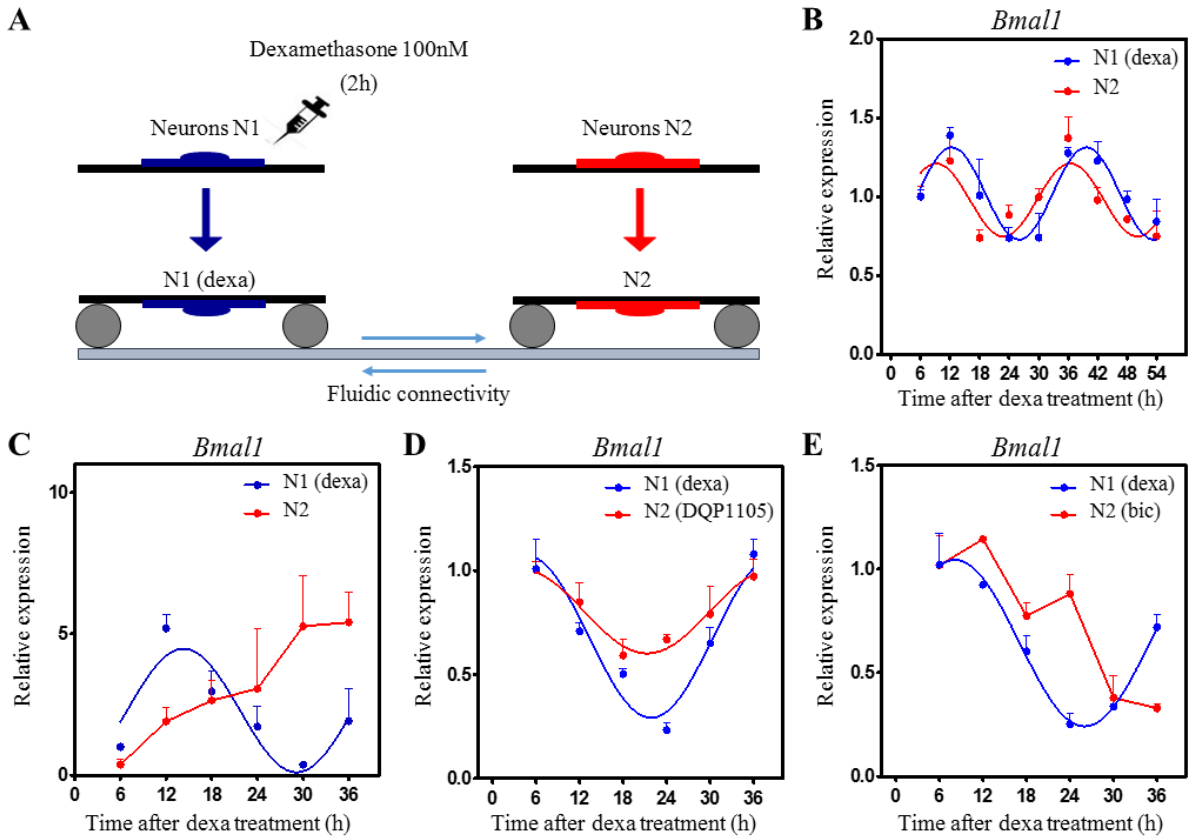

Figure 7: Synchronous neurons synchronize a segregated neuronal population via GABA signaling. A) Schematic illustration of the cell culture in the PDMS microfluidic device. N1=neurons synchronized with Dexamethasone (dexa) 100nM. N2=asynchronous neurons. B) *Bmal1* expression in N1 and N2 in a condition of fluidic connectivity between the two chambers. C) *Bmal1* expression in N1 and N2 without fluidic connectivity between the two chambers. D) *Bmal1* expression in N1 and N2 in a condition of fluidic connectivity between the two chambers and in presence of the NMDA receptor antagonist DQP1105 50µM in N2. E) *Bmal1* expression in N1 and N2 in a condition of fluidic connectivity between the two chambers and in presence of the $GABA_A$ receptor antagonist Bicuculline (bic) 30µM in N2. *Bmal1* was analyzed at the indicate time points by qPCR. All graphs show the mean ± s.e.m. of the cosine-fitted curves from an experiment performed in triplicate.

2.5.3 Astrocytes-mediated neurons (N1)-to-neurons (N2) synchronization

As it is difficult to think that in the brain the synchronization among distant neuronal populations occurs only through the release of neuronal paracrine factors, and given the emerging role of astrocytes in neuronal synchronization, I hypothesized that these glial cells may act as a channel for the transmission of clock rhythms between two distant and segregated neuronal populations. Before experimentally investigate this hypothesis, I first assessed if the constant perfusion of cell culture media used to segregate the cell populations in the two wells might have effects on the expression profile of astrocytes clock genes. In order to do this, a monolayer of asynchronous astrocytes (i.e. not treated with Dexa), was plated in the

microfluidic device. Successively, astrocytes were harvest at different time points, before and during the perfusion, and the expression profile of the clock gene *Bmal1* was analyzed by qPCR (Figure 8A).

Results show the presence of a rhythmic expression of *Bmal1* already before the perfusion. Most likely, this synchronization is induced by changes of the cell culture medium, an effect already reported by Prolo and colleagues (Prolo et al., 2005). Moreover, these data show the persistence of the rhythmicity during the perfusion, with an increase of *Bmal1* expression but without a significant increase in the amplitude of the oscillation. The increase of *Bmal1* expression is attributable to the effect on astrocytes of B27, a serum-free culture supplement present in the medium used for the perfusion (Beaulé et al., 2009). Following experiments were implemented by considering this result.

Next, I investigated whether astrocytes might define communication channels to transfer circadian rhythms to distant neural populations. First, cortical astrocytes were plated in the microchannel and in the two wells of the microfluidic device, while cortical neurons were plated on coverslips and cultured in 24-well dishes. Astrocytes and neurons were cultured separately. When astrocytes were confluent (3-4 DIVs) and neuronal cultures were at 22-24DIVs, the fluidic connectivity between the two chambers of the microfluidic device with cultured astrocytes was blocked. Then, neurons grown on coverslips were synchronized with 100nM of Dexa (2h) and placed upside-down on one well of the device (N1), while coverslips with asynchronous neurons (N2) were placed in the other well of the device. Under this condition, the only way of communication between the two populations of neurons was through astrocytes (Figure 8B-C). Upon cell harvesting, the expression of the clock gene *Bmal1* was analyzed by qPCR (Figure 8D). Remarkably, results show a rhythmic expression of this clock gene in all populations, thus suggesting that astrocytes can transfer circadian information among different neuronal populations.

These first experiments reveal that a synchronous population of neurons can transfer, through an astrocyte network, circadian information to a segregated neuronal population. Following these experimental results, to confirm that the cell culture media induced synchronization of astrocytes does not determines the N2 synchronization, I investigated what happens if both neuronal populations (N1 and N2) are initially asynchronous. To do so, I performed two experiments, by changing the cell culture medium in astrocytes 24h (Figure 8E) or 14h (Figure 8F) before starting the co-culture. For the same reason described above, for this and next experiments with astrocytes I decided to reduce the time points analyzed, going from 6 to 36 h after Dexa treatment. Results show that astrocytes have a circadian rhythmicity of *Bmal1*,

whose phase changes according to the time the cell culture medium was changed. However, in both cases astrocytes are not able to synchronize any of the neuronal populations. This result suggests that media- and synchronous neurons-induced astrocyte synchronizations act differently, but also that the synchronization induced by the cell culture medium is not effective in synchronizing neurons.

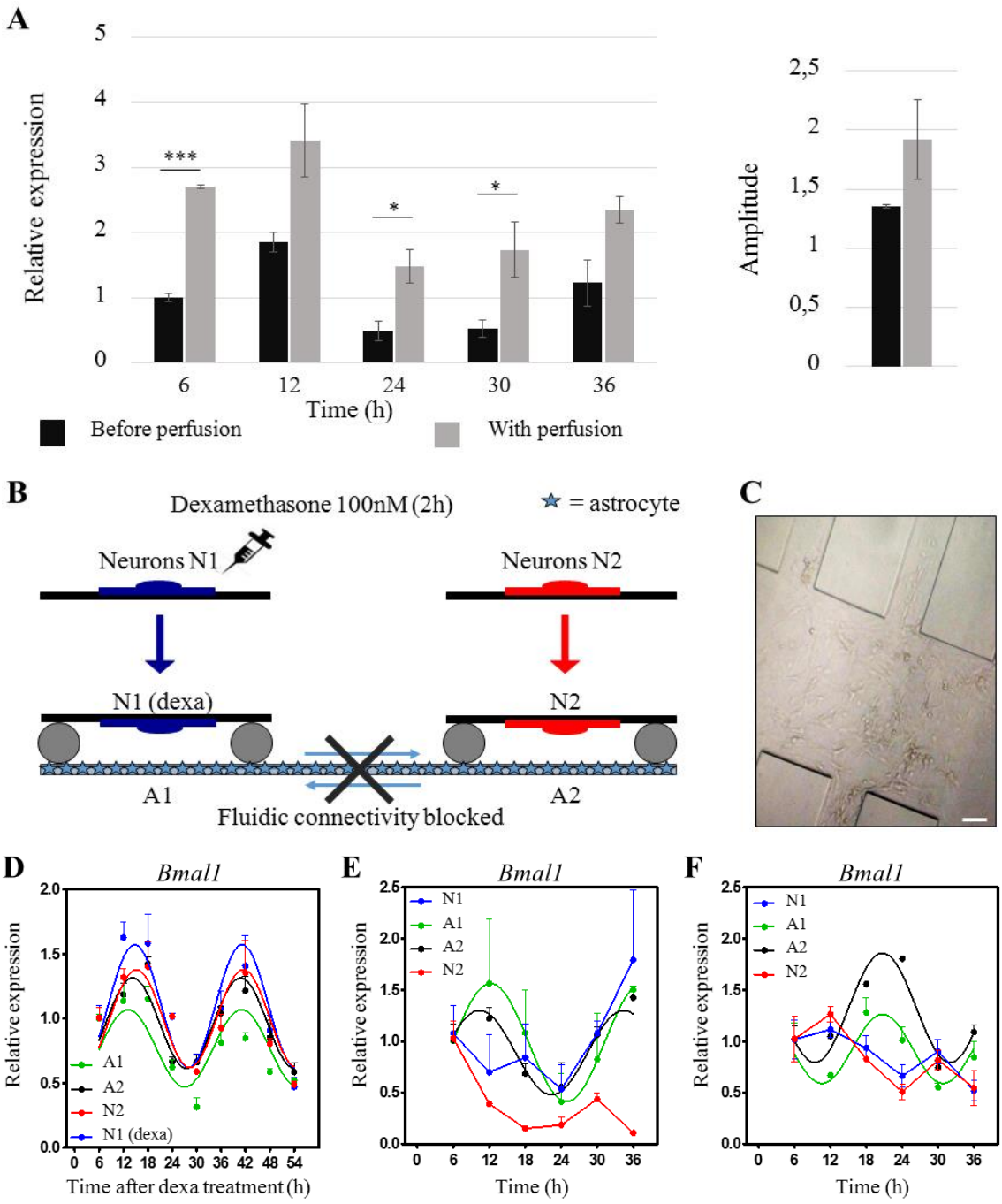

Figure 8: Astrocytes can transfer circadian information among distant and segregated neuronal populations. A) Left: *Bmal1* expression in astrocytes before (blue) and with (orange) perfusion used to segregate the wells of the microfluidic device. *Bmal1* was analyzed at the indicate time points by qPCR. The graph shows the mean ± s.e.m. from an experiment performed in triplicate. Right: Amplitude of *Bmal1* oscillation in astrocytes before (blue) and with (orange) perfusion. Paired t-test: *P<0.05,

**P<0.01 and ***P<0.001 versus astrocytes before perfusion. B) Schematic illustration of the cell culture in the PDMS microfluidic device. N1=neurons synchronized with Dexa 100nM. N2=asynchronous neurons. A1,A2=asynchronous astrocytes. C) Optical micrograph of astrocytes plated in the channel of the microfluidic device. Scale bar: 50 µm. D) *Bmal1* expression in each cellular population (N1, A1, A2, N2). Only N1 was synchronized with Dexa 100nM. E) *Bmal1* expression in each cellular population (N1, A1, A2, N2), with medium changed 24h before starting the experiment. N1,N2=asynchronous neurons. A1,A2=asynchronous astrocytes. F) *Bmal1* expression in each cellular population (N1, A1, A2, N2), with medium changed 14h before starting the experiment. N1,N2=asynchronous neurons. A1,A2=asynchronous astrocytes. In D), E), F), *Bmal1* was analyzed at the indicate time points by qPCR. All graphs show the mean ± s.e.m. of the cosine-fitted curves from an experiment performed in triplicate.

In order to investigate the mechanisms involved in this astrocytes-mediated synchronization, I decided to divide all the process in three steps: *i*) neurons (N1)-to-astrocytes (A1) synchronization; *ii*) astrocytes (A1)-to-astrocytes (A2) synchronization; *iii*) astrocytes (A2)-to-neurons (N2) synchronization. These three components are studied individually in the next sections.

2.5.3.1 Neurons (N1)-to-Astrocytes (A1) synchronization

In the process of astrocytes-mediated synchronization, astrocytes receive "time" information from the synchronous neuronal population. Most likely neurons release factors which, by acting on astrocytes, initiate a signaling that is transmitted through astrocytes and then determines the synchronization of other neurons. To investigate what are the possible factors involved in the neurons-to-astrocytes synchronization, I decided to start from the two main neurotransmitters, glutamate and GABA.

Astrocytes were plated in the channel and the wells of the microfluidic device (A1-A2), co-cultured with asynchronous neurons placed in one well (N2) and treated with glutamate 400µM (20min) or GABA 100µM (2h) in the other well (A1). Both experiments were performed in a condition of fluidic connectivity blocked to ensure that the induced effects from one well to the other are mediated by cell-to-cell communication in the astrocytic network (Figure 9A). As shown in Figure 9C, neurons do synchronize in both cases, thus suggesting that the action of glutamate and GABA on astrocytes is required for the synchronization of a neuronal population.

To confirm this result, three different experiments additionally were performed by using inhibitors of glutamate and GABA receptors. In this case, astrocytes were placed in the channel and the wells of the microfluidic device (A1-A2), a synchronous neural population (N1) in one well and an asynchronous neural population (N2) in the other one. The fluidic connectivity between the two chambers was blocked (Figure 9B).

To study the involvement of glutamate, A1 was incubated with the NMDA receptor antagonist DQP1105 (50µM) (Figure 9D) or with the AMPA/kainite receptor antagonist CNQX (10µM) (Figure 9E). Additionally, to study the involvement of GABA, A1 was incubated with the $GABA_A$ receptor antagonist Bicuculline (30µM) (Figure 9F). Results show that N2 remains asynchronous regardless of the inhibitors used, confirming that both glutamate and GABA are involved in the first step of the astrocytes-mediated synchronization observed between two segregated neuronal populations. Released by synchronous neurons, glutamate and GABA act on astrocytes and trigger a cell-to-cell signaling that leads to the transmission of clock rhythms to a distant neuronal population.

When released from synchronous neurons, glutamate and GABA bind their respective receptors on astrocytes, triggering a cascade of events. Indeed, it was shown that GABA activates astrocytes by binding to ionotropic $GABA_A$ receptor. This leads to glial calcium transients, which can induce the release of gliotransmitters, rendering GABA an important mediator of neuron-glia interactions (Nilsson et al., 1993; Meier et al., 2008; Mariotti et al., 2016). The same behavior was demonstrated for glutamate, which in astrocytes induces an intracellular calcium increase through the activation of NMDA and AMPA receptors (Zhang et al., 2003; Hu et al., 2004), induces calcium waves for a long-range signaling (Cornell-Bell et al., 1990; Kim et al., 1994) and upregulates gap-junctional communication (Rouach et al., 2000). There are also evidences indicating that the NMDA receptor in astrocytes could have a non-canonical metabotropic-like function, regulating Ca^{2+} exit from the endoplasmic reticulum and consequently increasing the intracellular calcium (Montes de Oca Balderas and Aguilera, 2015).

In light of this, knowing also that astrocytes synchronized by Dexa can synchronize neurons (Barca-Mayo et al., 2017) and that Dexa potentiates astrocytic signaling via long-range calcium waves (Simard et al., 1999), it is plausible to consider that glutamate and GABA released from synchronous neurons might act on astrocytes by determining an intracellular calcium increase and consequently an intercellular calcium signaling (ICS) that allows the transmission of circadian information to a distant neuronal population. Interestingly, it was also reported that the extent of the propagation of intercellular waves in astrocytes depends on the glutamate concentration: at low concentrations (< 1 µM), distinct areas of an astrocyte flickered asynchronously, and intracellular waves typically propagated only through portions of cells. At higher concentrations (1 to 10 µM), Ca^{2+}i waves more commonly propagated through entire cells, and intracellular waves began to propagate into neighboring cells. At still higher concentrations (10 to 100 µM), intercellular waves began to propagate over long distances

(Cornell-Bell et al., 1990). This could explain why only astrocytes in contact with synchronous neurons are able to synchronize a distant neuronal population: differently from asynchronous neurons, synchronous neurons release factors in a circadian manner. Consequently, in certain period of time glutamate concentration is high enough to trigger the formation of calcium waves is astrocytes. This explanation would be in line also with the study of Ananthasubramaniam et al., showing that timing of coupling determines synchrony and entrainment in the mammalian circadian clock (Ananthasubramaniam et al., 2014).

It has also to be noted that the increase of the astrocytic gap-junctional communication is not due to an upregulation of gap junction expression in astrocytes, as suggested by the analysis of the expression of Connexin43 (Cx43), the major astroglial Cx detected in cultured astrocytes (Giaume et al., 1991). For this, Cx43 expression was analyzed in A1 population of the two main experimental conditions, i.e. astrocytes in contact with synchronous neurons and astrocytes in contact with asynchronous neurons, and it does not show a significant difference (Figure 9G). This result is in line with other studies reported in literature where, in different experimental conditions, an increase of gap-junctional communication without an upregulation of Cx43 expression was shown (Simard et al., 1999; Rouach et al., 2000).

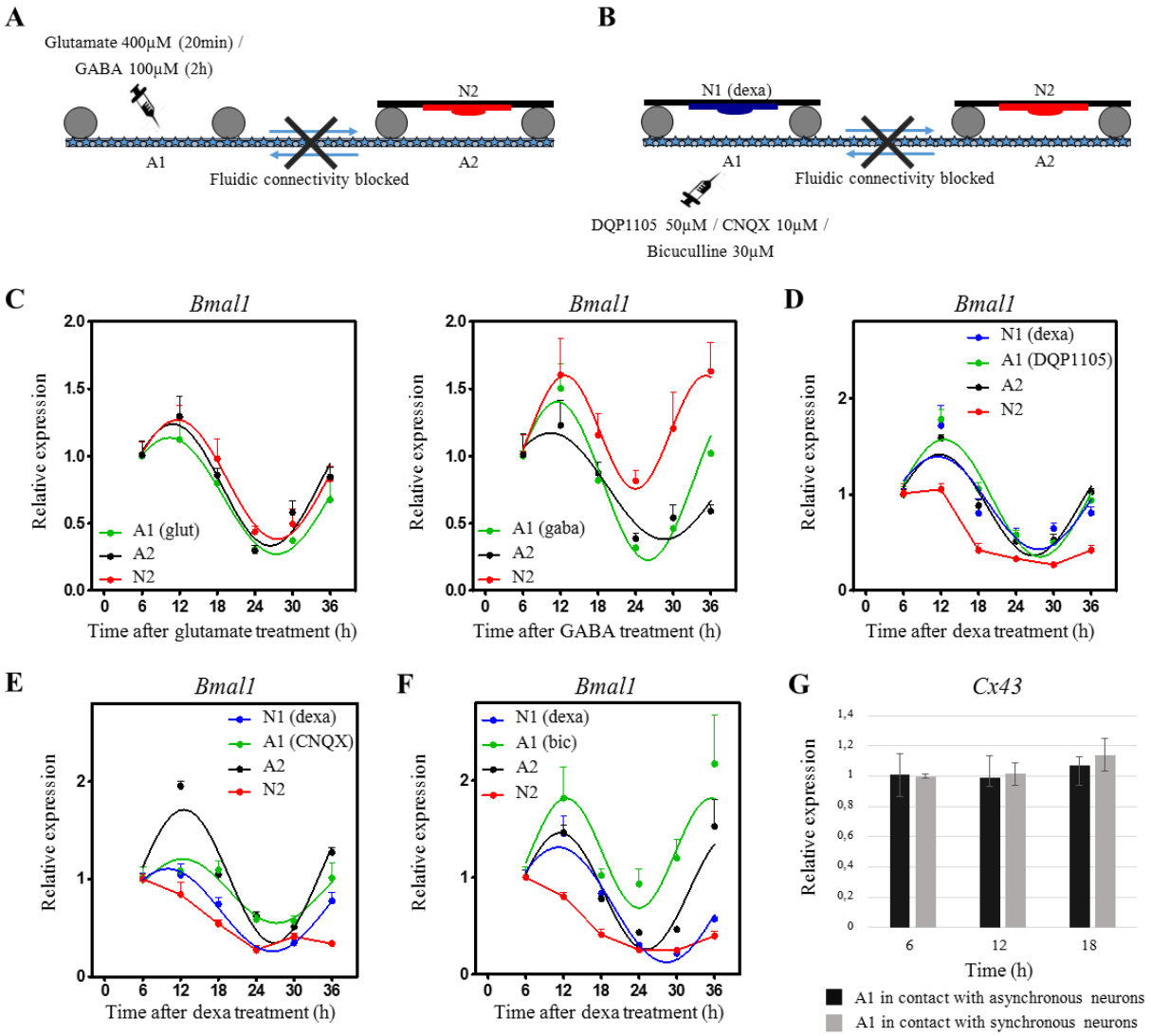

Figure 9: Glutamate and GABA are involved in the first step of the astrocytes-mediated neuronal synchronization. A) Schematic illustration of the cell culture in the PDMS microfluidic device, with glutamate 400µM or GABA 100µM added in the left well. A1,A2=asynchronous astrocytes. N2=asynchronous neurons. B) Schematic illustration of the cell culture in the microfluidic device, with DQP1105 50µM, CNQX 10µM or Bicuculline 30µM added in the left well in order to block respectively glutamate and GABA receptors in astrocytes (A1). N1=neurons synchronized with Dexa 100nM. N2=asynchronous neurons. A1,A2=asynchronous astrocytes. C) *Bmal1* expression in each cellular population in case of glutamate treatment (left panel) and GABA treatment (right panel). D) *Bmal1* expression in each cellular population, after blocking NMDA receptors with DQP1105 50µM in A1 astrocyte population. E) *Bmal1* expression in each cellular population, after blocking AMPA receptors with CNQX 10µM in A1 astrocyte population. F) *Bmal1* expression in each cellular population, after blocking $GABA_A$ receptors with Bicuculline (bic) 30µM in A1 astrocyte population. G) qPCR analysis of *Cx43* at different time points in astrocytes A1 in contact with asynchronous neurons (black) or synchronous neurons (gray). Paired t-test: *P<0.05, **P<0.01 and ***P<0.001 versus astrocytes in contact with asynchronous neurons. In B), D), E), F), *Bmal1* was analyzed at the indicate time points by qPCR. All graphs show the mean ± s.e.m. of the cosine-fitted curves from an experiment performed in triplicate.

2.5.3.2 Astrocytes (A1)-to-Astrocytes (A2) synchronization

To study the mechanisms involved in the transmission of circadian information through astrocytes, I first investigated whether the direct intercellular communication is required. To do so, I performed a synchronization assay under two different conditions: at first with astrocytes not in direct contact with each other, and secondly with astrocytes in direct contact.

For the first condition (Figure 10A), the A1 astrocyte population was plated on coverslips (in 12-well dishes) and grown until confluence. The A2 population was plated on 12-well dishes with paraffin feet that were successively used to avoid direct contact between the cultures (see Barca-Mayo et al., 2017). Astrocytes grown on coverslips (A1) were synchronized with 100nM of Dexa (2h) and placed upside-down in the dish containing the A2 astrocytes while sharing the same culture media. Then the A1 and A2 populations were harvested at different time points for subsequent analysis. For the second condition (Figure 10B), astrocytes were plated in the microfluidic channel and in the two wells of the microfluidic device. Once confluent, the fluidic connectivity between the two wells was blocked. Therefore, the only way of communication between the two populations of astrocytes was through astrocytes in the channel. Only one population (A1) was synchronized with 100nM of Dexa (2h). Finally, both A1 and A2 populations were harvested at different time points and the expression of clock genes analyzed. For both conditions, the expression of the clock gene *Bmal1* of A1 and A2 populations was analyzed by qPCR. Results show that synchronous astrocytes (A1) induce rhythmic expression of *Bmal1* in previously asynchronous astrocytes (A2) only in the second condition, when the two populations are in direct contact. Therefore, our results reveal that astrocyte populations require their direct cellular interconnection to acquire clock rhythms, and that the closed proximity is not sufficient.

Next, I aimed at investigating a possible mechanism that might be enabling this astrocyte-to-astrocyte intercellular signaling of clock rhythms. It is well known that gap junctions mediate intercellular communication among cells by providing ultrastructural cytoplasmic continuity and that they are integral to formation of the functional syncytium of astrocytes (Bennett et al., 2003). For this reason, I decided to block gap junctions, and in particular Cx43, the major astroglial connexin (Cx) detected in cultured astrocytes (Giaume et al., 1991).

Therefore, I performed the same experiment described in Figure 8B, but under the condition of blocking hemichannels and gap junctions between astrocytes in the first or in the second well of the microfluidic device by using Gap26 (100μM). This compound is a mimetic peptide corresponding to a short linear sequence in the first extracellular loop of Cx43 (Desplantez et al., 2012; Li et al., 2015), which makes it specific for astrocytes.

Interestingly, results show (Figure 10C) that, under blockade of hemichannels and gap junctions in the A1 or A2 astrocyte population, the second neuronal population (N2) remains asynchronous and does not synchronize with the Dexa-treated N1 neuronal population. This result suggests that the intercellular communication between astrocytes through gap junctions is required for transmitting neuronal-clock rhythms among distant and segregated neuronal populations.

Another important aspect for the astrocyte-to-astrocyte communication is the intercellular calcium signaling (ICS). Inositol trisphosphate (IP3) appears to be the best candidate to play the role of "fuel" in the propagation of ICS in astrocytes (Giaume and Venance, 1998). Therefore, to investigate if calcium signaling is required for the transmission of clock rhythmicity among astrocytes, I performed a synchronization assay in the microfluidic device, by incubating one astrocyte population (A1) with 2-APB (100μM, 2h), an IP3 receptor antagonist, in a condition of fluidic connectivity blocked (Figure 10D). Since 2-APB is not specific for astrocytes but blocks the release of calcium also in neurons, I did not used the N1 neuronal population but synchronized directly A1 with Dexa 100nM. Results show that the neuronal population (N2) remains asynchronous, thus suggesting that the intercellular calcium signaling in astrocytes is required for the synchronization of distant neuronal populations.

All these results support our hypothesis regarding the required glutamate-/GABA-induced intercellular calcium signaling in astrocytes for the synchronization of distant and segregated neuronal populations.

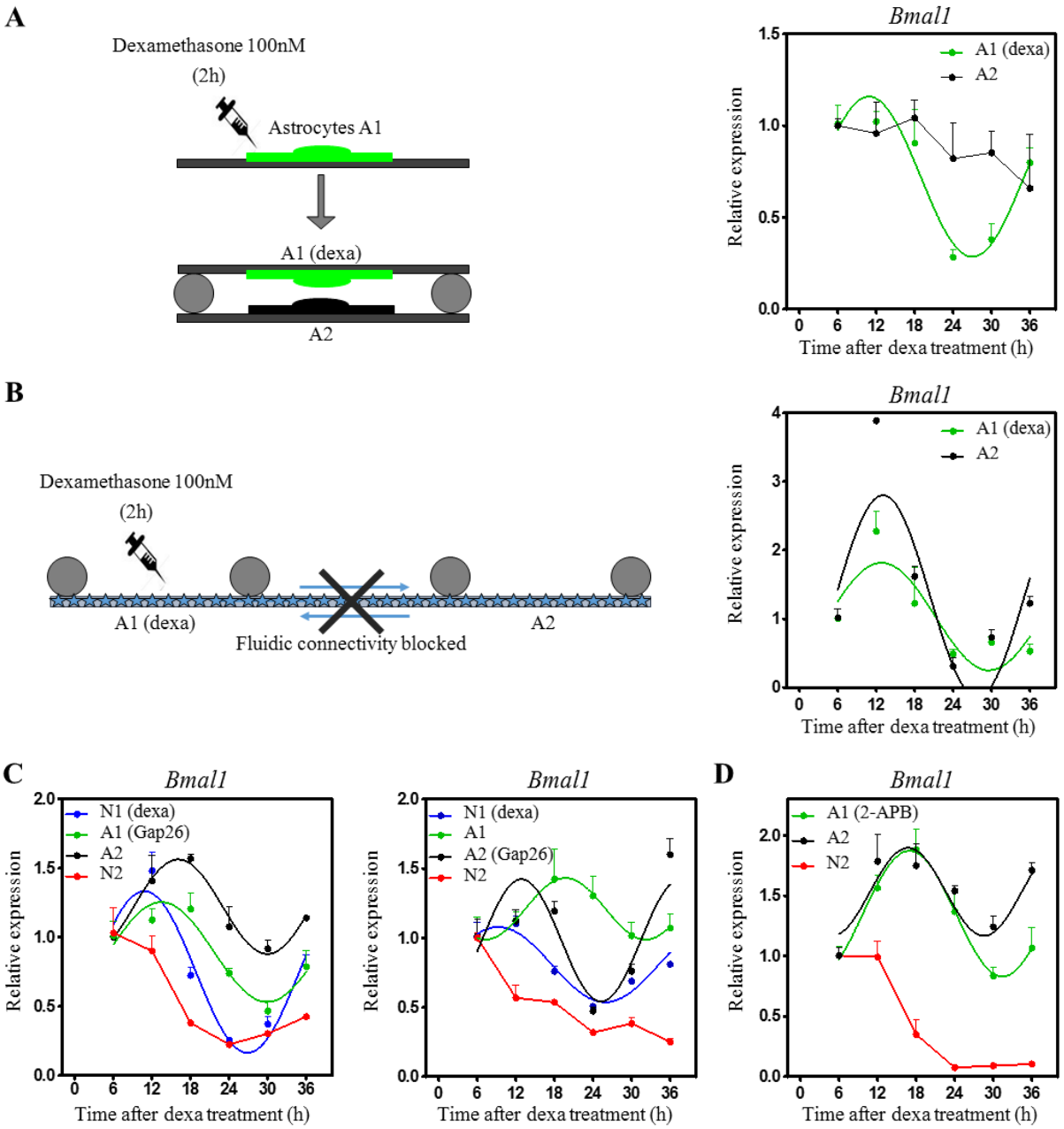

Figure 10: Astrocytes require their direct intercellular communication to acquire and transmit clock rhythms. A) Schematic illustration of the astrocyte culture in the 12-well dishes used for experiment without cellular contact (left) and *Bmal1* expression in both astrocyte populations (right). A1=astrocytes synchronized with Dexa 100nM. A2=asynchronous astrocytes. B) Schematic illustration of the astrocyte culture in the microfluidic device providing only cellular interconnections (left) and *Bmal1* expression in both astrocyte populations (right). A1=astrocytes synchronized with Dexa 100nM. A2=asynchronous astrocytes. C) *Bmal1* expression when intercellular communication between astrocytes is blocked with Gap26 100µM in A1 (left) or A2 (right). N1=neurons synchronized with Dexa 100nM. N2=asynchronous neurons. A1,A2=asynchronous astrocytes. D) *Bmal1* expression after blocking calcium signaling in A1 with 2-APB 100µM. A1=astrocytes synchronized with Dexa 100nM. A2=asynchronous astrocytes. N2=asynchronous neurons. In all graphs, *Bmal1* was analyzed at the indicate time points by qPCR and the mean ± s.e.m. of the cosine-fitted curves from an experiment performed in triplicate is represented.

2.5.3.3 Astrocytes (A2)-to-Neurons (N2) synchronization

The astrocytes-mediated transmission of clock rhythms from a synchronous to an asynchronous neuronal population, a signaling from astrocytes to neurons is necessary.

In 2017, Barca-Mayo and colleagues demonstrated, by an experiment of co-culture with synchronous astrocytes and asynchronous neurons, that GABA, through $GABA_A$ receptor signaling, mediates astrocyte to neuron communication (Barca-Mayo et al, 2017). In the same year, in a demonstration of functional gliotransmission in the SCN, Brancaccio et al. showed that astrocytes release glutamate rhythmically and that blocking this release or uptake by dorsal SCN neurons suppressed and desynchronized circadian oscillations, suggesting a glutamatergic signaling between astrocytes and neurons (Brancaccio et al., 2017). Two years after, by two independent pharmacological approaches, i.e. interference with glutamate release by astrocytes (via Cx43 inhibition) and with neuronal glutamate sensing (via NMDA receptor antagonism), the same group demonstrated that glutamate is a necessary mediator of astrocytic control of circadian function in the SCN (Brancaccio et al., 2019).

By taking these findings into consideration, I investigated on our microfluidic device whether both GABA and glutamate are involved in the astrocytes-to-neurons synchronization. To do so, I performed the same experiment described in Figure 8B, with astrocytes in the channel and the wells of the device, a synchronous neuronal population in one chamber and an asynchronous neuronal population in the other chamber, in a condition of fluidic connectivity blocked. In order to block NMDA receptors or $GABA_A$ receptors in the asynchronous neuronal population, I added DQP1105 50mM or Bicuculline 30μM respectively in the second chamber (Figure 11A). As shown in Figure 11B-C, the N2 neuronal population remains asynchronous, thus confirming the involvement of both GABA and glutamate in the astrocytes-to-neurons communication of clock rhythms.

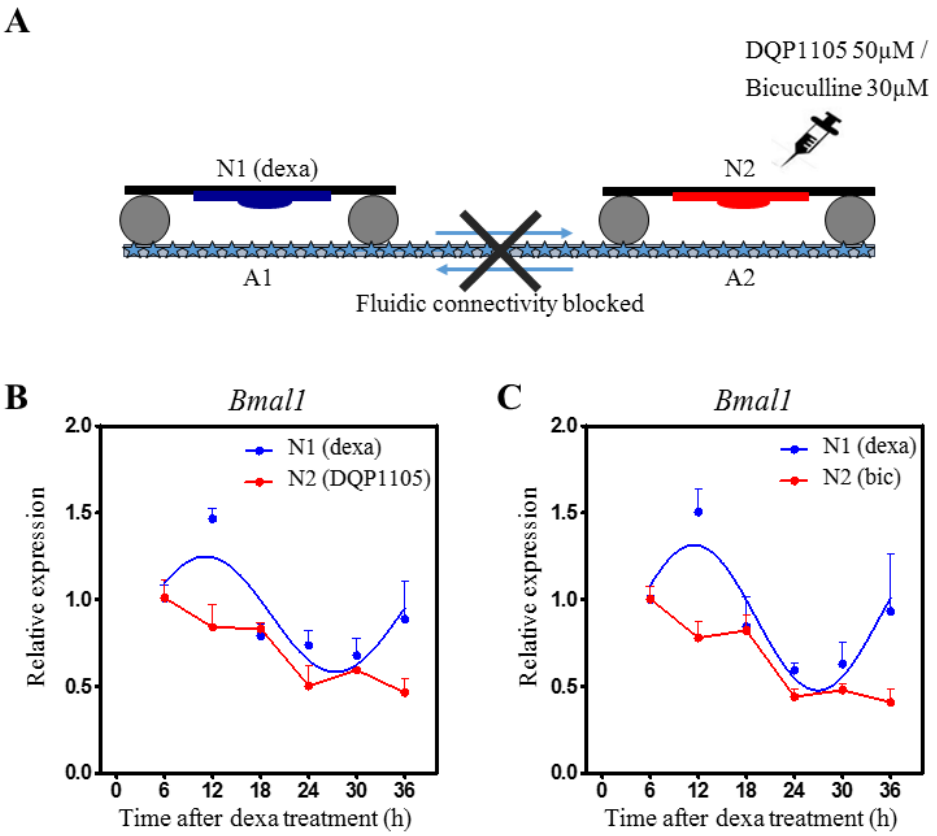

Figure 11: Astrocytes synchronize neurons via a glutamatergic and GABAergic signaling. A) Schematic illustration of the cell culture in the microfluidic device, with DQP1105 50µM or Bicuculline 30µM added in the right well in order to block respectively glutamate and GABA receptors in neurons (N2). N1=neurons synchronized with Dexa 100nM. N2= asynchronous neurons. A1, A2 = asynchronous astrocytes. B) *Bmal1* expression in both neuronal populations (N1-N2) with glutamate receptors blocked in N2 with DQP1105 50µM. C) *Bmal1* expression in both neuronal populations (N1-N2) with GABA receptors blocked in N2 with Bicuculline (bic) 30µM. In B) and C), *Bmal1* was analyzed at the indicate time points by qPCR. All graphs show the mean ± s.e.m. of the cosine-fitted curves from an experiment performed in triplicate.

2.5.4 Synchronization between neuronal populations at different distances

So far, our experimental results revealed the presence of two pathways for the synchronization of distant and segregated neuronal populations: a neural paracrine factors-mediated synchronization and an astrocytes-mediated synchronization.

To investigate if these two pathways may act regardless of the distance between neural populations, I performed specific experiments on microfluidic devices with an increased length of 10 and 17 mm channel, and that were realized by exploiting the flexibility of the established microfabrication process. With these devices I performed the same experiments that were previously reported in Figure 7A and 8B, both without and with astrocytes in the channel connecting the two neural populations.

Graphs of the qPCR data collected each 6 hours for 54 hours (Figure 12) show the expression of *Bmal1* in the two neuronal populations in case of the "empty" channel condition, i.e. without astrocytes and only cell culture medium, and in the case of the channel with pre-seeded astrocytes used for studying astrocytes-mediated synchronization.

As shown in panel A, paracrine factors released from a synchronous neuronal population are able to synchronize an asynchronous neuronal population at a distance of 10 mm, while not at a distance of 17 mm. For the case of the longer channel, the asynchronous neural population seems receiving an input for the synchronization but the neural population is not entrained over time. Differently, in the second condition shown in panel B, astrocytes are able to transmit neuronal clock rhythms also at the maximum distance of 17 mm, thus revealing the capacity of astrocytes to act as an active communication channel that can synchronize distant neural populations.

It is important to highlight that in the first condition, paracrine factors released from the first neural population reach the second one primarily by diffusion through the channel. Thus, an increase in the length of the microchannel, leads to an increase of the time for a factor to diffuse to the second. Furthermore, a variation in concentration of a factor imposed in the first chamber over a certain time, leads to a variation in concentration in the second chamber that is distributed over a longer time. It has to be noted that the volume variation among the different devices due to the channel length is of 0.168 µl, and does not introduce significant variations in the concentration of paracrine factors among the different devices. Further, all these experiments, as previous ones, were performed with a fine control on the volumes of media and in triplicate. These considerations allow us to interpret the results of these experiments. Indeed, our data collected for the 17 mm long microchannel show that the second population receives an initial kick to start synchronizing, but, because of the microchannel fading over time of the variation in concentration of the paracrine factors released by the first neural population, this release of paracrine factors is not sufficient to entrain the synchronization. Interestingly, this also suggests that the entrainment of the second neural population requires continuous impulses of paracrine factors from the first population.

Overall, the results of these experiments on different channel lengths reveal that neural populations can be entrained in synchronization through two pathways that could imply very different potential roles in brain circuits. Neuronal paracrine factors could be involved for local (or short-range) synchronization, while astrocytes can act as active communication channels to transfer circadian information to more distant (long-range) neurons.

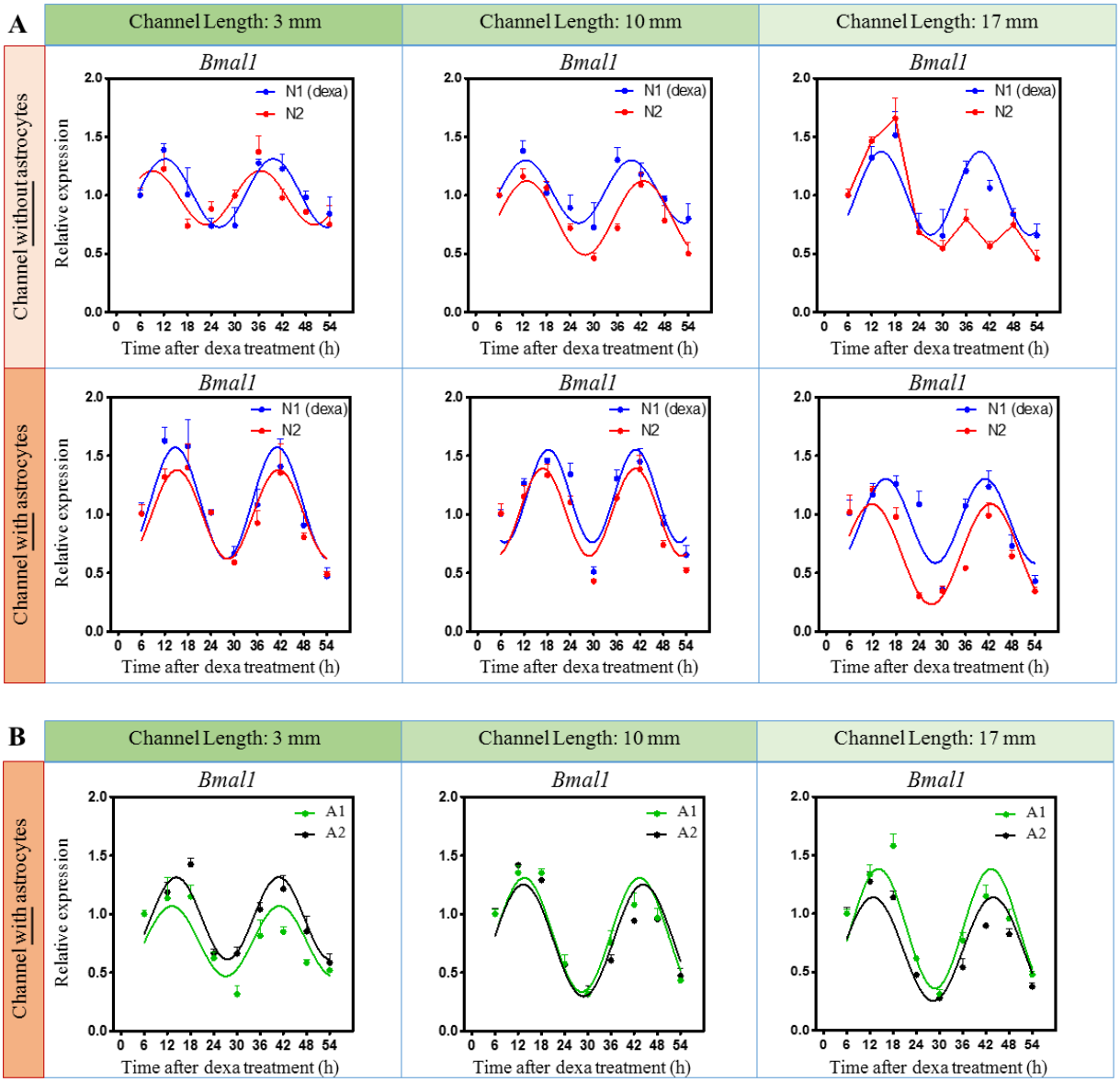

Figure 12: Astrocytes, but not neuronal paracrine factors, are able to transfer clock rhythms to longer distances. A) *Bmal1* expression in both neuronal populations (N1,N2) in microfluidic devices with different lengths of the channel. Going from left to right, channel length is 3, 10 and 17 mm. Upper panels: case of paracrine factors-mediated synchronization, with channel "empty", by means without astrocytes and with only cell culture medium. Lower panels: case of astrocytes-mediated synchronization. N1=neurons synchronized with Dexa 100nM. N2=asynchronous neurons. In all graphs, *Bmal1* was analyzed at the indicate time points by qPCR and the mean ± s.e.m. of the cosine-fitted curves from an experiment performed in triplicate is represented. B) *Bmal1* expression in both astrocytes populations (A1,A2) in microfluidic devices with different lengths of the channel. Going from left to right, channel length is 3, 10 and 17 mm. A1,A2=asynchronous astrocytes. In all graphs, *Bmal1* was analyzed at the indicate time points by qPCR and the mean ± s.e.m. of the cosine-fitted curves from an experiment performed in triplicate is represented.

2.5.5 Effects of astrocyte reactivity on neuronal synchronization

Alterations in the intercellular communication of astrocytes or in the expression of astrocytic clock genes contributes to the impairment of the neurobehavioral outputs, such as cognition, or to disorders associated with the timekeeping system (McKee et al., 2020). Based on this evidence, and knowing the important role of reactive astrocytes in brain diseases, I wondered whether the capabilities of astrocytes that I previously identified, to synchronize neuronal populations and to transfer molecular clocks among distant neuronal populations, are maintained by reactive astrocytes.

Reactive astrogliosis is a term coined for the morphological and functional changes seen in astrocytes responding to CNS injury and other neurological diseases (Pekny and Pekna, 2014). A way to obtain reactive astrocytes is based on Tumor Necrosis Factor alpha (TNFα) treatments. TNFα is known to induce apoptosis in CNS and contributes to brain injuries in many neurological diseases. However, in contrast to neurons and oligodendrocytes, astrocytes exposed to TNFα do not show apoptosis and become reactive in response (Dietrich et al., 2003; Song et al., 2006; Zvalova et al., 2001). Moreover, TNFα was demonstrated to induce proliferation and viability in cultured astrocytes (Wang et al., 2018). In my experiments, I treated rat cortical astrocytes with TNFα 200ng/ml for 2h (Duhart et al. 2013). Such induced reactivity was confirmed by analyzing some of the major reactivity markers, such as *GFAP*, *Serpina3n* and *Lcn2*, whose expression level increases significantly after the treatment (Figure 13A). By immunofluorescence analysis with an anti-cleaved caspase3 antibody, I also confirmed that the treatment with TNFα 200ng/ml does not induce apoptosis in cultured astrocytes (Figure 13B).

To address the first question and investigate if reactive astrocytes are able to synchronize a neuronal population, co-culture experiments in single wells were performed. The well was seeded with astrocytes treated with TNFα and synchronized with Dexa, while an asynchronous neuronal population was placed in the same well and separated by paraffin feet. As shown in Figure 13C, the quantification of qPCR data collected from multiple preparations at different time points reveals that astrocytes seem to lose their capability to locally synchronize a neuronal population.

To address the second question, and investigate if reactive astrocytes are still able to transfer circadian information to distant neuronal populations, I performed an experiment in the microfluidic device having astrocytes in both wells, reactive astrocytes only in the channel, a synchronous neuronal population in one chamber and an asynchronous neuronal population in the second chamber. Results obtained by fluidically segregating the two well populations

(Figure 13D) are reported in Figure 13E, and reveal how the asynchronous neuronal population can still get synchronized even in case of reactive astrocytes interconnecting the two chambers. This suggests that reactive astrocytes maintain their capability to transfer the required signaling for the synchronization of distant neuronal populations. However, this result is the consequence of an experiment performed just 24h after the treatment of astrocytes with TNFα. These astrocytes, therefore, can be considered in an acute-like phase of their reactivity. Ongoing experiments are targeting to investigate the same question also for a chronic-like phase of reactivity, as it can be obtained with longer treatments with TNFα.

Despite being still preliminary, however, these first results highlight the possible link (so far demonstrated only for local synchronization) between reactive astrocytes and alteration of circadian rhythms. Consequently, this also suggests that it might be important to consider astrocytes as a cellular target for neuropharmacology studies on brain diseases involving transient or chronic perturbation of circadian rhythms.

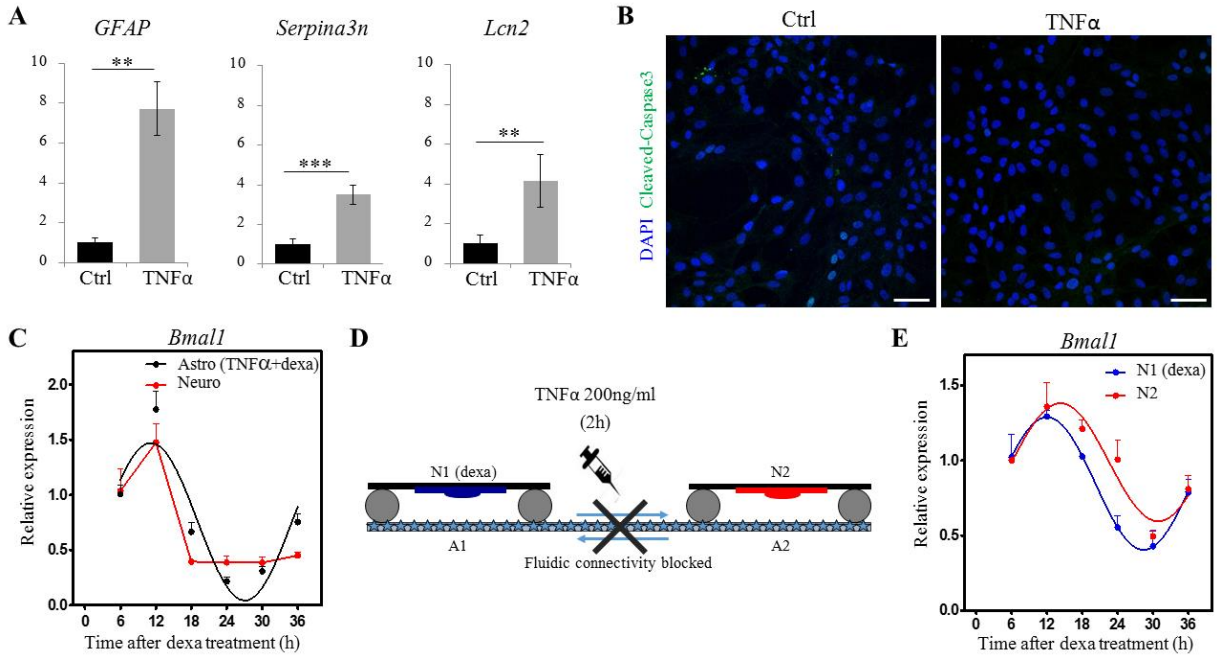

Figure 13: Role of reactive astrocytes for neuronal synchronization. A) qPCR analysis (mean ± sd) of *GFAP*, *Serpina3n* and *Lcn2* in astrocytes treated with TNFα 200ng/ml and in astrocytes not treated (Ctrl). The experiment was performed in triplicate. Paired t-test: *P<0.05, **P<0.01 and ***P<0.001 versus Ctrl. B) Representative immunofluorescence images of cultured astrocytes treated with TNFα 200ng/ml or not treated (Ctrl), stained with anti-cleaved caspase3 (green). Nuclei are labelled with DAPI (blue). Scale bar: 50µm. C) *Bmal1* expression in reactive astrocytes treated with Dexa 100nM (black) and in neurons (red) in a condition of co-culture in single well. D) Schematic illustration of the cell culture in the microfluidic device. Only astrocytes in the channel were treated with TNFα 200ng/ml for 2h. N1=neurons synchronized with Dexa 100nM. N2=asynchronous neurons. A1, A2 = asynchronous astrocytes. E) *Bmal1* expression in both neuronal populations (N1,N2) in the condition described in D).

In C) and E), *Bmal1* was analyzed at the indicate time points by qPCR. All graphs show the mean ± s.e.m. of the cosine-fitted curves from an experiment performed in triplicate.

2.6 Summary and Perspectives

Circadian rhythms are essential in coordinating the proper timing of physiology and behavior (Hastings et al., 2003). The SCN of the hypothalamus is the master clock of the body and it is believed to control the body's main circadian rhythm and communicate with peripheral brain and body regions about how and when to oscillate. What is unknown is how SCN neurons can transfer these information to distant neurons.

In this work, by taking advantage of a microfluidic device developed in our laboratory, I investigated two possible hypotheses: i) a synchronous neuronal population might release paracrine factors for the synchronization of a distant neuronal population; ii) astrocytes might define communication channels to transfer circadian rhythms to distant neural populations.

Results reveal that both pathways can occur. Indeed, synchronous neurons release paracrine factors that can diffuse and synchronize a distant, yet not too far, neuronal population. In particular, among the possible factors released by neurons, I found that GABA, but not glutamate, is necessary for the molecular clocks synchronization of a neuronal population through the binding of $GABA_A$ receptors. Glutamate, however, could have a role in determining the amplitude of the clock genes expression.

Additionally, I also found that astrocytes can have a role in the transmission of circadian rhythms to distant neuronal populations. Following this finding, I investigated the possible mechanisms that allow such transmission and synchronization, and divided this study in three steps: i) neurons-to-astrocytes synchronization; ii) astrocytes-to-astrocytes synchronization; iii) astrocytes-to-neurons synchronization. Results reveal that, in the first step, the synchronous neuronal population releases GABA and glutamate, which bind respectively $GABA_A$ receptors and AMPA or NMDA receptors on astrocytes. As suggested in literature (Hu et al., 2004; Mariotti et al., 2016; Meier et al., 2008; Montes de Oca Balderas et al. 2015), most likely this binding determines an increase in the intracellular concentration of Ca^{2+} leading to the formation of calcium waves that spread among astrocytes. In fact, blocking this spreading by using an IP3 receptor antagonist or a gap junctions blocker specific for astrocytes, I found that the distant neuronal population remains asynchronous. These results suggest that astrocyte gap junctions, and consequently the astroglial intercellular communication, and Ca^{2+} signaling are required for the transmission of the molecular clock synchronization to neurons. Of course, these findings do not exclude the involvement of ATP as another messenger for the spreading

of calcium waves among astrocytes (Fujii etr al., 2017; Guthrie et a al., 1999) and further analysis are needed to better understand the mechanisms involved in the transmission of molecular clock through astrocyte networks.

Finally, concerning the astrocytes-to-neurons synchronization, my results show that both GABA and glutamate are involved. This is in line with the findings reported by Brancaccio (Brancaccio et al., 2017; Brancaccio et al., 2019) and Barca-Mayo (Barca-Mayo et al., 2017) in two different works, in which, by using different approaches, show that astrocytes can synchronize neurons respectively through a glutamate and GABA signaling.

Based on these results, therefore, two mechanisms that allow the transmission of circadian information to distant neural clocks can be proposed (Figure 14): a paracrine factors-mediated synchronization through a GABA signaling, and an astrocytes-mediated synchronization with the involvement of both GABA and glutamate. Such two mechanisms can be complementary and ensure a robust synchronization of neuronal clocks in the brain.

Further, our findings do not exclude the presence of other pathways or other molecules being involved. For example, in recent years it has become clear that neuropeptides are critically involved in the circadian timekeeping. One of such neuropeptide, the vasoactive intestinal peptide (VIP), was found to modulate molecular oscillations within individual oscillators, to synchronize individually oscillating neurons with each other and to synchronize SCN neurons with light cues (Vosko et al., 2007). Moreover, Marpegan et al. showed that VIP synchronizes and sustains rhythmicity in astrocytes *in vitro*, thus indicating that VIP can be a potent entrainment factor for cultured astrocytes. Importantly, this suggests that VIP might play a role as a neuron-to-glia coupling signal *in vivo* (Marpegan et al., 2009). Therefore, in future experiments that could use our microfluidic device, it will be interesting to investigate the possible role of neuropeptides in the transmission of molecular clocks among distant neuronal populations.

Interestingly, by taking advantage of our microfluidic device, and by increasing the length of the channel, I found that paracrine factors-mediated synchronization occurs only on short distances, while astrocytes are able to transfer circadian information even at longer distances. This finding suggests the presence of at least two complementary mechanisms that could operate in parallel to ensure a robust synchronization of cellular clock in the whole brain. This is reasonable especially considering the limitations of diffusive paracrine factors to reach far neural populations in the brain. Therefore, in addition to indicate astrocytes as an “active channel” for the synchronization of distant neural clocks, my work strength the role of astrocytes in the circadian field.

In perspective, the *in vivo* study of these two pathways and their implication in health and disease is a fascinating and original perspective for future studies.

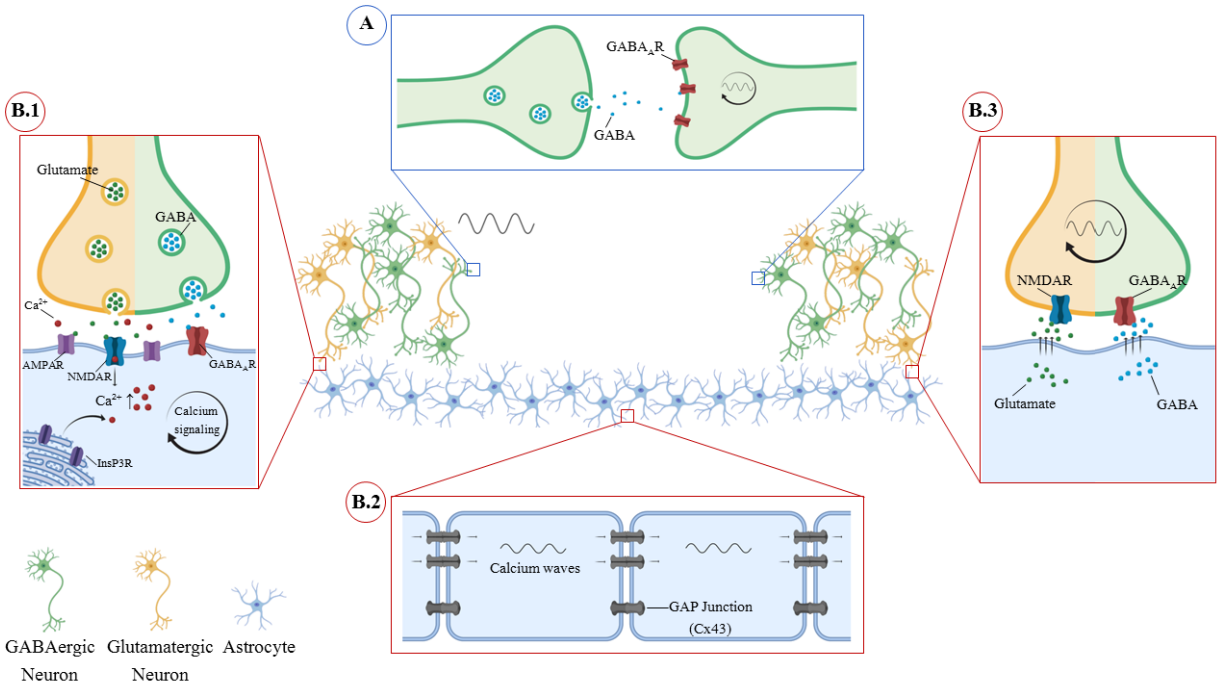

Figure 14: Mechanisms proposed for the synchronization of distant neuronal population. Two pathways have been identified in this work. A) Paracrine factors-mediated synchronization. Neurons release GABA that diffuses and, by binding $GABA_A$ receptors, trigger a signaling that allows the synchronization of neurons. B) Astrocytes-mediated synchronization. Neurons release GABA and glutamate, which bind respectively $GABA_A$ receptors and AMPA or NMDA receptors presents on astrocytes. This binding determines an increase in the intracellular concentration of Ca^{2+}, triggering a calcium signaling (B.1). Through GAP junctions, calcium waves propagate in the astrocyte network (B.2). This signaling ends with the release of glutamate and GABA from astrocytes that, binding respectively NMDA and $GABA_A$ receptors on neurons, trigger the synchronization of neurons (B.3).

A large amount of studies on mouse models have shown that astrocytes play a complex role in the pathogenesis of neurodegenerative diseases. The dysfunction of astrocytes may contribute to either neuronal death or the process of neural disturbances. Also, it has been found that reactive astrocytes always lose their supportive role and gain toxic function in the progression of neurodegenerative diseases (Li et al., 2019; Liddelow and Barres, 2017). It has to be noted that an alteration in the astrocyte intercellular communication or of astrocytic clock genes contributes to the impairment of neurobehavioral outputs, such as cognition, or to disorders associated with the timekeeping system (McKee et al., 2020).

Based on these evidences, in my PhD I also started to investigate if reactive astrocytes maintain their capability to synchronize a neuronal population and to transfer molecular clocks among

distant neuronal populations. Preliminary results highlight that astrocyte reactivity does not impair the propagation of clock rhythms through astrocytes, but causes an impairment in the capacity of astrocytes to synchronize neuronal populations locally. This suggests a possible link between reactive astrocytes and alteration of circadian rhythms, but experiments on this topic are still in progress.

Advancing in understanding the role of neuro-glia interactions in molecular clocks is a relevant topic for disorders linked to alterations in circadian rhythms, from mild disorders related to dysregulation of daily life to more sever pathologies. In perspective, this will undoubtedly lead to increasing the importance of considering astrocytes as a new cellular target for neuropharmacology of transient or chronic perturbation of circadian rhythms.

2.7 Cited references

Abe M, Herzog ED, Yamazaki S, Straume M, Tei H, Sakaki Y, Menaker M, Block GD. Circadian rhythms in isolated brain regions. J. Neurosci. (2002) 22:350–6.

Abrahamson EE, Moore RY. Suprachiasmatic nucleus in the mouse: Retinal innervation, intrinsic organization and efferent projections. Brain Res. (2001) 916:172–191.

Albers HE, Walton JC, Gamble KL, McNeill JK, Hummer DL. The dynamics of GABA signaling: revelations from the circadian pacemaker in the suprachiasmatic nucleus. Frontiers in Neuroendocrinology. (2017) 44:35–82.

Ananthasubramaniam B, Herzog ED, Herzel H. Timing of Neuropeptide Coupling Determines Synchrony and Entrainment in the Mammalian Circadian Clock. PLoS Comput. Biol. (2014) 10(4): e1003565.

Aton SJ, Herzog ED. Come together, right... now: synchronization of rhythms in a mammalian circadian clock. Neuron. (2005) 48:531–4.

Aton SJ, Huettner JE, Straume M, Herzog ED. GABA and Gi/o differentially control circadian rhythms and synchrony in clock neurons. Proc. Natl. Acad. Sci. USA. (2006) 103:19188–93.

Barca-Mayo O, Boender AJ, Armirotti A, De Pietri Tonelli D. Deletion of astrocytic BMAL1 results in metabolic imbalance and shorter lifespan in mice. Glia. (2020) 68(6):1131-1147.

Barca-Mayo O, Pons-Espinal M, Follert P, Armirotti A, Berdondini L, De Pietri Tonelli D. Astrocyte deletion of Bmal1 alters daily locomotor activity and cognitive functions via GABA signalling. Nat. Commun. (2017) 8:14336.

Beaule´ C, Swanstrom A, Leone MJ, Herzog ED. Circadian modulation of gene expression, but not glutamate uptake, in mouse and rat cortical astrocytes. PLoS ONE. (2019) 4(10): e7476.

Bennett MVL, Contreras JE, Bukauskas FF, Saez JC. New roles for astrocytes: Gap junction hemichannels have something to communicate. Trends Neurosci. (2003) 26:610–617.

Brancaccio M, Edwards MD, Patton AP, Smyllie NJ, Chesham JE, Maywood ES, Hastings MH. Cell-autonomous clock of astrocytes drives circadian behavior in mammals. Science. (2019) 363:187–192.

Brancaccio M, Patton AP, Chesham JE, Maywood ES, Hastings MH. Astrocytes control circadian timekeeping in the suprachiasmatic nucleus via glutamatergic signaling. Neuron. (2017) 93:1420–1435.

Callaway E, Ledford H. Medicine Nobel awarded for work on circadian clocks. Nature (2017) 550:18.

Cho H, Zhao X, Hatori M, Yu RT, Barish GD, Lam MT, Chong LW, DiTacchio L, Atkins AR, Glass CK, Liddle C, Auwerx J, Downes M, Panda S, Evans RM. Regulation of circadian behaviour and metabolism by rev-erb-alpha and rev-erb-beta. Nature. (2012) 485:123–127.

Chun LE, Woodruff ER, Morton S, Hinds LR, Spencer RL. Variations in phase and amplitude of rhythmic clock gene expression across prefrontal cortex, hippocampus, amygdala, and hypothalamic paraventricular and suprachiasmatic nuclei of male and female rats. J. Biol. Rhythms. (2015) 30(5):417-436.

Coluccio ML, Perozziello G, Malara N, Parrota E, Zhang P, Gentile F, Limongi T, Raj PM, Cuda G, Candeloro P, Di Fabrizio E. Microfluidic platforms for cell cultures and investigations. Microelectron. Eng. (2019) 208:14-28.

Colwell CS, Michel S, Itri J, Rodriguez W, Tam J, Lelievre V, Hu Z, Liu X, Waschek JA. Disrupted circadian rhythms in VIP- and PHI-deficient mice. Am. J. Physiol. Integr. Comp. Physiol. (2003) 285:R939–49.

Cornell-Bell AH, Finkbeiner SM, Cooper MS, Smith SJ. Glutamate induces calcium waves in cultured astrocytes: Long-range glial signaling. Science. (1990) 247(4941): 470–473.

Csáki Á, Kocsis K, Halász B, Kiss J. Localization of glutamatergic/aspartatergic neurons projecting to the hypothalamic paraventricular nucleus studied by retrograde transport of [^{3}H]D-aspartate autoradiography. Neuroscience. (2000) 101:637–655.

de Mairan J. Observation botanique. Hist. Acad. Roy. Sci. (1729) 35–36.

Desplantez T, Verma V, Leybaert L, Evans WH, Weingart R. Gap26, a connexin mimetic peptide, inhibits currents carried by connexin43 hemichannels and gap junction channels. Pharmacol. Res. (2012) 65:546–552.

Dietrich PY, Walker PR, Saas P. Death receptors on reactive astrocytes: a key role in the fine tuning of brain inflammation? Neurology. (2003) 60:548–554.

Duhart JM, Leone MJ, Paladino N, Evans JA, Castanon-Cervantes O, Davidson AJ, Golombek DA. Suprachiasmatic astrocytes modulate the circadian clock in response to TNF-α. J. Immunol. (2013) 191(9):4656-64.

Dunlap JC, Loros JJ, DeCoursey P. Chronobiology: Biological Timekeeping. Sinauer Associates. (2004)

Dunlap JC. Molecular bases for circadian clocks. Cell. (1999) 96:271–290.

Fields RD, Araque A, Johansen-Berg H, Lim SS, Lynch G, Nave KA, Nedergaard M, Perez R, Sejnowski T, Wake H. Glial biology in learning and cognition. Neuroscientist. (2014) 20:426–431.

Fujii Y, Maekawa S, Morita M. Astrocyte calcium waves propagate proximally by gap junction and distally by extracellular diffusion of ATP released from volume-regulated anion channels. Sci. Rep. (2017) 7:13115.

Gachon F, Nagoshi E, Brown SA, Ripperger J, Schibler U. The mammalian circadian timing system: from gene expression to physiology. Chromosoma. (2004) 113:103–12.

Gao Y, Majumdar D, Jovanovic B, Shaifer C, Lin PC, Zijlstra A, Webb DJ, Li D. A versatile valve-enabled microfluidic cell co-culture platform and demonstration of its applications to neurobiology and cancer biology. Biomed. Microdevices. (2011) 13:539–548.

Gerstner JR, Yin JCP. Circadian rhythms and memory formation. Nat. Rev. Neurosci. (2010) 11:577–588.

Giaume C, Fromaget C, El Aoumari A, Cordier J, Glowinski J, Gros D. Gap junctions in cultured astrocytes: single-channel currents and characterization of channel-forming protein. Neuron. (1991) 6:133-143.

Giaume C, Venance L. Intercellular calcium signaling and gap junctional communication in astrocytes. Glia (1998) 24:50–64.

Goers L, Freemont P, Polizzi KM. Co-culture systems and technologies: taking synthetic biology to the next level. J. R. Soc. Interface. (2014) 11:20140065.

Golombek DA, Bussi IL, Agostino PV. Minutes, days and years: molecular interactions among different scales of biological timing. Philos. Trans. R. Soc. Lond. B. Biol. Sci. (2014) 369(1637):20120465.

Guthrie PB, Knappenberger J, Segal M, Bennett MV, Charles AC, Kater SB. ATP released from astrocytes mediates glial calcium waves. J. Neurosci. (1999) 19(2):520-8.

Halassa MM, Fellin T, Haydon PG. The tripartite synapse: roles for gliotransmission in health and disease. Trends. Mol. Med. (2007) 13:54–63.

Harbour VL, Weigl Y, Robinson B, Amir S. Phase differences in expression of circadian clock genes in the central nucleus of the amygdala, dentate gyrus, and suprachiasmatic nucleus in the rat. PLoS One. (2014) 9(7):e103309.

Harmar AJ, Marston HM, Shen S, Spratt C, West KM, Sheward WJ, Morrison CF, Dorin JR, Piggins HD, Reubi JC, Kelly JS, Maymood ES, Hasting MH. The VPAC(2) receptor is essential for circadian function in the mouse suprachiasmatic nuclei. Cell. (2002) 109:497–508.

Hastings MH, Maywood ES, Brancaccio M. Generation of circadian rhythms in the suprachiasmatic nucleus. Nat. Rev. Neurosci. (2018) 19:453–69.

Hastings MH, Maywood ES, Brancaccio M. The Mammalian Circadian Timing System and the Suprachiasmatic Nucleus as Its Pacemaker. Biology. (2019) 8:13.

Hastings MH, Reddy AB, Maywood ES. A clockwork web: circadian timing in brain and periphery, in health and disease. Nat. Rev. Neurosci. (2003) 4(8):649-661.

Herzog ED, Hermanstyne T, Smyllie NJ, Hastings MH. Regulating the suprachiasmatic nucleus (SCN) circadian clockwork: interplay between cell-autonomous and circuit-level mechanisms. Cold Spring Harb. Perspect. Biol. (2017) 9:a027706.

Higashimori H, Yang Y. Imaging analysis of neuron to glia interaction in microfluidic culture platform (MCP)-based neuronal axon and glia co-culture system. J. Vis. Exp. (2012) 68:4448.

Hu B, Sun SG, Tong ET. NMDA and AMPA receptors mediate intracellular calcium increase in rat cortical astrocytes. Acta Pharmacol. Sin. (2004) 25:714–720.

Jackson FR. Glial cell modulation of circadian rhythms. Glia. (2011) 59:1341–50.

Jin X, Shearman LP, Weaver DR, Zylka MJ, de Vries GJ, Reppert SM. A molecular mechanism regulating rhythmic output from the suprachiasmatic circadian clock. Cell. (1999) 96:57–68.

Kalsbeek A, Palm IF, La Fleur SE, Scheer FA, Perreau-Lenz S, Ruiter M, Kreier F, Cailotto C, Buijs RM. SCN outputs and the hypothalamic balance of life. J. Biol. Rhythms. (2006) 21:458–69.

Karatsoreos IN, Bhagat S, Bloss EB, Morrison JH, McEwen BS. Disruption of circadian clocks has ramifications for metabolism, brain, and behavior. Proc. Natl. Acad. Sci. USA. (2011) 108(4):1657–1662.

Kiesel A. Untersuchungen zur Physiologie des facettierten Auges. Sitzungsber. Akad. Wiss. Wien (1894) 103:97–139.

Kim HJ, Park JW, Byun JH, Vahidi B, Rhee SW, Jeon NL. Integrated microfluidics platforms for investigating injury and regeneration of CNS axons. Ann. Biomed. Eng. (2012) 40:1268–1276.

Kim SM, Lee SH, Suh KY. Cell research with physically modified microfluidic channels: a review. Lab Chip. (2008) 8:1015–1023.

Kim WT, Rioult MG, Cornell-Bell AH. Glutamate-induced calcium signaling in astrocytes. Glia. (1994) 11:173–184.

Klein DC, Moore RY, Reppert SM, editors. Suprachiasmatic Nucleus: The Mind's Clock. New York: Oxford University Press (1991).

Ko GY, Shi L, Ko ML. Circadian regulation of ion channels and their functions. J. Neurochem. (2009) 110:1150–1169.

Kyriacou CP, Hastings MH. Circadian clocks: genes, sleep, and cognition. Trends Cogn. Sci. (2010) 14(6):259-67.

Lavialle M, Servie` re J. Circadian fluctuations in GFAP distribution in the Syrian hamster suprachiasmatic nucleus. Neuroreport. (1993) 4:1243–1246.

Li H, Liu TF, Lazrak A, Peracchia C, Goldberg GS, Lampe PD, Johnson CM. Properties and regulation of gap junctional hemichannels in the plasma membranes of cultured cells. J. Cell Biol. (1996) 134:1019–1030.

Li K, Li J, Zheng J, Qin S. Reactive Astrocytes in Neurodegenerative Diseases. Aging Dis. (2019) 10(3):664-675.

Li R, Lv X, Zhang X, Saeed O, Deng Y. Microfluidics for cell-cell interactions: A review. Front. Chem. Sci. Eng. (2016) 10:90–98.

Li X, Zhao H, Tan X, Kostrzewa RM, Du G, Chen Y, Zhu J, Miao Z, Yu H, Kong J, Xu X. Inhibition of connexin43 improves functional recovery after ischemic brain injury in neonatal rats. Glia. (2015) 63(9):1553–1567.

Liddelow SA, Barres BA. Reactive Astrocytes: Production, Function, and Therapeutic Potential. Immunity. (2017) 46:957-967.

Liu C, Reppert SM. GABA synchronizes clock cells within the suprachiasmatic circadian clock. Neuron. (2000) 25:123–8.

Lopez-Molina L, Conquet F, Dubois-Dauphin M, Schibler U. The DBP gene is expressed according to a circadian rhythm in the suprachiasmatic nucleus and influences circadian behavior. EMBO J. (1997) 16:6762–6771.

Majumdar D, Gao Y, Li D, Webb DJ. Co-culture of neurons and glia in a novel microfluidic platform. J. Neurosci. Methods. (2011) 196:38–44.

Mao S, Zhang J, Li H, Lin JM. Strategy for signaling molecule detection by using an integrated microfluidic device coupled with mass spectrometry to study cell-to-cell communication. Anal. Chem. (2013) 85(2):868-76.

Mariotti L, Losi G, Sessolo M, Marcon I, Carmignoto G. The inhibitory neurotransmitter GABA evokes long-lasting Ca^{2+} oscillations in cortical astrocytes. Glia. (2016) 64:363–373.

Marpegan L, Krall TJ, Herzog ED. Vasoactive intestinal polypeptide entrains circadian rhythms in astrocytes. J. Biol. Rhythms. (2009) 24(2):135-43.

Maywood ES, Chesham JE, O'Brien JA, Hastings MH. A diversity of paracrine signals sustains molecular circadian cycling in suprachiasmatic nucleus circuits. PNAS. (2011) 108:14306–14311.

McClung CR. Plant circadian rhythms. Plant Cell. (2006) 18:792–803.

McKee CA, Lananna BV, Musiek ES. Circadian regulation of astrocyte function: implications for Alzheimer's disease. Cell. Mol. Life Sci. (2020) 77:1049–1058.

Meier SD, Kafitz KW, Rose CR. Developmental profile and mechanisms of GABA-induced calcium signaling in hippocampal astrocytes. Glia. (2008) 56:1127–1137.

Moldavan M, Cravetchi O, Allen CN. GABA transporters regulate tonic and synaptic GABAA receptor-mediated currents in the suprachiasmatic nucleus neurons. J. Neurophysiol. (2017) 118:3092–3106.

Montes de Oca Balderas P, Aguilera P. A metabotropic-like flux-independent NMDA receptor regulates Ca2+ exit from endoplasmic reticulum and mitochondrial membrane potential in cultured astrocytes. PLoS One. (2015) 10(5):e0126314.

Nahavandi S, Tang SY, Baratchi S, Soffe R, Nahavandi S, Kalantar-zadeh K, Mitchell A, Khoshmanesh K. Microfluidic platforms for the investigation of intercellular signalling mechanisms. Small. (2014) 10:4810–4826.

Newman EA. Propagation of intercellular calcium waves in retinal astrocytes and Müller cells. J. Neurosci. (2001) 21(7):2215–23.

Nielsen HS, Hannibal J, Fahrenkrug J. Vasoactive intestinal polypeptide induces per1 and per2 gene expression in the rat suprachiasmatic nucleus late at night. Eur. J. Neurosci. (2002) 15:570–4.

Nilsson M, Eriksson PS, Rönnbäck L, Hansson E. GABA induces Ca^{2+} transients in astrocytes. Neuroscience. (1993) 54:605–614.

Panda S, Antoch MP, Miller BH, Su AI, Schook AB, Straume M, Schultz PG, Kay SA, Takahashi JS, Hogenesch JB. Coordinated transcription of key pathways in the mouse by the circadian clock. Cell. (2002) 109:307–320.

Park J, Koito H, Li J, Han A. Multi-compartment neuron-glia co-culture platform for localized CNS axon-glia interaction study. Lab Chip. (2012) 12:3296–3304.

Park JW, Vahidi B, Taylor AM, Rhee SW, Jeon NL. Microfluidic culture platform for neuroscience research. Nat. Protoc. (2006) 1(4):2128-36.

Park SE, Georgescu A, Huh D. Organoids-on-a-chip. Science. (2019) 364(6444):960–965.

Parpura V, Haydon PG. Physiological astrocytic calcium levels stimulate glutamate release to modulate adjacent neurons. Proc. Natl. Acad. Sci. U.S.A. (2000) 97(15):8629–34.

Pekny M, Pekna M. Astrocyte reactivity and reactive astrogliosis: costs and benefits. Physiol. Rev. (2014) 94(4):1077-98.

Perea G, Navarrete M, Araque A. Tripartite synapses: astrocytes process and control synaptic information. Trends Neurosci. (2009) 32:t421–t431.

Preitner N, Damiola F, Lopez-Molina L, Zakany J, Duboule D, Albrecht U, Schibler U. The orphan nuclear receptor rev-erb alpha controls circadian transcription within the positive limb of the mammalian circadian oscillator. Cell. (2002) 110:251–260.

Prolo LM, Takahashi JS, Herzog ED. Circadian rhythm generation and entrainment in astrocytes. J. Neurosci. (2005) 25:404–408.

Prosser RA, Edgar DM, Heller HC, Miller JD. A possible glial role in the mammalian circadian clock. Brain Res. (1994) 643:296–301.

Richter CP. A behavioristic study of the activity of the rat. Comp. Psychol. Monogr. (1922) 1:1–55.

Rothbauer M, Zirath H, Ertl P. Recent advances in microfluidic technologies for cell-to-cell interaction studies. Lab on a Chip. (2018) 18:249–270.

Rouach N, Glowinski J, Giaume C. Activity-dependent neuronal control of gap-junctional communication in astrocytes. J. Cell Biol. (2000) 149:1513–1526.

Santos J, Arau´ jo J, Cunha M, Costa S, Barbosa A, Mesquita J, Costa M. Circadian variation in GFAP immunoreactivity in the mouse suprachiasmatic nucleus. Biol. Rhythm Res. (2005) 36:141–150.

Simard M, Couldwell WT, Zhang W, Song H, Liu S, Cotrina ML, Goldman S, Nedergaard M. Glucocorticoids-potent modulators of astrocytic calcium signaling. Glia. (1999) 28:1–12.

Sofroniew MV, Vinters HV. Astrocytes: biology and pathology. Acta Neuropathologica. (2010) 119(1):7–35.

Song JH, Bellail A, Tse MC, Yong VW, Hao C. Human astrocytes are resistant to Fas ligand and tumor necrosis factor-related apoptosis-inducing ligand-induced apoptosis. J. Neurosci. (2006) 26(12):3299-308.

Stratmann M, Schibler U. Properties, entrainment, and physiological functions of mammalian peripheral oscillators. J. Biol. Rhythms (2006) 21:494–506.

Takahashi JS. Transcriptional architecture of the mammalian circadian clock. Nat. Rev. Genet. (2017) 18:164–179.

Taylor AM, Dieterich DC, Ito HT, Kim SA, Schuman EM. Microfluidic local perfusion chambers for the visualization and manipulation of synapses. Neuron. (2010) 66:57–68.

Tazawa H, Sato K, Tsutiya A, Tokeshi M, Ohtani-Kaneko ER. A microfluidic cell culture system for monitoring of sequential changes in endothelial cells after heat stress. Thromb. Res. (2015) 136:328–334.

Tso CF, Simon T, Greenlaw AC, Puri T, Mieda M, Herzog ED. Astrocytes regulate daily rhythms in the suprachiasmatic nucleus and behavior. Curr. Biol. (2017) 27:1055–1061.

Vosko AM, Schroeder A, Loh DH, Colwell CS. Vasoactive intestinal peptide and the mammalian circadian system. Gen. Comp. Endocrinol. (2007) 152(2-3):165-75.

Vu TQ, Castro RMde, Qin L. Bridging the gap: microfluidic devices for short and long distance cell-cell communication. Lab Chip. (2017) 17:1009–1023.

Wang X, Huang S, Jiang Y, Liu Y, Song T, Li D, Yang L. Reactive astrocytes increase the expression of P-gp and Mrp1 via TNF-α and NF-κB signaling. Mol. Med. Rep. (2018) 17(1):1198-1204.

Watts AG, Swanson LW, Sanchez-Watts G. Efferent projections of the suprachiasmatic nucleus: studies using anterograde transport of Phaseolus vulgaris leucoagglutinin in the rat. J. Comp. Neurol. (1987) 258(2):204–229.

Weaver DR. The suprachiasmatic nucleus: A 25-year retrospective. J. Biol. Rhythms. (1998) 13:100–112.

Welsh DK, Logothetis DE, Meister M, Reppert SM. Individual neurons dissociated from rat suprachiasmatic nucleus express independently phased circadian firing rhythms. Neuron. (1995) 14:697–706.

Welsh DK**,** Takahashi JS**,** Kay SA**.** Suprachiasmatic nucleus: cell autonomy and network properties. Annu. Rev. Physiol. (2010) 72:551–77.

Yamaguchi S, Isejima H, Matsuo T, Okura R, Yagita K, Kobayashi M, Okamura H. Synchronization of cellular clocks in the suprachiasmatic nucleus. Science. (2003) 302:1408–1412.

Yamazoe H, Ichikawa T, Hagihara Y, Iwasaki Y. Generation of patterned coculture system composed of adherent cells and immobilized non adherent cells. Acta Biomater. (2016) 31:231–240.

Young MW, Kay SA. Time zones: a comparative genetics of circadian clocks. Nat. Rev. Genet. (2001) 2:702–715.

Yu EA, Weaver DR. Disrupting the circadian clock: gene-specific effects on aging, cancer, and other phenotypes. Aging. (2011) 3(5):479–493.

Zhang Q, Hu B, Sun S, Tong E. Induction of increased intracellular calcium in astrocytes by glutamate through activating NMDA and AMPA receptors. J. Huazhong Univ. Sci. Technol. Med. Sci. (2003) 23:254–257.

Zhong Q, Ding H, Gao B, He Z, Gu Z. Advances of microfluidics in biomedical engineering. Adv. Mater. Technol. (2019) 4:1800663.

Zvalova D, Formstecher E, Fauquet M, Canton B, Chneiweiss H. Keeping TNF-induced apoptosis under control in astrocytes: PEA-15 as a 'double key' on caspase-dependent and MAP-kinase-dependent pathways. Prog. Brain Res. (2001) 132:455-67.

3. Surface-functionalized self-standing microdevices exhibit predictive localization and seamless integration in 3D neural spheroids

3.1 Abstract

Three-dimensional (3D) brain models hold great potential for the generation of functional *in vitro* models to advance studies on human brain development, diseases and possible therapies. The routine exploitation of such models, however, is hindered by the lack of technologies to chronically monitor the activity of neural aggregates in three dimensions. A promising new approach consists in growing bio-artificial 3D brain model systems with seamless tissue-integrated biosensing artificial microdevices. Such devices could provide a platform for in-tissue sensing of diverse biologically relevant parameters. To date there is very little information on how to control the extracellular integration of such microscale devices into neuronal 3D cell aggregates.

In this direction, in the present work I contributed to investigated the growth of hybrid neurospheroids obtained by the aggregation of silicon sham microchips (100x100x50µm^3) with primary cortical cells. Interestingly, by coating microchips with different adhesion-promoting molecules, we reveal that surface functionalization can tune the integration and final 3D location of self-standing microdevices into neurospheroids. Morphological and functional characterization suggests that the presence of an integrated microdevice does not alter spheroid growth, cellular composition, nor network activity and maturation. Finally, we also demonstrate the feasibility of separating cells and microchips from formed hybrid neurospheroids for further single-cell analysis, and quantifications confirm an unaltered ratio of neurons and glia.

These results uncover the potential of surface-engineered self-standing microdevices to grow untethered three-dimensional brain-tissue models with inbuilt bioelectronic sensors at predefined sites.

3.2 Introduction

The brain is one of the most complex and intriguing organs in humans, responsible for the advanced intellectual and cognitive ability. Although primates are capable of performing cognitive tasks, their abilities are less evolved. One of the reasons for this is the vast differences in the brain of humans compared to other mammals. Features that are unique to the human brain include its shape, large size and complexity.

Unraveling the molecular and cellular mechanisms regulating brain development, as well as the evolutionary differences seen across species and the need to understand human brain disorders, are some of the reasons that make the study of human brain development fascinating and have attracted the attention of many scientists throughout centuries.

However, our understanding of how human brain develops and functions is still very primitive. The main reason is that we cannot address these questions by studying the human brain itself. Indeed, the brain is formed largely *in utero*, and there are obvious important ethical considerations that limit access to the developing human brain. In addition, the brain, compared to tissues endowed with regenerative capacities, cannot be easily grown and expanded in the dish. Consequently, even the small live-tissue resections discarded from certain types of brain surgery make for very limited experimental platforms (Arlotta, 2018).

For all these reasons, model systems are usually used to study the brain. Conventional models are standard *in vitro* two-dimensional (2D) cell cultures and *in vivo* animal models (Figure 15). 2D cell cultures provide low cost and simplified approaches for studying the brain development and its diseases. Recently, pharmaceutical companies and research labs have enhances the 2D cell culture studies by utilizing human cells, including primary cells, embryonic stem cells, and induced pluripotent stem cells (iPSC). However, despite the progress on the availability of cells for 2D cultures, they fail to mimic the complexity of the human brain and its unique features and functions (Jorfi et al., 2018). First, cell-to-cell or cell-to-extracellular matrix interactions, which regulate important steps of neurodevelopment, are largely missing in a monolayer culture. Second, gradient of growth factors, patterning factors, nutrients, and gas exchange are critical for regional specification of the human brain, which is a challenge to model with a monolayer system. Third, a planar culture cannot recapitulate certain important cellular properties, such as cell polarity and guided cell migration (Koo et al., 2019). Moreover, 2D cultures cannot provide information regarding behavioral responses, many functional responses, or systemic responses (organ-organ interactions), and are therefore considered to be too simplistic for many practical applications (Nikolakopoulou et al., 2020).

Animal models, in turn, offer complexity but are often unable to recapitulate the human brain pathophysiology accurately and are associated with many specific interspecies differences. In addition, they are expensive, their throughput is low, and they raise ethical concerns.

The lack of adequate models causes, for example, many drugs to fail in the transition from animal to human clinical trials. This has spurred academic and industrial researchers to seek out new technologies for mimicking brain physiology and functionality in health and disease, by using tools such as iPSCs, organ-on-a-chip (OoC) systems, organoids, 3D printed gels and neuronal machine interfaces. Though none of these methods can fully capture the complex physiology, anatomy and functionality of the human brain, they are nonetheless showing very promising results in terms of their capacity to recapitulate certain human functions or pathological mechanisms, as well as to reveal new physiological interactions that could not have been identified with current standard tools *in vitro* or *in vivo* (Nikolakopoulou et al., 2020).

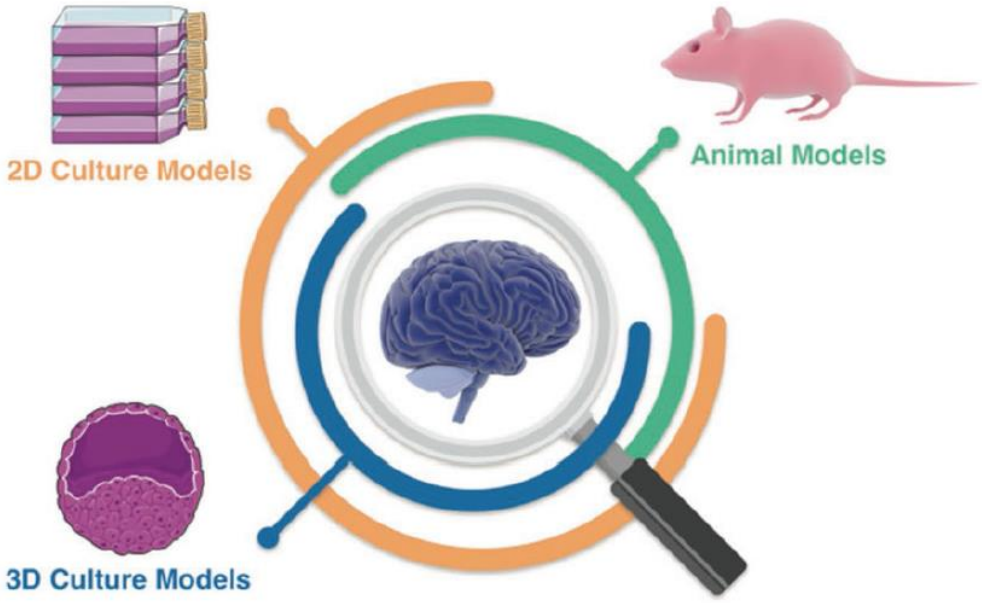

Figure 15: Schematic representation of available experimental models to study the human brain development and its diseases. This image was adapted from Jorfi et al., 2018.

3.2.1 Mimicking the complexity of the human brain: 3D cellular models

Over the last decade, there has been a dramatic effort to develop 3D *in vitro* brain models. This was mainly driven by the emergence of unprecedented enabling technologies, including stem cells, biomaterials and microfabrication techniques. These 3D physiologically relevant cell culture systems aim to closely mimic the human tissues and provide high-throughput and reproducible studies at molecular, cellular and circuit scales. The 3D cell-cell interactions and physiological cues provided by the extracellular matrix (ECM) tend to offer an *in vivo*-like

environment to cells. This is a core concept that has been applied for building 3D models of the central nervous system, such as brain-on-chips, neurospheroids and cerebral organoids. Nowadays, these 3D models offer a very powerful potential platform for understanding the human brain as well as for drug development and discovery in pharmaceutical industry for neurological diseases such as Alzheimer's disease (AD), Parkinson's disease (PD), traumatic brain injury and related damage to the brain. Additionally, these experimental models could be invaluable test beds for assessing toxicology and the responses of the human brain cells and circuits to a variety of therapeutics (Jorfi et al., 2018). Here below I shortly introduce these 3D models by starting with organotypic brain slices, an experimental model that initially enabled several studies on brain circuits *in vitro*.

3.2.1.1 Organotypic Brain Slice cultures

Organotypic brain slice cultures (BSCs) have been the first attempt to bridge *in vitro* and *in vivo* models by creating a platform that resemble the brain *in vivo* environment while attempting to keep key *in vitro* characteristics (Shamir and Ewald, 2014; Humpel, 2015). These models now represent an established model for a variety of studies in neuroscience that can exploit them, for instance, with electrophysiology, immunohistochemistry and other techniques to dig into molecular, cellular and circuit level processes in health and disease.

They are typically obtained from rodents but can also be obtained from human postmortem or biopsy brains (Humpel, 2015).

The use of BSCs of postnatal rodent brain to model physiological and developmental properties was first established in the 1980s with the introduction of the roller-tube method (Gähwiler, 1981). However, brain tissue cultured in this manner did not preserve the cytoarchitecture of the region of interest. To overcome this issue, in 1990s an alternative culture method referred as the interface-slice culture method, was introduced. This method is based on the properties of the air-liquid interface to drive nutrients inside the tissue and it involves culturing the tissue region of interest on a porous membrane interface between a humidified atmosphere and the culture medium. The explant of tissue attaches to the membrane and receives nutrition from the slice culture medium through the membrane via capillary action (Stoppini et al., 1991). The majority of BSCs are typically prepared from mice or rats up to postnatal day 12. At this age the cytoarchitecture is established, the brain is larger and easier to manipulate and neuronal cells are likely to survive the explantation (Bahr 1995). BSCs also display high levels of plasticity and therefore show resistance to the mechanical trauma incurred when neuronal processes are cut (De Simoni et al., 2003).

A main advantage of BSCs is that they retain a certain degree of the native 3D organization in culture, maintain vascular cells and are, at least partially, anatomically intact and representative of the area of which they are derived (Humpel, 2015; Hutter-Schimid et al., 2015). Neuronal and non-neuronal cells from the brain grown *ex vivo* in BSCs are representative of the populations found *in vivo* (Staal et al., 2011). This system therefore allows all cell types in the brain to be studied in a quite well anatomically preserved environment. A further advantage of this *ex vivo* system is that the development of cells and synapses mimics the development of the brain *in vivo*: neurons morphologically develop *ex vivo* as they do *in vivo* in acute preparations and retain similar synaptic connectivity, intact neuronal function and circuitry as observed in intact brain (De Simoni et al., 2003). Other advantages are the easy preparation, the low cost maintenance and the minimization of ethical issues compared to animal models (Shamir and Ewald, 2014).

Organotypic brain models have been mainly used for assessing physiological and pharmacological properties of different tissues and for studying neurodegenerative disorders, serving as *ex vivo* models for diseases such as AD, PD, Huntington's, and cerebral ischemia (Cavaliere et al., 2016; Croft et al., 2019). BSCs also represent a valuable platform for studying cell therapy approaches based on the grafting of engineered cells into slices and monitoring the induced effects. This allows researchers to assess cell-cell, and cell-cellular matrix interactions, cell migration, and stem cells phenotype changes (Daviaud et al., 2013).

Despite all the advantages presented so far, organotypic brain slices also show key disadvantages that halted people from using them widely as a standard model. Indeed, these models can be maintained in cultures only for few weeks; they are very thin and fragile tissue (≈100–400 μm) and they can be distorted during the culture maintenance. Although organotypic slices derived from young animals (P3 to P10 – rats or mice) offer the most resilient slices, these slices do not represent a valuable model for adult neurodegenerative diseases (Jorfi et al., 2019).

3.2.1.2 Brain-on-a-Chip models

The last decade has seen a growing trend towards engineering microphysiological systems (MPSs) called 'organs-on-chip'. These are microfluidic-based microsystems capable of mimicking *in vivo* human physiology at small scale, reconstituting the key physiological elements and functions of different organs in a miniaturized and well-controlled microenvironment (Bhatia and Ingber, 2014; Jiang et al., 2014). Organ-on-chips can be used for a wide variety of applications such as drug discovery, personalized medicine or fundamental

research on cellular mechanisms. They accelerate pharmaceutical testing by harnessing the potential of microfluidic high-throughput technologies to lower cost, increase reproducibility, and speed up drug screening for adsorption, distribution, metabolism, excretion and toxicity compared to animal models that tend to be expensive and poor predictors (Guan et al., 2017). For all these reasons, organs-on-chip has already captured the attention of many pharmaceutical and medical companies as well as government regulatory agencies including the United States Food and Drug Administration (FDA).

The MPSs offer the possibility of a 3D simulation also of the brain physiology and functionalities. The so called brain-on-a-chip has been a significant technological advancement in making human-relevant brain models for mimicking higher-order physiological and pathophysiological responses. They can be used to test the potential neurotoxicity of new drugs and to study the biochemical mechanisms underlying neurological disorders. Aside from ethical considerations, brain-on-chips overcome the high cost of animal care, the complexity of tissue isolation, the need for transgenic animals, as well as many of the uncertainties of translation of animal models to human physiology (Jorfi et al., 2019). The model reliability is strongly improved by using human-derived cells that are more relevant than animal models for pharmacological screening and disease studies. Patient-derived neurons from different regions of the brain can be directly grown and differentiated on a brain-on-a-chip device (Figure 16). The selected cells are capable of organizing themselves in the *in vivo* environment thanks to the device architecture, materials selection and bio-chemical functionalization (Miccoli et al., 2018). In addition to this, brain-on-chips offer more control over the cell culture environment: the microfluidic channels connected to the cell culture microchamber allow continuous exchange of nutrients and growth factors along with discarding the waste, and the continuous flow ensures the cells get exposed to the nutrients equally (Jahromi et a., 2019).

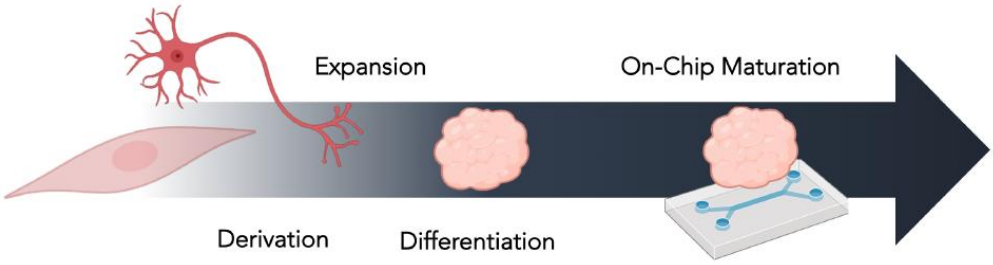

Figure 16: Concept representation of the growth of brain-on-chips starting from human-derived cells. This image was adopted from Spitz et al., 2019.

3.2.1.3 Neurospheroids

Neural cells can be cultured through self-assembly and without using scaffolds into spheroids structures, forming the so called neurospheroids. Spheroids have been employed to recapitulate the fundamental features of brain tissues in terms of cell diversity, electrophysiology, extracellular matrix (ECM) production and mechanical stiffness (Zhuang et al., 2017). Typically, these cellular aggregates secret their own ECM instead of requiring other foreign ECM-mimicking materials, hence, maintaining the native ECM composition.

Dingle et al. generated 3D spheroids with rat neonatal cortical cells. Their immunohistochemical analysis revealed the presence not only of neurons, but also of multiple glial cell types, including astrocytes, oligodendrocytes, and even microglia. Remarkably, after 14 days *in vitro*, patch-clamp recordings revealed that neurons were electrically active and participated in synaptic networks. In addition, such cortical spheroids secreted laminin and exhibited elastic modulus that was similar to that of newborn rat cortex (Dingle et al., 2015).

Spheroid formation is one of the most well characterized models for 3D culture and screening due to its simplicity, reproducibility, and similarity to physiological tissues. Most importantly, spheroids can be monitored easily for practical daily observations. As a result, spheroid cultures have been valued as a physiologically relevant alternative to 2D cultures for decades (Tung et al., 2011) and are widely used for assays on non-brain tissues.

Typical spheroid formation methods include hanging drops on the underside of culture plate lids, culture of cells on non-adherent surfaces, spinner flask cultures, and rotary cell culture systems (Del Duca et al., 2004; Friedrich et al., 2007). These traditional spheroid formation and culture systems, however, are often tedious, produce variable size spheroids, low-throughput, and hard to handle (Tung et al., 2011). To increase spheroid formation efficiency, offer better control of spheroid sizes, as well as simplify handling procedures, various microfluidic (spheroids on a chip) devices have also been developed (Torisawa et al., 2007; Sakai and Nakazawa, 2007; Torisawa et al., 2007; Wu et al., 2008).

Using spheroid models, researchers have drawn great insights into tumor development and neurotoxicity (Ivanov et al., 2014; Avci et al., 2015; Terrasso et al., 2015). In addition, thanks to the possibility to obtain neurospheroids with neural progenitor cells, which are self-renewing multipotent cells that have the capacity to differentiate into neurons as well as glial cells, the neurosphere culture system has gained a great importance in studies investigating differentiation, neurotoxicological studies, and biological studies of developmental processes (Khan et al., 2018). Moreover, in recent years spheroids have been extended to model degenerative neurological diseases such as AD (Choi et al., 2013) and PD (Simao et al., 2015).

However, despite of the potentials in using neurospheroids, the major issue with this kind of culture is its sensitivity to the variable culture methods. This has made it difficult to formulate a unified culture procedure and therefore it has been difficult to merge discoveries from different groups to gain a complete understanding of a particular phenomenon (Khan et al., 2018).

3.2.1.4 Brain organoids

Brain organoids are organ-like 3D tissue cultures derived from hPSCs that self-assemble to form an organized architecture, composed of progenitor, neuronal and glial cell types, resembling the fetal human brain (Jo et al., 2016; Lancaster et al., 2013; Pasca et al., 2015). They have been demonstrated to capture some fundamental features of human brain: not only brain organoids recapitulate the human brain at the cellular level, but also in terms of general tissue structure and developmental trajectory, providing in this way a unique opportunity to model human brain development and function (Qian et al., 2019) (Figure 17).

In general, two different types of methodologies can be used to generate brain organoids. These are the so called “unguided methods” and “guided methods”.

Unguided methods harness the intrinsic signaling and self-organization capacities of hPSCs to differentiate spontaneously into tissues mimicking the developing brain. In the protocol developed by the Knoblich group, embryoid bodies (EBs) derived from hPSC aggregates were embedded into an extracellular matrix (ECM), such as Matrigel, and subsequently cultured in spinning bioreactors to promote tissue expansion and neural differentiation (Lancaster and Knoblich, 2014). Cerebral organoids produced by this approach exhibit a variety of cell lineage identities ranging from forebrain, midbrain and hindbrain, to retina, choroid plexus and mesoderm (Camp et al., 2015; Lancaster et al., 2013). The stochastic nature of hPSC spontaneous differentiation, however, results in unpredictable proportions and a heterogeneous arrangement of each lineage and cell type across batches of differentiated organoids and across hPSC lines. Although this cell-type diversity in cerebral organoids offers a unique opportunity to model the interactions between different brain regions, the high variability and heterogeneity present significant challenges for systematic and quantitative studies (Qian et al., 2019).

In “guided” organoid, small molecules and growth factors are used throughout the differentiation process to instruct hPSCs to form cells and tissues representative of certain brain regions (Jo et al., 2016; Pasca et al., 2015; Sakaguchi et al., 2015; Yoon et al., 2019). For example, a hindbrain neural tube-like structure that differentiates to form cerebellum-like organoids was generated by the sequential addition of FGF19 and SDF1 (Muguruma et al.,

2015). These directed organoid cultures are sometimes capable of generating mixtures of cell types with relatively consistent proportions, exhibiting less variation across batches and cell lines (Sloan et al., 2017). However, directed organoids typically contain relatively small neuroepithelial structures and their cytoarchitecture is sometimes not well-defined, possibly owing to the interference of hPSC self-organization and cell-cell interactions by excessive use of external factors.

The number and combination of external factors used in differentiation protocols varies, and the choice between unguided and guided approaches is often seen as a trade-off between diversity and consistency and will depend on the specific focus of investigation. For instance, unguided organoids are suitable for exploring cell-type diversity during whole-brain development, while brain region-specific organoids better recapitulate brain cytoarchitecture with less heterogeneity (Qian et al., 2019).

Although cerebral organoid methods can produce tissues resembling various interacting brain regions, their proportion and spatial organization are highly heterogeneous and unpredictable. To improve modeling of inter-regional interactions, several groups concurrently developed new approaches, first differentiating hPSCs into different brain region-specific organoids separately, and then fusing them together to form organoids with multiple distinct region identities in a controlled manner (Bagley et al., 2017; Birey et al., 2017; Xiang et al., 2017). These fused organoids are called assembloids, a term coined by S. Paşca to describe the anatomical and functional assembly of multiple organoids (or spheroids), wherein infiltrating nerve fiber branching among two or more masses mimics interconnected brain areas (Paşca, 2018). Assembloids are a unique means to study the development of interconnections among brain areas in a controlled setting. Therefore, they carry the tremendous potential of enabling the replication (and characterization) of interconnected brain areas at the highest level of complexity so far witnessed in the tissue bioengineering field (Marton and Paşca, 2020; Forro et al., 2021).

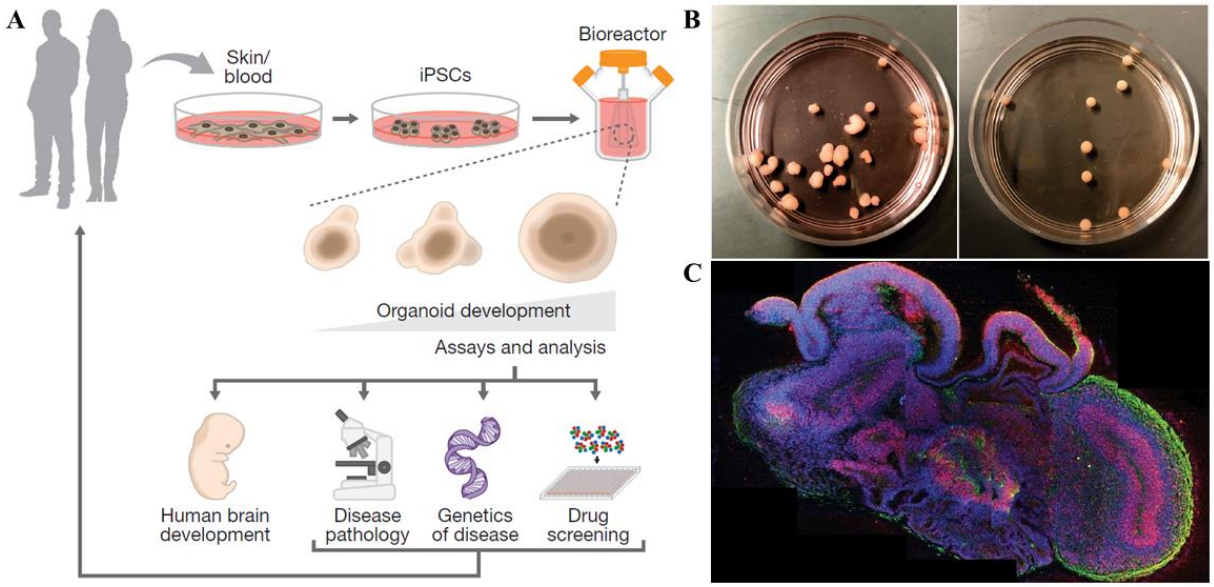

Figure 17: Brain organoids derived from human pluripotent stem cells. A) Brain organoids enable a better understanding of human brain development and of the impact of genetic variation on brain development and function (Arlotta, 2018). B) Culture of whole-brain organoids (left) and dorsally patterned forebrain organoids (right) (Velasco et al., 2019). C) Sectioning and immunohistochemistry of a cerebral organoid (Lancaster et al., 2013).

The brain organoid system is a highly accessible and genetically modifiable model by which to study the gene expression program during human brain development (Koo et al., 2019). Indeed, comprehensive transcriptome comparisons between forebrain organoids and the human fetal cortex at different stages showed that organoid development is reminiscent of fetal human brain development at the transcriptome level (Marton et al., 2019; Qian et al., 2016). Moreover, the profiles of the N6-methyladenosine (m6A) modification on mRNA from forebrain organoids and the human fetal cortex showed significant overlap, suggesting that the epitranscriptome landscape during human brain development is well recapitulated by brain organoids (Yoon et al., 2017a).

Over the last few years, brain organoids derived from hPSCs, especially patient-derived iPSCs, have been widely used to model and investigate neurodevelopmental brain disorders (Arlotta, 2018; Chen et al., 2018; Di Matteo et al., 2020; Klaus et al., 2019; Kyrousi and Cappello, 2020). The mechanisms of such disorders are frequently attributed to disrupted progenitor cell regulation, including premature differentiation, reduced proliferation, and cell cycle disruption, all of which can be analyzed reliably in brain organoids.

Brain organoids have also attracted great interest as neurodegenerative disease models, but attempts so far have had limited success (Arber et al., 2017; Gonzalez et al., 2018). Because

most neurodegenerative diseases are late onset and age related, brain organoids mimicking embryonic brain development may not robustly reproduce disease-relevant endophenotypes.
Brain organoids have been used also in cancer studies: they provide an accessible, scalable, and easily manipulable system to understand the progression and the resistance of cancer and to screen anti-cancer drugs with patient-derived samples (Hubert et al., 2016; Linkous et al., 2019).
These so promising model, however, suffer from several limitations. Firstly, they are extremely variable in size and shape. In addition, as the composition of Matrigel is not completely understood, many organoids that involve the use of Matrigel appear to be unstable and suffer from batch to batch inconsistency. This in turn restricts their use in high throughput screenings. Moreover, necrosis has been observed in most studies due to insufficient nutrient/oxygen exchange in the center of these structures. Thus, proper vascularization that integrates capillary networks into the organoid structures may be necessary to facilitate gas and nutrient exchange (Zhuang et al., 2018).

3.2.3 Challenges of 3D cellular models

Although 3D cellular models faithfully recapitulate a number of key features of the human brain, they are not perfect replica, and several biological and technical challenges need to be overcome in order to greatly expand our ability to investigate human brain development and disorders.

3.2.2.1 Biological challenges

The design and creation of these complex 3D cellular systems is not a simple process, and different biological limitations hinder the formation of an "ideal" model.
The small size of current 3D models remains the fundamental limiting factor that prohibits from using them to fully recapitulate late stages of human brain development. Because of the lack of vascular cells and so of a circulation system with blood vessels, the viable thickness is restricted by the physical distance over which oxygen and nutrients can diffuse from the surface, which is typically less than 400 μm (Rambani et al., 2009). When culturing occurs over a long period, a substantial number of cells undergo apoptosis. Moreover, because neural progenitor cells (NPCs) with high metabolic demands are often located in the most interior part of the cortical structures, they are the first to succumb to the diffusion limit, and neurogenesis cannot be sustained in long-term cultures. The formation of a cortical plate with six distinct layers and cortical folding is therefore still out of reach (Qian et al., 2019). Methods to create a more

permissive environment to alleviate this condition include the use of spinning bioreactors or orbital shakers to enhance diffusion (Kadoshima et al., 2013; Lancaster et al., 2017; Qian et al., 2016). Recently, a blood vessel organoid was successfully generated from human PSCs, containing endothelial cells and pericytes that self-assemble into capillary networks. Human blood vessel organoids can be transplanted into mice to form a stable, perfused vascular tree, including arteries, arterioles and venules (Wimmer et al., 2019). In the future, human brain organoid technology could be combined together with a blood vessel organoid to establish a functional closed circulation system, to support long-term culture and to study neurovascular interactions. Another promising approach for long-term culture is the transplantation of organoids into animals, allowing the host vasculature to grow into the organoid graft (Mansour et al., 2018). Alternatively, the incorporation of biomaterials and microfluidic systems could be used to engineer vascular-like networks with perfusion to supply the organoid interior with adequate oxygen and nutrients (Qian et al., 2019).

Another important biological challenge is the differentiation into various cell types: the brain consists of so many different cell types (different kind of neurons, astrocytes, oligodendrocytes, microglia, pericytes, and endothelial cells) that need to be present in precise ratio and have substantial cell–cell interactions to reach organ functionality (Pamies et al., 2014).

In addition, variability, consistency and reproducibility in cell types should be considered carefully to perform fine quantitative studies and large-scale unbiased screening. Over the last few years, researchers have been working on protocols for 3D cultures with minimal variability, mainly focusing on homogenizing morphologies. By using single cell RNA-seq, a study of Yoon et al. highlighted that multiple human cortical spheroids showed similar cell-type composition and proportions (Yoon et al., 2019). In the same year, single-cell RNA-seq analysis revealed that dorsal forebrain organoids derived from different stem cell lines showed consistent cell-type composition after three months or six months. The developmental trajectories of cells in different batches of organoids were also consistent and reproducible, and dorsal organoids had transcriptomic profile similar to that of a human fetal cortex (Velasco et al., 2019).

Lastly, the fact that 3D cellular models dynamically mimic the temporal progression of human brain development is both an advantage and a disadvantage for researchers. On the one hand, 3D cellular systems of different ages recapitulate their corresponding *in vivo* counterparts, offering researchers a versatile platform to probe different developmental stages. On the other hand, from a practical point of view, these models take a long time to grow and mature, raising the cost and hindering the efficiency of experiments (Qian et al., 2019). Methods for speeding

up the maturation process, or to parallel the growth of organoids in a highly reproducible way, thus need to be advanced.

3.2.2.2 Technological challenges

The routine experimental use of 3D brain tissue models remains largely unpractical also because of several technological limitations.

First of all, 3D brain models are more difficult to evaluate than traditional monolayer cultures, which are normally more easily accessible. Studies are largely confined to cell morphology assessments, and barely extend to the evaluation of physiological functions of cells. Available biosensing technologies, developed for 2D cultures, are not yet adapted for the routine monitoring of biosignals such as neural activity or physiological paramters inside individual 3D models. This hinders studies aiming towards a better understanding of the emergence of spontaneous neural activity in these models as well as the optimization of culture methods and protocols to reliably generate electrically active brain-tissue models for functional assays.

Current functional analysis of 3D models most commonly relies on optical technologies, such as calcium imaging, as overall screening technique of the tissue functionality (Aleksandra et al., 2014). However, these approaches are limited to measures on the superficial outer layer of the sample, without the possibility to resolve in detail the 3D network dynamics, and are subject to alignment issues, which makes them unpractical to study large number of samples. Electrophysiology techniques so far used to study 3D models function are patch-clamp and multielectrode arrays (MEAs) recording. Patch-clamp has been used to address the presence of Na^+ and K^+ currents involved in action potential dynamics, the firing properties of neurons, as well as to address the presence of excitatory and inhibitory synaptic activity (Birey et al., 2017; Sakaguchi et al., 2015; Trujillo et al., 2019; Xu et al., 2016; Logan et al., 2010). In this regard, however, the available information remains qualitative, whereas a quantitative analysis as well as a direct comparison with the native brain structure of reference is yet to be completed.

Similarly as 2D neural cultures, 3D cultures can grow on top of biosensing devices, such as MEAs for multisite extracellular electrophysiology with planar or protruding electrode morphologies. These devices comprise passive MEAs with a few tens of individually electrically wired microelectrodes, as well as more recent generations of monolithic active multielectrode arrays realized in complementary metal-oxide semiconductor technology (CMOS-MEAs) with on-chip front-end and multiplexing circuits to continuously monitor extracellular neural activity from several thousands of closely spaced microelectrodes (Heer et al., 2004; Frey et al., 2007; Berdondini et al., 2001; Berdondini et al., 2009). MEA recording

not only allows detailed network dynamics studies of the 3D tissue, but it also enables a direct comparison with the human brain electrical patterns (Trujillo et al., 2019; Fair et al., 2020). However, this approach requires that each 3D cell culture model grows on a dedicated biosensing device, thus challenging the development of low-cost consumable biosensing chips and constraining sample number. Another technical limitation of such tool is in achieving a good electrical contact between the electrodes and the tissue, as the latter does not offer a flat surface that can optimally adhere to the planar MEA substrate. To overcome this issue, two main approaches may be considered: sample processing and recording device. In terms of sample processing, one strategy consists of letting the intact tissue sit on the MEA, previously coated with adhesion-promoting molecules typically used in neuronal culture and that have no interference with recording capabilities (poly-(d)-lysine, poly(l)-ornithine, laminin) (Amin et al., 2016). However, such procedure could induce cell spreading and organoid disaggregation, and the recorded signal might as well represent the result of a secondary 2D network activity established upon guidance by the coating biomolecule. The other strategy could consist of slicing the tissue to obtain thin (200-300 µm) sections. In this way, it is possible to get access to the inner tissue layers and bypass its surface, which most frequently contains not electrically active stem cells (Qian et al., 2020). The negative aspect of this approach is that it does not preserve the original 3D circuitry in full, whereas, ideally, electrophysiological measurements should be performed on the intact tissue assembly in order to obtain a global picture of its network dynamics. In terms of recording devices for organoids, silicon array probes inserted directly into the intact tissue sample have been successfully employed to overcome the technical limitations posed by planar MEA (Quadrato et al., 2017). Silicon probes enable recording local field potentials, as well as single- and multi-unit activity, with the added advantage of enabling a depth electrophysiology profile of the bioengineered brain tissue. The invasiveness of these implantable devices and consequent tissue-damage, however, leads to low yield electrical read-outs and restricts measures to acute (non-chronic) experimental conditions.

In the light of the limitation of current technologies, a promising alternative approach to overcome these issues consists in the development of bio-artificial 3D brain model systems with seamless tissue-integrated biosensing artificial microdevices, without perturbing 3D model in terms of development, morphology, composition and functionality. Optically-interfaced self-standing microscopic silicon particle devices internalized in cells (Gomez-Martinez et al., 2010) or even in embryos (Fernandez-Rosas et al., 2010) were proposed. These micrometric intracellular devices were demonstrated for tasks such as cell tracking using a barcode system (Fernandez-Rosas et al., 2009), intracellular pressure sensing (Gomez-Martinez

et al., 2013) or to implement multistage delivery systems (Tasciotti et al., 2019). However, because of alignment and light scattering issues, the functional performances of these very small area optically-interfaced devices were demonstrated so far only on isolated cells or 2D cell cultures.

On the other hand, a new class of extracellular tissue-integrated microdevices might be developed by exploiting recent achievements in the massive downscaling of free-floating microelectronic independent biosensor nodes down to 10-100 μm in size (Angotzi et al., 2019). Such extracellular CMOS-based microdevices, or "neural dusts", would allow label-free routine electrophysiological measures from the inside of each self-standing 3D model, such as spheroids or complex brain organoids. So far, neural dusts were proposed for stable chronic brain machine interfaces in vivo and are meant to communicate neural data back to an interrogator by modulating the amplitude, frequency, and/or phase of an incoming ultrasound wave (Neely et al., 2018; Seo et al., 2013). Early proof-of-concepts report electroneurograms (ENG) obtained with a single neural dust mote anchored to the sciatic nerve of an anesthetized rat (Seo et al., 2016). Other studies used commercial radio frequency identification (RFID) chips of 460 x 480 μm2 in size integrated into re-aggregated iPSC-derived endoderm spheroids to demonstrate phenotypic screenings of a pool of RFID-modified organoids (Kimura et al., 2018). Finally, McDonald et al., with inspiration from implantable mesh electronics and growth of organoids on polymer scaffolds, proposed the fabrication of suspended hammock-like mesh microelectrode arrays for neural organoids (McDonald et al., 2020).

Recently, at IIT we proposed a circuit architecture for large-scale radiofrequency (RF) based, low-power active CMOS microdevices (100 x 100 μm^2) providing integrated circuits for extracellular sensing of neural activity in organoids (Angotzi et al., 2018). While bioelectronic and wireless technologies to realize such microdevices are under study, to date there is very little information on how to integrate extracellular Si microchips into neuronal 3D cell aggregates. Further, the potential impact of extracellular Si microdevices on cell viability, 3D construct morphology and network functionality is still unexplored.

3.3 Aim

Three-dimensional (3D) neural cell assemblies are rapidly emerging as more comprehensive *in vitro* model systems of the brain tissue to study neurological diseases and for next-generation screening assays in drug-discovery. However, despite remarkable recent progresses, establishing and applying such models is hindered by the lack of technologies to chronically monitor the activity of neural aggregates in three dimensions.

A promising new approach consists in self-standing biosensing microdevices capable of achieving seamless tissue integration during cell aggregation and *in vitro* culture.

Recently, we proposed a circuit architecture for large-scale radiofrequency (RF) based, low-power active complementary metal-oxide semiconductor (CMOS) microdevices (100x100x50µm^3) providing integrated circuits for extracellular sensing of neural activity in organoids (Angotzi et al., 2018) (Figure 18). These dimensions were chosen so that microdevices would be smaller than a typical rat cortical spheroid (typically 200-300 µm in diameter at 21 days *in vitro* (Dingle et al., 2015)), yet large enough to integrate all the required circuits for wireless biosensing (Angotzi et al., 2018; Burke et al., 2010; Seo et al., 2015).

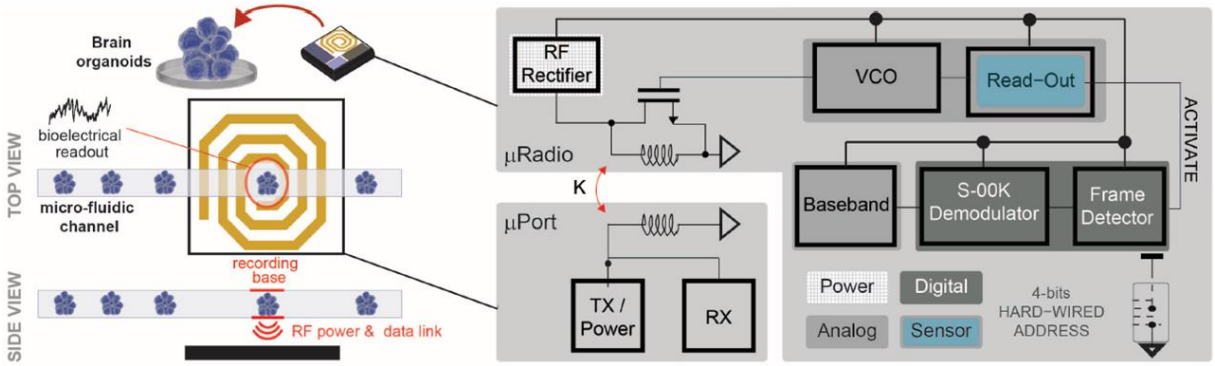

Figure 18: Perspective of the developing technology. Functional description of a prototypical lab-on-chip platform application in which bionic organoids are individually guided along a micro-fluidic channel toward a recording base integrating a µPort device for RF wireless powering and data readout from µRadios fused into 3D human brain organoids (left); block diagram of the µPort and of the CMOS µRadio devices (right). This image was adopted from Angotzi et al., 2018.

While bioelectronic and wireless technologies to realize such microdevices are under study, to date there is very little information on how to integrate extracellular Si microchips into neuronal 3D cell aggregates. Further, the potential effects of aggregating artificial Si microdevices with cells on cell viability, 3D morphology and network functionality are still unexplored.

To address these questions, in this work I contributed to this development by investigating the 3D assembling of neurons with microfabricated Si sham devices, and the growth of bio-artificial hybrid spheroids from rat primary cortical neurons.

3.4 Materials and methods

3.4.1 Silicon microchip fabrication

The fabrication of Si microchips requires standard microelectronic processes (Figure 19A). First, squares of 100 x 100 µm² of 100 nm sputtered aluminum were patterned via lift-off (Microchem S1813 photoresist) onto an N-type 50µm silicon wafer (Si-Mat) and acted as a mask for the silicon etching step (Figure 19A-1). The thin silicon wafer was then transferred onto a thicker substrate by means of a dissolvable glue (Xtal bond SPI 555, Figure 19A-2). A standard Bosch process at 5°C allowed to etch through the 50 µm-thick wafer (ICP-RIE Si 500, SE Tech instruments) (Figure 19A-3).

3.4.2 Silicon microchip surface modifications

3.4.2.1 (3-aminopropyl)triethoxysilane (APTES)

Following this step, both SiO_2 (10 nm) and (3-aminopropyl)triethoxysilane (APTES, 40 cycles, dose 30") were deposited through atomic layer deposition (FlexAL, Oxford Instruments) onto the substrate (Figure 19A-4). Finally, the microchips were released in deionized water in a glass vial. To avoid having molten glue residues in the vial, the deionized water was cold (4°C) and a gentle ultrasound was applied on the vial for a few seconds to completely release the small silicon microchips into the vial (Figure 19A-5). The microchips were then rinsed twice in deionized water before being sterilized under hood UV for 1 hour (Figure 19A-6).

3.4.2.2 Protein coatings

For each trial, the microchips were separated in different sterile vials. For protein immobilization, water was replaced with either 800µl of poly-DL-ornithine (0.1 mg ml^{-1}, Sigma P0671), poly-D-lysine (0.1 mg ml^{-1}, Sigma P6407) or Matrigel (0.5%, Corning 354230), and incubated overnight at 37°C and 5% CO_2. The next day, the vials were rinsed three times with sterile Milli-Q water. In the end, one vial per condition was obtained: microchips without coating (No coat.), microchips with Matrigel coating (MG), microchips with PDL coating (PDL) and microchips with PDLO coating (PDLO).

3.4.3 Characterization of the coating-induced wettability

To characterize surface wettability and their stability over time, water droplet contact angle measurements were performed onto macro pieces of silicon using Dataphysics OCAH200

contact angle instrument equipped with a 2/3'' CCD Chip camera. Four inches silicon wafers type N 500µm were cleaned in piranha for 2 min (1:3 H_2SO_4:H_2O_2, Sigma Aldrich), then subjected to the same surface modifications as described above. The wafers were then cut in 8 and kept in dry box. For each time point, one piece for each condition was retrieved, blown under nitrogen flow and 5 contact angle measurements were made using 5µL droplets of deionized water.

3.4.4 Spheroids formation

All animal procedures carried out in this work were approved by the institutional IIT Ethics Committee and by the Italian Ministry of Health and Animal Care (Authorization No. 110/2014-PR of the 19th of December 2014).

Primary neuronal spheroids were established from cerebral cortices of Embryonic day 18 (E18) Sprague–Dawley rats and maintained at 37°C in a humidified atmosphere of 5% CO_2. The following solutions and media were used: Hanks Balanced Salt Solution (HBSS) (Sigma H6648); digestion solution − Trypsin (0.125%, Thermo Fisher Scientific 25050014) in HBSS + DNase (0.25 mg ml^{-1}, Sigma D5025) in HBSS 5mM $CaCl_2$; complete Neurobasal medium (NB, Thermo Fisher Scientific 21103049) supplemented with B27 (2%, Thermo Fisher Scientific 17504044), Glutamax (1%, Thermo Fisher Scientific 35050038) and Penicillin/Streptomycin (1%, Sigma P4333); FBS (Sigma F7524). Briefly, embryos were removed and decapitated, brains were extracted from the skulls and placed in cold HBSS. After dissection, cortices were placed in the digestion solution and incubated in water bath at 37°C for 30 minutes. Few milliliters of complete NB + FBS (10%) were added to the cell solution, centrifuged at 1200 rpm for 5 min, and the supernatant was removed. The cell pellet was resuspended in fresh complete NB + FBS (10%) and gently pipetted for no more than 10 times with P1000 pipette. The solution was filtered with a cell strainer (Biologix 15-1040, 40µm pore size), centrifuged at 700 rpm for 7 min, and the supernatant was removed. The cell pellet was resuspended in complete NB. Cell viability at the time of isolation was determined by a Trypan Blue Exclusion Assay (Sigma T8154). Cortical cells were then seeded at a density of 6500 cells in 75µL medium in ultra-low attachment plates (GravityTRAP ULA plate 96-wells). In order to avoid bubbles in the wells, first 25µL of warm NB was plated in the wells, then the plate was centrifuged at 250g for 2 minutes, before adding 6500 cells in 50µL in each well. Following cell plating, silicon microchips were seeded by carefully pipetting 1µL of water in each glass vial, visually inspecting that it contained only one device, before plating it one by one in the wells. For each condition (control, µchip with and without protein), a minimum of 24 wells

were plated. Device-less wells were re-plated after inspection. After a few hours, the plates were centrifuged at 250g for 2 minutes before being kept in incubator for 21 days. At DIV 5, 10, 14 and 19, the medium was partially replaced with 30µL of fresh complete NB.

3.4.5 Morphology assessment

3.4.5.1 Optical microscopy

At DIV 3, 5, 7 10, 14, 17 and 21, plates were retrieved from the incubator and images were taken from all wells using a Leica DMI 6000 B inverted microscope with a x10 objective. At each time point, the circularity of the spheroids, its area therefore its mean radius and the distance between the center of the device compared to the centroid of the spheroid were measured using ImageJ software (Schneider et al., 2012). Contaminated wells, dirty wells (residues) and wells containing more than 1 device, were not taken into account in the morphology assessment. They represented approximately 8-15% of all wells. Besides, at early time points, wells containing more than one single spheroid were also excluded. Overall, between 13 and 23 wells were considered at each time point for each condition and each trial (3 distinct trials, at different time during the year and with distinct animal dissection).

3.4.5.2 Scanning electron microscopy (SEM)

At DIV5, 10, 14, 17 and 21, six spheroids per condition (Ctrl, No Coat., MG, PDL, PDLO) were fixed in paraformaldehyde (PFA, 2% v/v, Santa Cruz Biotechnology 30525-89-4) and glutaraldehyde (GA, 2% v/v, Sigma G5882) in phosphate-buffered saline (PBS) (Thermo Fisher Scientific 10010056) for 2 hours, followed by three washes in PBS. The samples were post-fixed in osmium tetroxide (1%) in Milli-Q water for 2h and washed with Milli-Q water. The spheroids were subsequently dehydrated with a series of 10min incubations in rising concentrations of ethanol in water solutions (from 30% to 100%), 1:1 ethanol:hexamethyldisilazane (HMDS, Sigma-Aldrich) and HMDS (100%) and dried overnight in air. Finally, the samples were sputtered with Au (10 nm) and analyzed by SEM (FEI NanoLab 600 dual beam system).

3.4.5.3 Immunofluorescence imaging and analysis

At DIV5 and DIV21, a few spheroids from each condition were fixed in PFA (2%) and GA (2%) (see previous section). All the following steps were performed on a shaker at 4°C. The following antibodies were used: mouse anti-tubulin β3 (BioLegend 801213, 1:50), rabbit anti-glial fibrillary acidic protein (GFAP, DAKO Z0334, 1:250), Alexa488 goat anti-rabbit

(Invitrogen A11034, 1:200) and Alexa647 goat anti-mouse (Invitrogen A21236, 1:200). Spheroids were permeabilized and blocked with Triton X-100 (TX, 1%, Sigma T9284), normal goat serum (NGS, 10%, Sigma G9023), and bovine serum albumin (BSA, 4%, Sigma A9647) in PBS (B-PBT) for 2h, and subsequently incubated in primary antibodies diluted in B-PBT overnight. Spheroids underwent two 2-h washes with TX (0.2%) in PBS (PBT), followed by one 2-h B-PBT wash. Spheroids were incubated with secondary antibodies in B-PBT overnight. Spheroids underwent two 2-h PBT washes and were incubated with Hoechst (BD Biosciences 561908, 1:300) in PBT for 1 h and returned to PBS. Spheroids were kept in PBS and transferred to glass-bottomed confocal dishes for imaging. All images were acquired with 40x objective lenses using a Leica SP5 inverted confocal microscope (Leica Microsystems). For each condition, the maximum intensity projection of a Z-stack from approximately half spheroid (from the bottom to the maximum diameter) is displayed.

3.4.6 Neural activity assessment

Calcium dye Fluo-4 AM (ThermoFisher 14201) was reconstituted in Dimethyl Sulfoxide (DMSO) according to manufacturer's instructions. Spheroids were incubated with Fluo-4 AM at the final concentration of 2.5 µg ml^{-1} in extracellular saline solution (HEPES 10mM, D-Glucose 5.5mM, NaCl 145mM, KCl 5mM, $CaCl_2$ 2mM, $MgSO_4$ 1mM, pH 7.3-7.4) and incubated at 37°C in the dark for 15 minutes. Spheroids were consequently washed twice in extracellular saline solution and transferred in 300 µl of the latter in a chamber with glass bottom for live imaging. Live imaging was performed with inverted confocal microscope Nikon A1 coupled with a Nikon Objective 20X Plan Apo A.N.0.75 (Nikon Instruments S.p.A.), using a 488nm laser for the green fluorescent dye. The focus plane was made on top of the spheroid, and the pinhole adjusted so that each manually-selected regions of interest (ROI, 5µm in diameter) could be reasonably be associated as the contribution of a single soma in the spheroid. Each recording session lasted 10 minutes and consisted of 8 minutes of unperturbed activity, followed by injection of KCl (2mM) to activate voltage-gated calcium channels and depolarize the cells. Fluorescence intensity from various regions of interest (ROI) was then exported from Nikon imaging software NIS 5.02 (Nikon Instruments S.p.A.) and analyzed with OriginLab. For each ROI, the linear decrease in fluorescent intensity due to bleaching was compensated, and the standard $\frac{\Delta F}{F_0} = \frac{F - F_0}{F_0}$ versus time was plotted, where F_0 represents the mean ROI baseline intensity when no activity is detected, after bleaching compensation. An event is defined by the sudden increase and decrease of fluorescent intensity over 3 times the noise standard deviation; a ROI is defined active if more than 2 events occur during the recording sessions. For each

recorded spheroid, the average number of active ROI on the focus plane considered was counted. Spheroids with less than 3 active ROI or for which the KCl control did not have a depolarization effect, were not considered.

3.4.7 Single-cell analysis by Fluorescence-Activated Cell Sorting (FACS)

Spheroids at DIV28 were desegregated with the Papain Dissociation System (Worthington Biochemical, LK003150) according to the manufacturer's instructions. Briefly, 156 spheroids per condition were pooled in a tube (one tube per condition), washed with PBS and placed in the papain solution (20 units/ml papain, 0.005% DNase). The tube was incubated at 37°C with constant agitation (550 rpm) for 1h. Every 10 minutes, spheroids were triturated with P200 pipette and the solution re-equilibrated with 95% O_2:5% CO_2. After 1h, while the freed devices remained at the bottom of the tube, the single cell suspension was transferred to a new tube and centrifuged at 300g for 5 min at room temperature. The pelleted cells were resuspended in albumin-inhibitor solution with DNase (according to the manufacturer's instructions) and centrifuged at 1200 rpm for 5 min. For FACS analysis, the pelleted cells were fixed in PFA (4%) for 20 min at room temperature, washed and centrifuged at 1200 rpm for 5 min. The pelleted cells were permeabilized with Triton X-100 (0.05%) in PBS for 20 min at room temperature, washed with cold FACS buffer (0.05% Triton X-100 and 0.5% BSA in PBS) and centrifuged at 1200 rpm for 5 min. The pelleted cells were stained with mouse anti-Neuronal Nuclei (NeuN, Alexa Fluor 488 conjugated, Millipore MAB377X, 1:1000) and mouse anti-GFAP (Alexa Fluor 647 conjugated, BD Pharmigen 561470, 1:250) in FACS buffer for 30 min on ice in the dark. Cells were washed, centrifuged at 1200 rpm for 5 min and resuspended in 200µl of FACS buffer. FACS analysis was performed with BD FACSAria™ III cytometer (BD Biosciences), at least 10000 events for each dot plot were acquired and data were analyzed with CellQuest™ software.

3.4.8 Data processing and statistical analysis

Data processing and analysis was performed by considering:

1. Pre-processing of data (e.g., transformation, normalization, evaluation of outliers): For cell culture analysis, wells excluded from the study were: dirty wells (residues, contamination), wells containing more than 1 device, wells containing more than one single spheroid 24h after seeding.
2. Data presentation (e.g., mean ± SD): Droplet contact angle: mean ± SD. Circularity and spheroid radius: mean ± SEM (standard error of the mean).

Internalization degree: mean ± SD. For FACS analysis, percentage of gated events compared to total events is represented.

3. Sample size for each statistical analysis: a) Droplet contact angle: n=5 per surface treatment and per time point. b) Circularity, mean spheroid radius and internalization degree: 3 trials were performed (1 trial = set of 21 DIV-long cultures from 1 sacrificed animal, at different times during the year), with for each trial 24 wells dedicated per surface treatment. Without excluded wells (contaminated etc. see previously), we have n=[13,23] for each data point represented. c) FACS: 1 trial with 156 spheroids per condition and at least 10000 events acquired for each dot plot.

Data analysis was performed using the following softwares: Matlab, OriginLab, CellQuest™ (FACS).

3.5 Results and discussion

3.5.1 Formation of hybrid neurospheroids from spontaneous aggregation of neurons and Si microchips

In this work, we first fabricated silicon dummy microchips (or µchips) to study their aggregation with primary neuronal cells and the growth of bio-artificial hybrid neurospheroids. The fabrication process of these generic Si microchips is depicted in Figure 19A and detailed in the "Materials and Methods" section. This rather simple process includes a single photolithography and a step of deep reactive ion etching (DRIE) of the 50 µm thick Si substrate. It results in the production of approximately 2000 microchips of dimensions 100x100x50 μm^3 per cm^2. Once structured, devices were top-side coated with a layer of silicon dioxide (SiO_2) and of (3-aminopropyl)triethoxysilane (APTES) through atomic layer deposition processes (ALD).

The deposition of SiO_2 underneath ensures that the squares sides, covered in fluorinated residues from the DRIE process, are then well coated with the same material all over the µchips, on which APTES can bond more uniformly. In this way, ALD deposition provides a conformal, repeatable, uniform layer on the silicon µchips surface.

The APTES was shown to stabilize protein immobilization on different substrates, including silicon, silicon dioxide and polydimethylsiloxane (PDMS), which in turn supports adhesion and long-term viability of neuronal and glial cells in cell cultures (Gunda et al., 2014; Kuddannaya et al., 2015). In order to handle microchips for the successive steps, devices were finally released in deionized water and sterilized under hood UV for 1 hour.

To investigate whether surface functionalization of the device can promote aggregation of cells around the microchips, I tested three different adhesion-promoting molecules typically used in neural cultures and that have shown no interference with recording capabilities (Amin et al., 2016), namely Matrigel (MG), Poly-D-lysine (PDL) and Poly-DL-ornithine (PDLO). MG is a solubilized basement membrane matrix, mainly containing extracellular matrix (ECM) components such as laminin, collagen I and entactin (Laplaca et al., 2010), and widely used as a biologically active embedding scaffold suitable for 3D neural cell culture (Lancaster et al., 2013; Meseke et al., 2012; Kunze et al., 2011). PDL and PDLO are also routinely used to promote adhesion and differentiation of primary neurons on glass or Si substrates through an increase of surface charge density (Harnett et al., 2007; Yavin et al., 1974). These three molecules can bind onto the APTES layer, as evidenced by the contact angle measured on clean

SiO_2 surfaces (Figure 19B). The APTES coating on SiO_2 surfaces increases the contact angle from 7.85° to 47.1°, a value in line with APTES deposition from aqueous solutions (Kuddannaya et al., 2015). Matrigel binding increases slightly the surface hydrophobicity to 60.2°, which is to be expected for a gel-like structure while PDL and PDLO significantly decrease the contact angle to 11.2° and 13.6° respectively. As evidenced by the contact angle measured at different times over 28 days (Figure 19C), the presence of amine-terminated silanes after APTES deposition allows for proteins to covalently bind on the surface, which in turn provides a stable interface over time (Cargill et al., 1999; Kim et al., 2011).

This is an important pre-requisite for future applications in organoid development, where cultures are maintained for extended periods (over 9 months) (Quadrato end Arlotta, 2017).

As illustrated in Figure 19D, primary cortical neurons prepared from rats at embryonic day 18 (E18) were seeded in ultra-low attachment 96-well plates and added with single Si microchips in each well. Despite involving different coatings on the devices and steps of manual manipulation of cells and microchips, this protocol reliably yielded bio-artificial 3D neurospheroids (between 78-87% for n=4 trials and over 96 plated wells per trial). As a step forward, production could be automated and scaled up by using pick-and-place and microfluidic techniques.

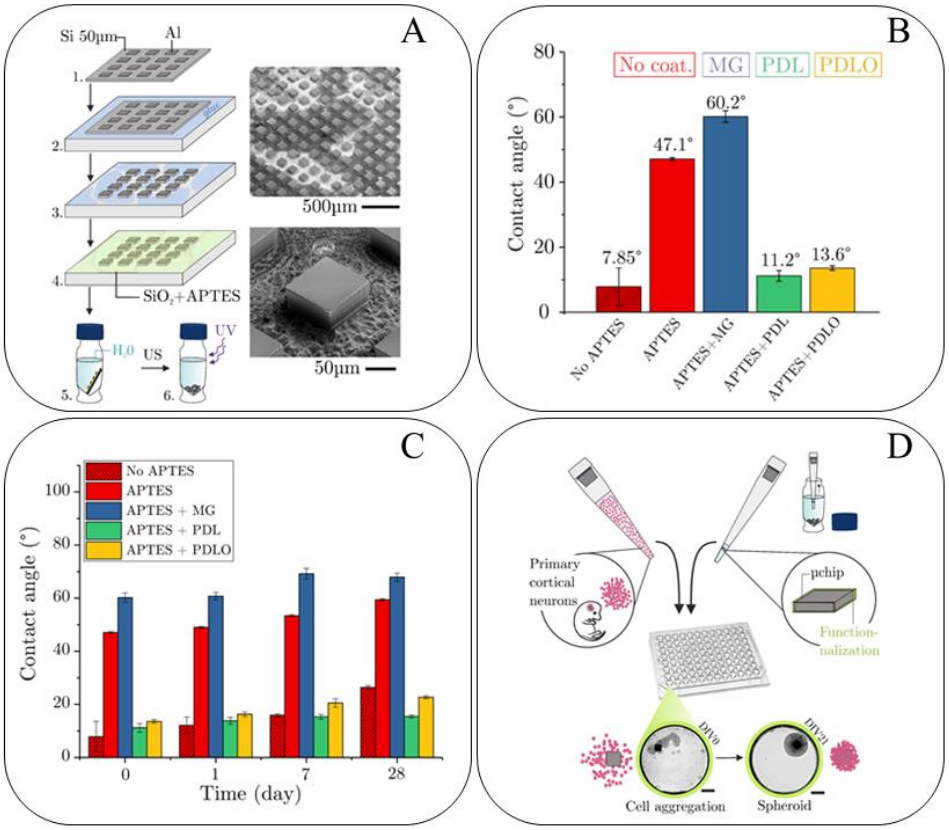

Figure 19: Aggregating bio-artificial hybrid neurospheroids with Si microchips. A. Schematic representation of generic microchip fabrication and SEM images of the realized Si devices. 1) Lift-off

of Al 100nm on an N-type 50µm-thick Si wafer. 2) Transfer of the wafer onto a thicker substrate by means of a water-dissolvable glue. 3) Standard Bosch process etching the whole 50µm-thick Si wafer. 4) ALD deposition of 10nm of SiO_2 and of a layer of APTES. 5) Release of the microchips in deionized water using a US bath and 6) Sterilization under UV light. B. Mean and standard deviation (SD) of contact angle measurements on Si substrates with different coatings (n=5). C. Mean and SD of contact angle measurements on Si substrates with different coatings at different time points. Overall, all protein immobilizations appear stable over time. n=5 per surface treatment and per time point. D. Schematic representation of the aggregating protocol and microscopy images of cells and devices at DIV0 and after the aggregation of a hybrid spheroid at DIV21. Primary cortical neurons from rat embryo were cultured in ultra-low attachment plate along with a 100x100x50µm^3 microchip previously functionalized with adhesion-promoting coatings. Scale bar 200µm.

3.5.2 Morphology of developing hybrid neurospheroids

The morphology of developing neurospheroids aggregated with differently coated microchips was characterized by optical microscopy imaging at multiple time-points and over 21 days of *in vitro* culture (DIV). These results provide an overall initial evaluation of whether the presence of the Si microchip might affect spheroid growth and its roundness. As shown in Figure 20, the quantification of the circularity and the mean radius does not reveal major differences among developing spheroids with and without microchips (see Figure 20C for an example), neither among spheroids integrating microchips with different coatings. Spheroids form and maintain a circular shape (circularity ratio > 0.84 after 3 DIVs) and grow progressively over the course of 3 weeks, reaching a plateau in their mean radius at around 14 DIVs, corresponding to approximately 500 µm in diameter. The dimensional increase observed between 3-14 DIVs (about 200 µm in diameter) is most likely due to an increase of the inter-cellular spacing which mainly results from network formation and astrocyte proliferation (Dingle et al., 2015). Slight inter-trial differences (Figure 21) are most likely due to variations in the ratio of astrocytes and neurons among primary cell culture preparations.

Overall, these results indicate that neither the presence of the microchip nor its functionalization affects the spheroid growth and its roundness, suggesting that the device does not disrupt the general morphology of self-aggregating spheroids.

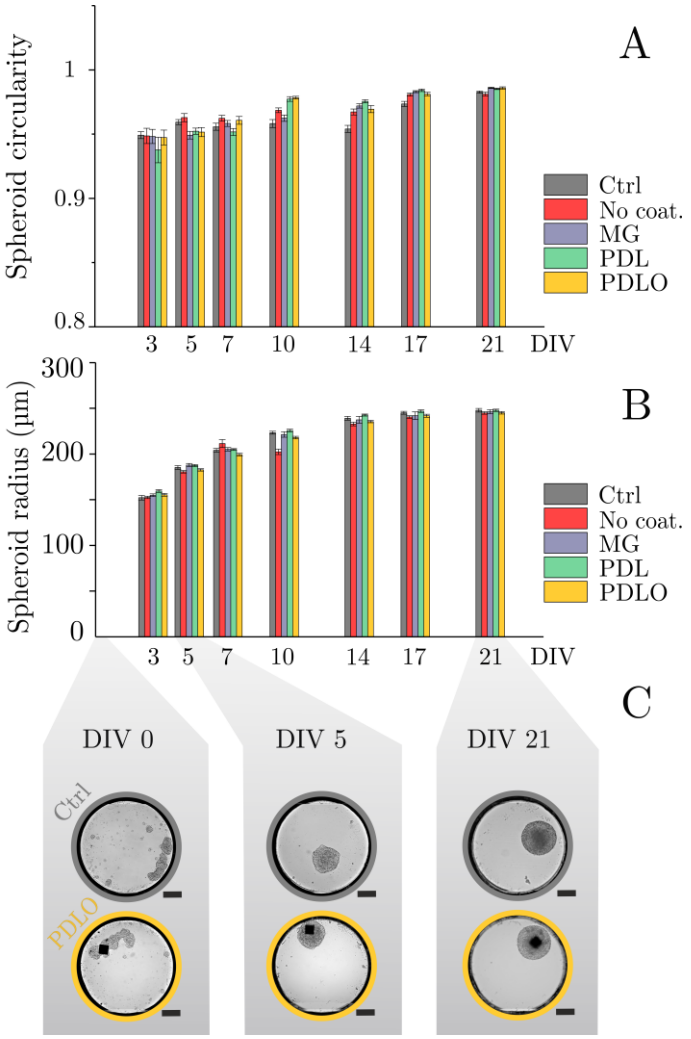

Figure 20: Morphology of bio-artificial hybrid neurospheroids. A. Spheroid circularity (mean ± SEM) and B. spheroid radius (mean ± SEM) of neurospheroids without microchip (Ctrl) or with differently functionalized microchips (No coating, MG, PDL, PDLO) as measured in 2D by optical contrast images. No major difference in the radius and circularity of spheroids is to be noted, neither between conditions with and without microchip, nor between the different coatings used. Depending on condition and time point, n=[13-23]. C. Examples of these optical micrographs showing the aggregation and spheroid formation in the absence and presence of a microchip (in this case, coated with PDLO) at DIV0, DIV5 and DIV21 (scale bar 150µm).

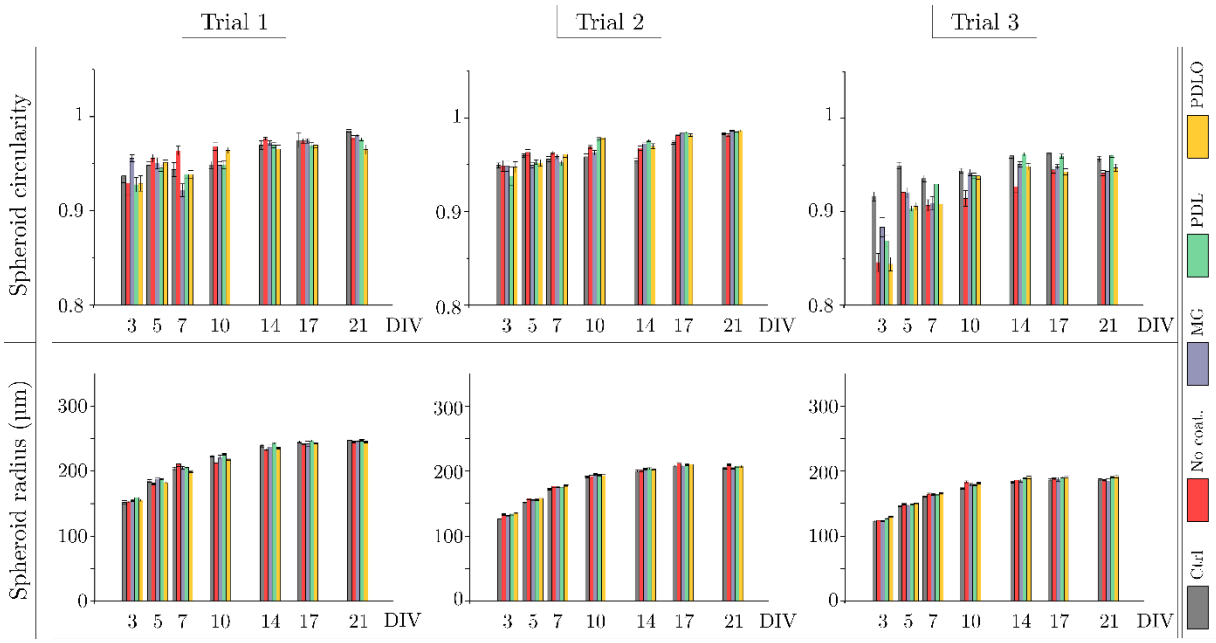

Figure 21: Inter-trial variability of neurospheroids circularity and radius. Both the circularity and the radius (mean+SEM) of neurospheroids without (Ctrl) and with microchip (No coating, MG, PDL, PDLO) are represented at different time points from DIV3 to DIV21. The size of spheroids varies from one trial to another throughout the time points, suggesting that the difference in spheroids dimensions results more from a difference in the number of cells plated (errors in cell counting, diverse proportion of astrocytes between neuronal preparations), than the speed of growth of the spheroids. Besides, from DIV7 on, all spheroids have a circularity above 0.9 for all conditions, approaching an ideal sphere as time goes. Depending on condition and time point, n=[13-23].

3.5.3 Surface functionalization of Si microchip determines its location inside neurospheroids

To investigate the extent of the Si microchip integration in the forming neurospheroid, optical microscopy imaging of the wells was used over 3 weeks. To quantify this integration, we defined a parameter, the internalization degree (ID), corresponding to the ratio between the distance from the spheroid center to the microchip center $D_{sph-to-\mu chip}$, and the radius of the spheroid r_{sph} (Figure 22):

$$ID\ (\%) = \frac{D_{sph-to-\mu chip}}{r_{sph}} x\ 100$$

An ID between 0 and 75% corresponds to the case where the microchip is located in the center of the spheroid; an ID between 75% and 125% to the case where the microchip is located in the periphery of the spheroid; while an ID above 125% indicates that the microchip is not integrated in the spheroid.

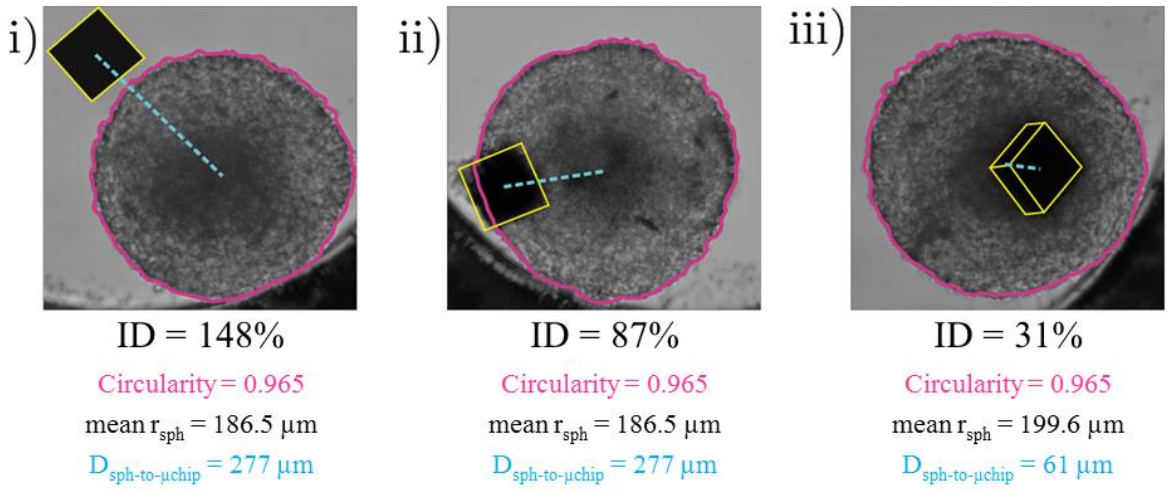

Figure 22: Phase-contrast analysis of neurospheroids with different levels of microchip integration. Three examples of phase-contrast image analysis taken at DIV21, in the case of an internalization degree (ID) of the microchip of i) 148% ii) 87% and iii)31%, corresponding to a microchip outside the spheroid, on the periphery and inside the spheroid, respectively.

In Figure 23 I report the internalization degree quantified for each condition (No coat., MG, PDL and PDLO) in the case of one representative experimental trial (see Figure 24 for all other trials). Results show a marked difference in the microchip integration depending on the functionalization used. Microchips without any coating (red) tend to remain on the surface of the spheroid and in some cases (between 12% and 33%, all trials and all time points included) they are not even in contact with the spheroid. This suggests the presence of a weak adhesion of the microchip that might have detached upon handling of the multiwell plate. In the case of Matrigel coating (blue), the majority of microchips, particularly from DIV14 to DIV21, is integrated in the inner part of the periphery of the spheroids, suggesting a much stronger interaction between cells and microchips. Finally, in the case of PDL and PDLO (green and yellow, respectively), the vast majority (between 65 and 100%, for all trials and all time points) of the microchips is instead internalized inside the spheroid.

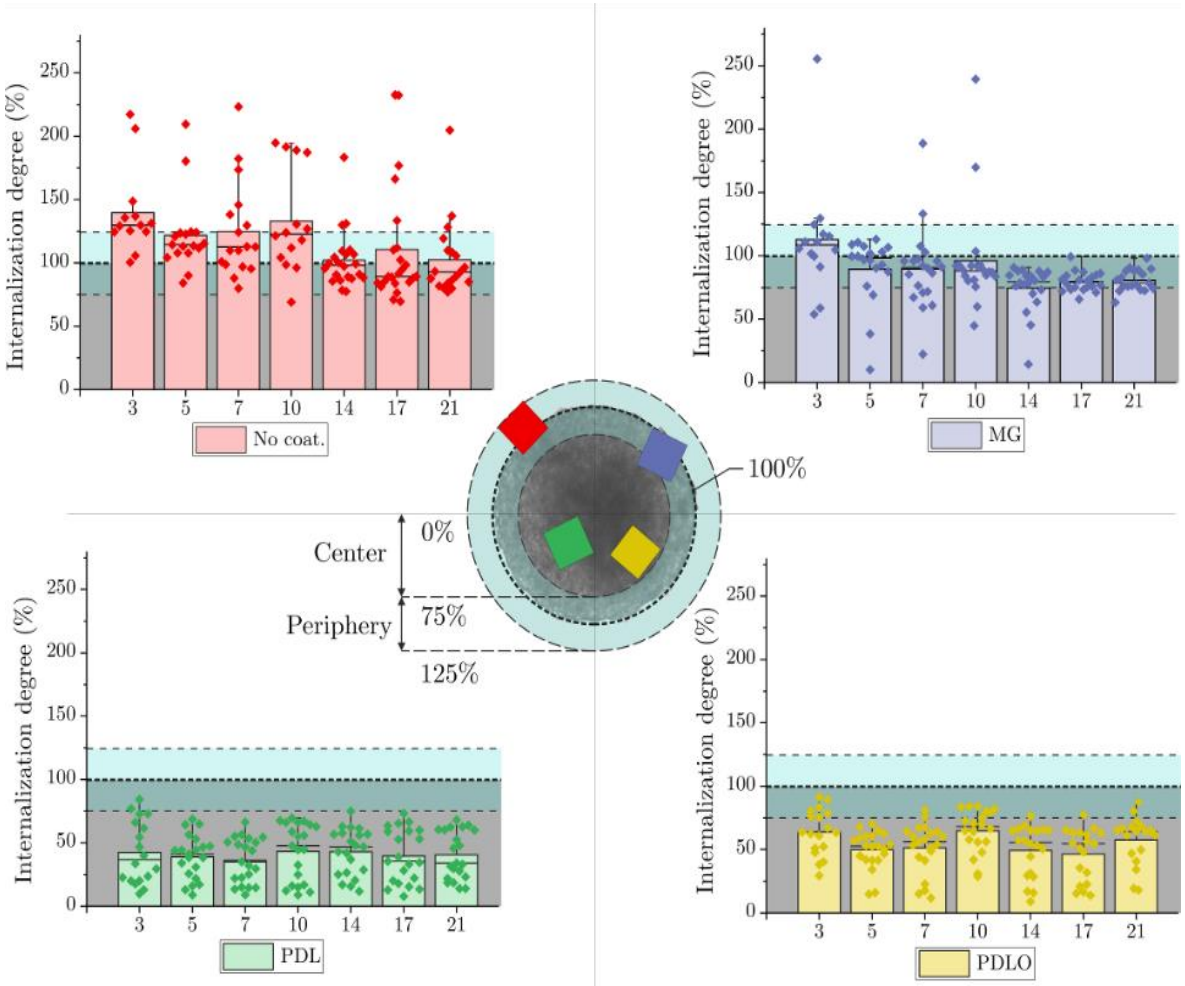

Figure 23: Internalization degree of the microchip inside neurospheroids. The ID (mean ± SD) is defined here as the inclusion ratio between the distance center-of-spheroid to center-of-microchip and the corresponding spheroid radius. As such, a microchip on the external part of the spheroid would have an ID of 75-125%, while a microchip in the spheroid center is represented with an ID close to 0%. Data points are represented for different surface functionalizations during 21 DIVs. Depending on condition and time point, n=[13-23].

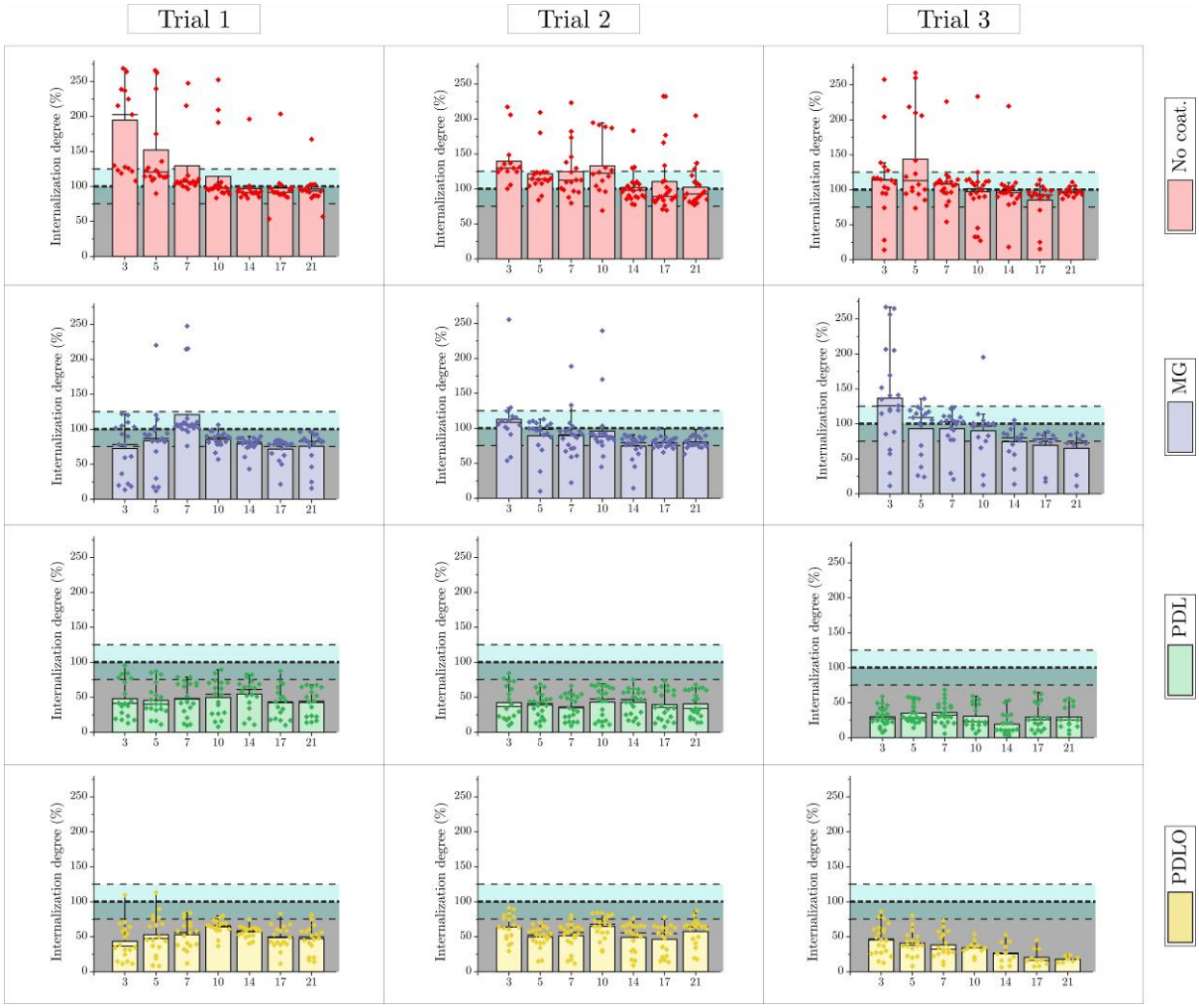

Figure 24: Inter-trial variability of the internalization degree. ID (mean ± SD) of microchips without (no coat) and with functionalization (MG, PDL, PDLO) into neurospheroids is represented. Overall, the different trials show very similar trends. Without coating, the microchip remains on the periphery of the spheroids or is not in contact with the spheroid in the well. With Matrigel coating, the majority of the microchips remain on the periphery of the spheroid, but as time goes, get internalized a little more, suggesting a highest coupling between the cells and the microchip. With PDL and PDLO, the microchip is internalized from early time points on, with an ID generally below 75%. Data points are represented. Depending on condition and time point, n=[13-23].

These results reveal the important role of the surface chemical properties of the microchips for the 3D assembling and growth of bio-artificial hybrid neural constructs. Since these results were obtained by quantifying parameters computed from the planar projection of the 3D spheroid in the well, I qualitatively verified them by scanning electron microscopy (SEM), which allows direct 3D visualization of the spheroids with microchips. Figure 25 displays representative examples of spheroids at different developmental time points for different functionalization conditions. These 3D micrographs confirm optical imaging results on the different levels of microchip integration depending on the surface functionalization. In particular, uncoated Si

microchips remain on the external surface of the spheroid, with a few neurites holding the device in place. This leads to a weak integration of the microchip into the spheroids and to a high number of devices detaching from the spheroid. Matrigel-coated microchips remain on the periphery of the spheroid, but exhibit more neurites that keep the device in place, which in turn supports a stronger interaction. Finally, for PDL and PDLO conditions, SEM images display much more neurite growth on the microchip at early time points and a higher level of microchip integration: at 21 DIV it is barely possible to distinguish the presence of the device in the neurospheroid.

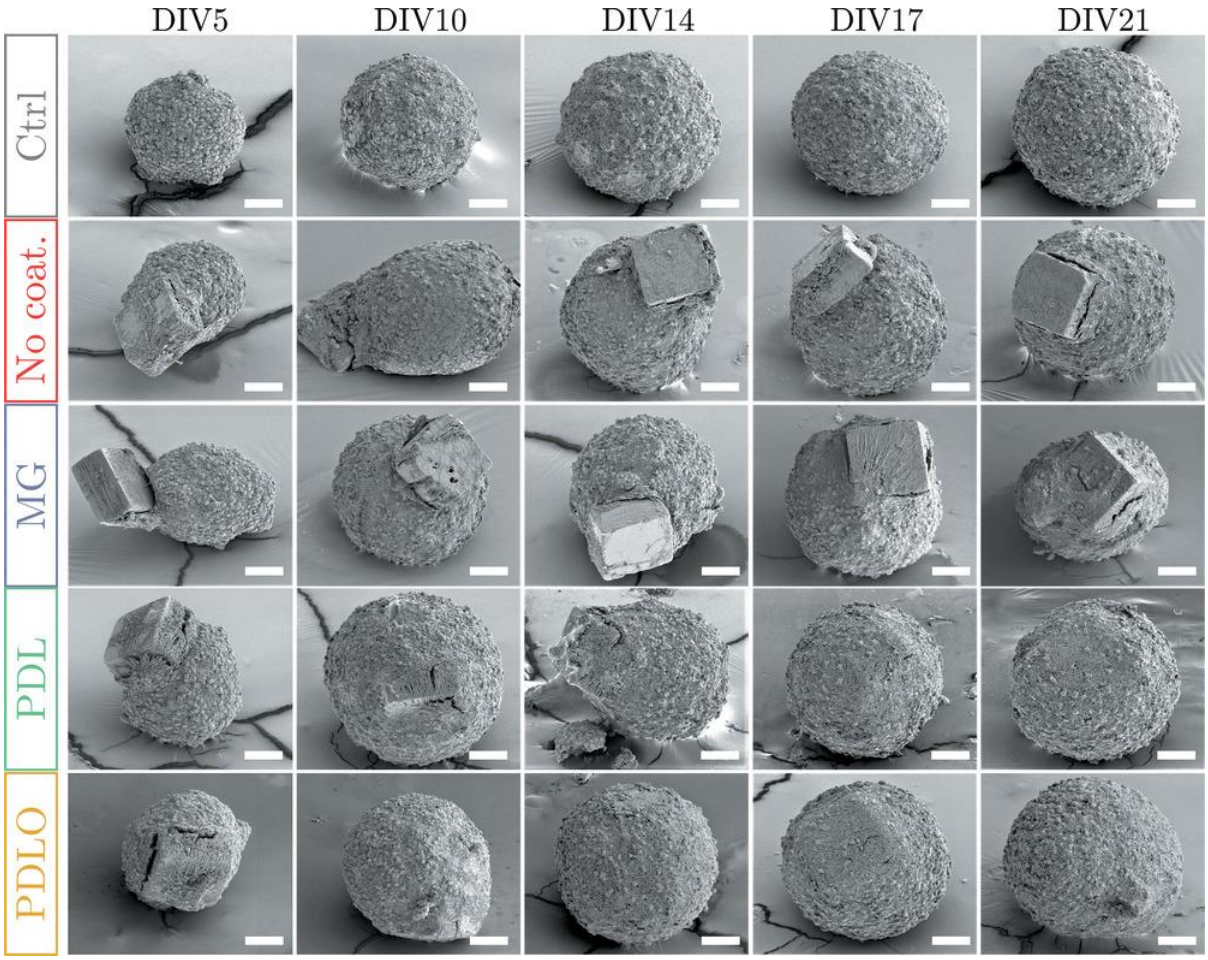

Figure 25: 3D inclusion of microchip in neurospheroids. SEM micrographs of fixed neurospheroids taken at different time points, without microchip (Ctrl) and with microchip, depending on the protein used on the microchip surface (No coating, MG, PDL and PDLO). When the microchip is either not coated (APTES) or coated with Matrigel (MG), it remains on the periphery of the spheroid, while as time goes, the spheroid englobes the microchip when the latter is coated with either PDL or PDLO. Scale bar 50µm.

These results indicate that surface functionalization allows to control the assembly of 3D bio-artificial neuronal constructs with different levels of in-tissue integrated self-standing micro-devices. Controlling the microdevice position in the 3D neural aggregate is particularly relevant for brain organoids. For instance, a microdevice with pH sensing capabilities internalized in the center of brain organoid would allow routinely monitoring the diffusion of nutrients and oxygen to detect the formation of a necrotic core, which in turn would provide crucial information to optimize organoid cultures efficiency (Jorfi et al., 2018). Besides, being able to control the placement of microdevices at different locations inside organoids would provide access to different cellular layers to routinely monitor neural activity or the chemical microenvironment, thus overcoming limitations of current imaging techniques for high-throughput read-outs.

3.5.4 Neuronal and astrocytic cell composition of hybrid neurospheroids

Using immunofluorescence analysis of neuronal and glial markers, I further investigated whether the presence of Si microchips might affect spheroids cellular composition. Neurospheroids at DIV5 and DIV21 from each condition were fixed, stained and analyzed through confocal microscopy (Figure 26). At DIV5, spheroids exhibit globular patterns of β-III-tubulin neuronal staining (red), and fewer GFAP-positive (Glial Fibrillary Acidic Protein) astrocytes (green), while cells are highly packed in the structure, as evidenced by Hoechst staining (blue). At DIV21, both neurons and astrocytes express more elongated neurites, bundles, and form a complex network, while the distance between nuclei increases under the effect of astrocyte proliferation and neurite extension complexity. No evident difference is observed in the composition and maturation of the network with respect to the presence of the microchip, independently of the coating used. These qualitative imaging data suggest that the Si microchip does not alter astrocyte proliferation, neurite branching nor the overall development of 3D neural constructs. As already observed, the position of the microchip highly depends on the coating used. Without adhesion-promoting protein (No coat.), the microchip remains on the periphery of the spheroid, with few neuronal branching keeping the microchip in place, and actually often losing it (9 times out of 10 the microchip is lost during the immunostaining process). With Matrigel (MG), the microchip remains on the periphery but is much more well-retained by both neuron and astrocyte branching. For both PDL and PDLO, the microchip is covered by dendrites as early at DIV5, and cell nuclei eventually migrate over the microchip, even giving at times the illusion that the microchip is absent.

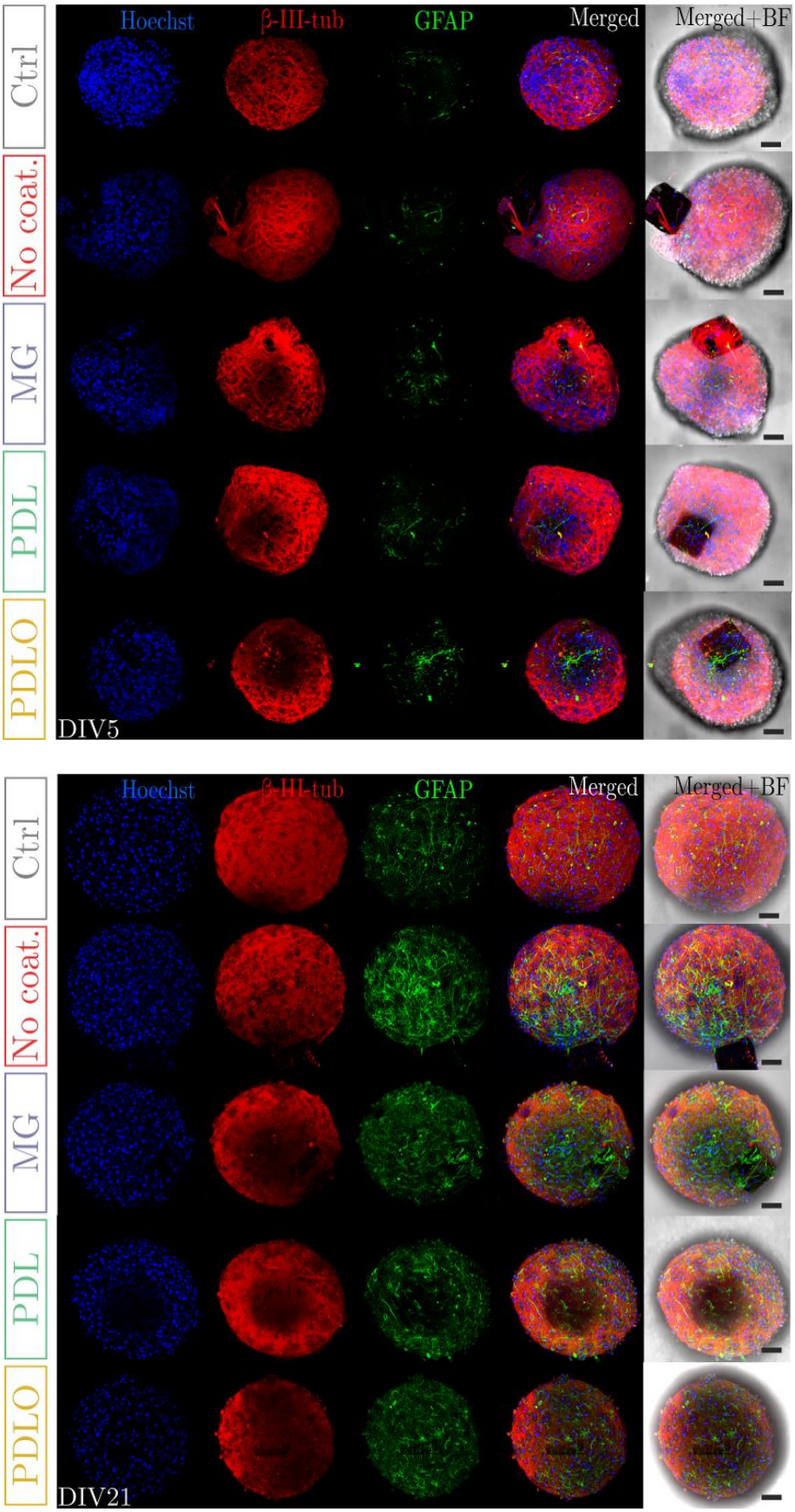

Figure 26: Fluorescence imaging of cortical spheroids with and without microchip. Confocal projections at DIV5 (upper panel) and DIV21 (lower panel) of spheroids reveal the presence of CNS

(Central Nervous System) cell types, including neurons (β-III-tubulin, red) and astrocytes (GFAP, glial fibrillary acidic protein, green). Nuclei are labeled with Hoechst (blue). Images are merged with and without bright field (BF). Data show a proliferation of neuronal connection between DIV5 and DIV21, and a great increase in GFAP-expressing astrocytes in the network in a similar fashion between spheroids with and without microchips. Scale bar 50µm.

3.5.5 Expression of spontaneous neural activity in hybrid neurospheroids

The integration of Si microchips might affect the expression of spontaneous neural activity. To verify this, I used calcium dye confocal microscopy imaging and compared the developmental activity in control spheroids without microchips with bio-artificial hybrid spheroids. Given the little influence of coatings observed on neurospheroid cellular composition, only PDL-coated devices were used. After one week in culture and throughout three weeks, Ca^{2+} oscillations represented as fluorescent variations are detected (Figure 27A-C). The pharmacologically-induced KCl depolarization confirms that this calcium activity is associated with neuronal activity. At DIV7, neurospheroids both with and without microchips exhibit signs of neuronal activity on a few regions of interest (ROI). At this stage of development, the activity is sparse, both spatially and temporally, and no synchronous activity is detected (Figure 27A). Upon network development, at DIV14, all spheroids exhibit more active ROIs, with in some cases the appearance of synchronous activity among distant ROIs (Figure 27B). After three weeks, neurospheroids tend to express a sustained spontaneous activity both in terms of numbers of active soma as well as in the frequency of spikes (Figure 27C). Figure 13D shows that the number of active ROIs for each tested spheroid increases over developmental time, and very similar activity levels are observed between control spheroids and spheroids containing a microdevice. This suggests that the presence of the Si microchips does not perturb the spontaneous functional development of neurospheroids over the observed experimental time window of three weeks.

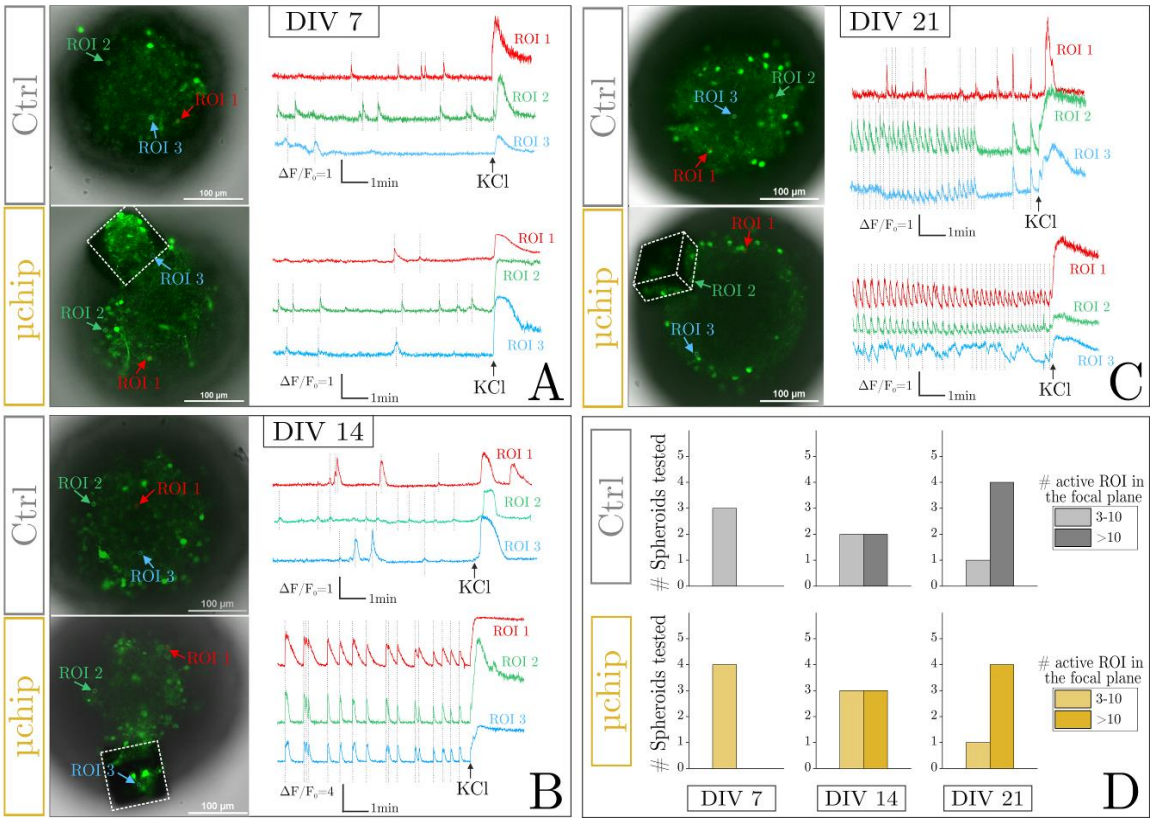

Figure 27: Calcium imaging frequency response of cortical neurons. Neurospheroids activity was measured using fluorescence indicators (Fluo-4 AM) of intracellular calcium oscillations. The fluorescence intensity displays representative activity during 8-10min of recording neurospheroids with and without microchip during development. A. After one week in culture, a few soma from the focus plane start exhibiting activity. B. After two weeks in culture, spheroids display single spikes from neurons, with in some cases synchronous activity among distant ROIs (region of interest). C. After three weeks in culture, spheroids with and without microchip exhibit synchronous spontaneous neural activity among many ROIs. Injection of 2mM KCl was used as a control. D. Graphs representing the level of activity exhibited from calcium imaging from spheroids at DIV7, DIV14 and DIV21, with or without the microchip. The bars correspond to the number of spheroids that exhibited either between 3 and 10 active ROI, or more than 10 active ROI in the focus plane. Only samples where KCl control was positive were considered. The results show that in both cases (with or without microchip), the level of maturation of spheroids is similar: spheroids with little active soma at DIV7, more at DIV14 and very active soma at DIV21.

3.5.6 Disaggregating bio-artificial neurospheroids for single-cell analysis

Finally, I explored whether cells and devices of bio-artificial hybrid neurospheroids can be separated for further single-cell analysis. By using a papain-based tissue dissociation, I found that it is possible to disaggregate formed spheroids to collect living single cells separated from microchips (Figure 28A). To demonstrate wheather the single cell suspension obtained from the disaggregation can be used for further single-cell analysis, I quantified by fluorescence-activated cell sorting (FACS) the ratio of neurons and glial cells in neurospheroids at DIV28

with and without microchips. As shown in Figure 28B, no differences between the two conditions was found. On average, spheroids without microchips are composed of 53.1% neurons (identified as $NeuN^+$ cells) and 35.4% astrocytes (identified as $GFAP^+$ cells), while spheroids with microchips are composed of 51.5% neurons and 39.6% astrocytes (see details in Table 2). Thus, beside confirming that the presence of microchips does not alter the spheroid cellular composition as previously observed by immunofluorescence analysis, this quantification demonstrates the feasibility of single-cell analysis on bio-artificial hybrid spheroids.

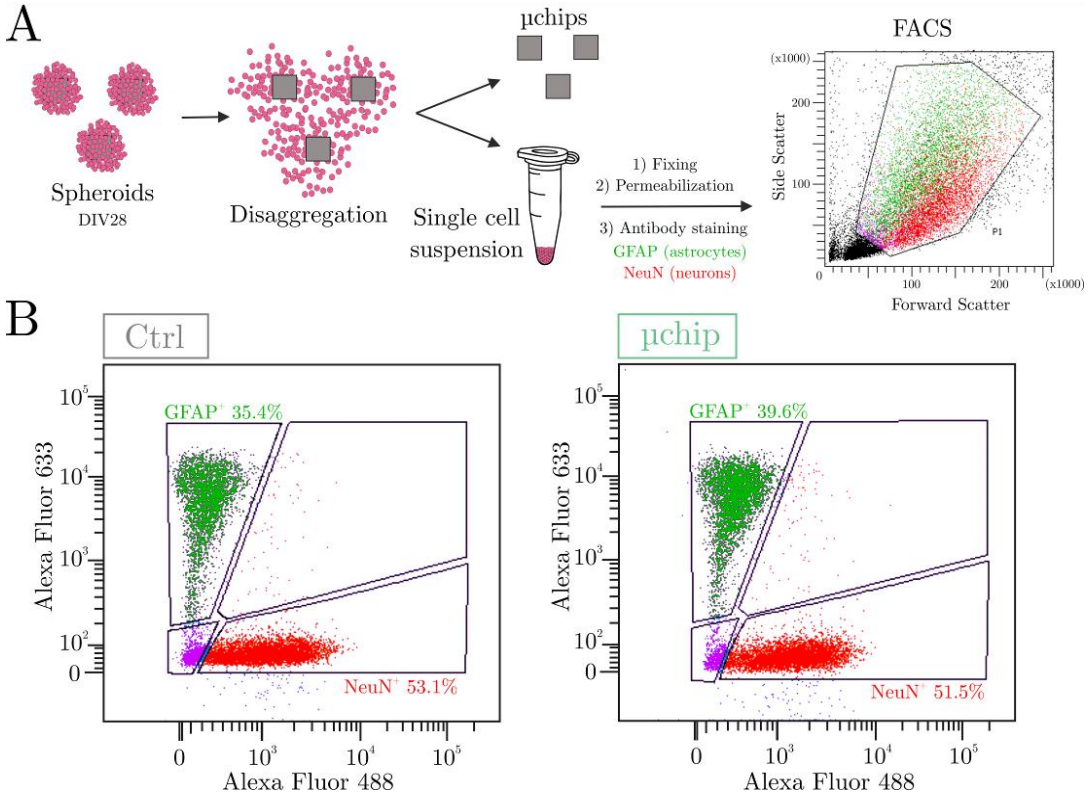

Figure 28: Single-cell analysis of disaggregated bio-artificial hybrid neurospheroids. A. Schematic representation of spheroids disaggregation. Cells and devices of formed bio-artificial hybrid neural spheroids were separated and the obtained single cell suspension was analyzed by FACS. B. FACS analysis of the ratio of neurons and astrocytes in spheroids without (ctrl, left) and with microchip (right). Neurons and astrocytes were labeled with anti-NeuN and anti-GFAP respectively. n=156.

Gated events	%Parent Ctrl	%Parent µchip
○$NeuN^+$ cells	53.1	51.5
○$GFAP^+$ cells	35.4	39.6
○$NeuN^+$ $GFAP^+$ cells	0.6	0.8
○$NeuN^-$ $GFAP^-$ cells	8.9	5.8

Table 2: FACS analysis after disaggregation of spheroids at DIV28 without (Ctrl) and with microchip. Single cells were fixed and stained for neuronal (NeuN) and astrocytic (GFAP) markers. At least 10000 gated events were analyzed.

3.6 Summary and Perspectives

Seamlessly tissue-integrated biosensing artificial microdevices can lead to bio-artificial hybrid 3D brain model systems with built-in biosensors for throughput functional assays. To this aim, parallel to the development of an untethered biosensing micro-device, there is the need of better understanding how to assemble and grow 3D neural cultures with built-in microscale devices.
My study focused on the integration of Si microchips into neuronal 3D cell aggregates through the assembling of primary cortical cells and microchips, and the growth of hybrid neurospheroids over 21 DIVs.
To do so, I successfully developed a method consisting in the manual seeding of cells and microchips, which enables the growth of bio-artificial hybrid neurospheroids with a high yield (>78%), although production could be automated and scaled up by using pick-and-place and microfluidic techniques. Results show that the presence of Si microchips of 100 x 100 x 50 μm^3 does not affect the developing 3D morphology, cellular composition and the development of spontaneous neural activity. Originally, by immobilizing various adhesion-promoting proteins on Si microdevices, our results reveal the role of the surface-chemical properties of these microchips in driving their assembling with cortical cells and their incorporation inside spheroids. In particular, uncoated microchips have poor interaction with cells, matrigel-coated microchips remain on the periphery of the spheroid, while PDL- and PDLO-coated microchips are integrated inside the spheroid. Finally, I also demonstrated the feasibility of separating cells and microchips from formed spheroids for further single-cell analysis.
Altogether, these findings support the feasibility of realizing a new generation of 3D brain tissue models with tissue integrated biosensing microscale devices. Importantly, this work reveals an original method to control the spatial integration of micro-devices into cellular constructs. This could provide built-in functionalities for routinely monitoring neural activity at sub-millisecond resolution and from deeply inside organoids, far behind the performances of currently available technologies, or for multiparametric monitoring of other biosignals (e.g. pH, temperature) during the growth of organoids or assays.
Moreover, these results open the possibility of studying the tuning of the surface chemical properties of Si microchips to finely control the assembling of 3D bio-artificial neuronal constructs with different levels of in-tissue integrated self-standing microdevices. This might lead to organoids integrating more than one microdevice, thus enabling to monitor functional biosignals within differently organized neuronal circuits as illustrated in the perspective Figure 29.

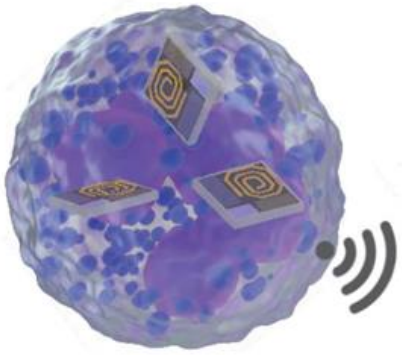

Figure 29: Findings of the present study open the perspective of integrating multiple, spatially controlled micro-scale untethered biosensing devices into organoids for accessing different compartments of complex 3D models.

Controlling the microdevice position in the 3D neural aggregate is particularly relevant for brain organoids. For instance, a microdevice with pH sensing capabilities internalized in the center of brain organoid would allow routinely monitoring the diffusion of nutrients and oxygen to detect the formation of a necrotic core, which in turn would provide crucial information to optimize organoid cultures efficiency (Jorfi et al., 2018). Besides, being able to control the placement of microdevices at different locations inside organoids would provide access to different cellular layers to routinely monitor neural activity or the chemical microenvironment, thus overcoming limitations of current imaging techniques for high-throughput read-outs.

In this work I focused on microscale Si devices having a square area of 100 x 100 μm^2 in size and 50 µm in thickness that were previously determined from the physical constraints of a RF biosensing circuit (Angotzi et al., 2018). However, shape and dimensions of microscale devices could provide additional degrees of freedom to tune the device integration inside 3D models and need to be evaluated in parallel with CMOS circuit design.

Future studies need to focus on the assembling of bio-artificial 3D models with human-derived neurons, extend the experimental time-window up to over several months and evaluate the microdevice performances to establish an efficient built-in-tissue seamless bioelectronic interface with normal neural tissue.

3.7 Cited references

Aleksandra B, Xiaonan RS, Andrea G, Laura AL, Samuel SHW. Fast calcium sensor proteins for monitoring neural activity. Neurophotonics. (2014) 1(2):1-12.

Amin H, Maccione A, Marinaro F, Zordan S, Nieus T, Berdondini L. Electrical Responses and Spontaneous Activity of Human iPS-Derived Neuronal Networks Characterized for 3-month Culture with 4096-Electrode Arrays. Front. Neurosci. (2016) 10:121.

Angotzi GN, Boi F, Lecomte A, Miele E, Malerba M, Zucca S, Casile A, Berdondini L. SiNAPS: An implantable active pixel sensor CMOS-probe for simultaneous large-scale neural recordings. Biosens. Bioelectron. (2019) 126:355-364.

Angotzi GN, Crepaldi M, Lecomte A, Giantomasi L, Rancati S, Depietri Tonelli D, Berdondini L. A uRadio CMOS device for real-time in-tissue monitoring of human organoids. IEEE Int. Conf. Biomed. Circuits Syst. (2018).

Arber C, Lovejoy C, Wray S. Stem cell models of Alzheimer's disease: progress and challenges. Alzheimers Res. Ther. (2017) 9:42.

Arlotta P. Organoids required! A new path to understanding human brain development and disease. Nat. Methods. (2018) 15:27-29.

Avci NG, Fan Y, Dragomir A, Akay YM, Gomez-Manzano C, Fueyo- Margareto J, Akay M. Delta-24-RGD induces cytotoxicity of glioblastoma spheroids in three dimensional PEG microwells. IEEE Trans. Nanobiosci. (2015) 14(8):946-951.

Bagley JA, Reumann D, Bian S, Levi-Strauss J, Knoblich JA. Fused cerebral organoids model interactions between brain regions. Nat. Methods. (2017) 14:743-751.

Bahr BA. Long-term hippocampal slices: a model system for investigating synaptic mechanisms and pathologic processes. J. Neurosci. Res. (1995) 42(3):294–305.

Berdondini L, Imfeld K, Maccione A, Tedesco M, Neukom S, Koudelka-Hep M, Martinoia S. Active pixel sensor array for high spatio-temporal resolution electrophysiological recordings from single cell to large scale neuronal networks. Lab on a Chip. (2009) 9(18):2644-2651.

Berdondini L, Overstolz T, Rooij NFd, Koudelka-Hep M, Wany M, Seitz P. High-density microelectrode arrays for electrophysiological activity imaging of neuronal networks. Proc. IEEE Int. Conf. Electron. Circuits Syst. (2001) 3:1239-1242.

Bhatia SN, Ingber DE. Microfluidic organs-on-chips. Nat. Biotech. (2014) 32:760.

Birey F, Andersen J, Makinson CD, Islam S, Wei W, Huber N, Fan HC, Metzler KRC, Panagiotakos G, Thom N, O'Rourke NA, Steinmetz LM, Bernstein JA, Hallmayer J,

Huguenard JR, Pasca SP. Assembly of functionally integrated human forebrain spheroids. Nature. (2017) 15:631-639.

Burke P, Rutherglen C. Towards a single-chip, implantable RFID system: is a single-cell radio possible?. Biomed. Microdevices. (2010) 12:589–596.

Camp JG, Badsha F, Florio M, Kanton S, Gerber T, Wilsch-Brauninger M, Lewitus E, Sykes A, Hevers W, Lancaster M, Knoblich JA, Lachmann R, Paabo S, Huttner WB, Treutlein B. Human cerebral organoids recapitulate gene expression programs of fetal neocortex development. Proc. Natl. Acad. Sci. USA. (2015) 112:15672-15677.

Cargill RS 3rd, Dee KC, Malcolm S. An assessment of the strength of NG108-15 cell adhesion to chemically modified surfaces. Biomaterials. (1999) 20(23-24):2417-25.

Cavaliere F, Benito-Muñoz M, Matute C. Organotypic cultures as a model to study adult neurogenesis in CNS disorders. Stem Cells Int. (2016) 2016:6.

Chen HI, Song H, Ming GL. Applications of human brain organoids to clinical problems. Dev. Dyn. (2018) 248:53-64.

Choi YJ, Park J, Lee SH. Size-controllable networked neurospheres as a 3D neuronal tissue model for Alzheimer's disease studies. Biomaterials. (2013) 34(12):2938-2946.

Croft CL, Futch HS, Moore BD, Golde TE. Organotypic brain slice cultures to model neurodegenerative proteinopathies. Mol. Neurodegener. (2019) 14:45.

Daviaud N, Garbayo E, Schiller PC, Perez-Pinzon M, Montero-Menei CN. Organotypic cultures as tools for optimizing central nervous system cell therapies. Exp. Neurol. (2013) 248:429.

De Simoni A, Griesinger CB, Edwards FA. Development of rat CA1 neurones in acute versus organotypic slices: role of experience in synaptic morphology and activity. J. Physiol. (2003) 550(1):135–47.

Del Duca D, Werbowetski T and Del Maestro RF. Spheroid preparation from hanging drops: characterization of a model of brain tumor invasion. J. Neuro-Oncol. (2004) 67:295–303.

Di Matteo F, Pipicelli F, Kyrousi C, Tovecci I, Penna E, Crispino M, Chambery A, Russo R, Ayo-Martin AC, Giordano M, Hoffmann A, Ciusani E, Canafoglia L, Götz M, Di Giaimo R, Cappello S. Cystatin B is essential for proliferation and interneuron migration in individuals with EPM1 epilepsy. EMBO Mol. Med. (2020) 12(6):e11419.

Dingle YT, Boutin ME, Chirila AM, Livi LL, Labriola NR, Jakubek LM, Morgan JR, Darling EM, Kauer JA, Hoffman-Kim D. Three-dimensional neural spheroid culture: an in vitro model for cortical studies. Tissue Eng. Part C. Methods. (2015) 21 (12):1274e1283.

Fair SR, Julian D, Hartlaub AM, Pusuluri ST, Malik G, Summerfied TL, Zhao G, Hester AB, Ackerman WEIV, Hollingsworth EW, Ali M, McElroy CA, Buhimschi IA, Imitola J, Maitre NL, Bedrosian TA, Hester ME. Electrophysiological Maturation of Cerebral Organoids Correlates with Dynamic Morphological and Cellular Development. Stem Cell Reports. (2020) 15(4):855-868.

Fernandez-Rosas E, Gómez R, Ibañez E, Barrios L, Duch M, Esteve J, Nogués C, Plaza JA. Intracellular polysilicon barcodes for cell tracking. Small. (2009) 5(21):2433-9.

Fernández-Rosas E, Gómez R, Ibañez E, Barrios L, Duch M, Esteve J, Plaza JA, Nogués C. Internalization and cytotoxicity analysis of silicon-based microparticles in macrophages and embryos. Biomed. Microdevices. (2010) 12(3):371-9.

Forro C, Caron D, Angotzi GN, Gallo V, Berdondini L, Santoro F, Palazzolo G, Panuccio G. Electrophysiology Read-Out Tools for Brain-on-Chip Biotechnology. Micromachines. (2021) 12(2):124.

Frey U, Sanchez-Bustamante CD, Ugniwenko T, et al. Cell recordings with a CMOS high-density microelectrode array. Conf. Proc. IEEE Eng. Med. Biol. Soc. (2007) 2007:167-170.

Friedrich J, Ebner R, Kunz-Schughart LA. Experimental anti-tumor therapy in 3-D: spheroids-old hat or new challenge? Int. J. Radiat. Biol. (2007) 83:849–871.

Gähwiler BH. Organotypic monolayer cultures of nervous tissue. J. Neurosci. Methods. (1981) 4(4):329–42.

Gómez-Martínez R, Hernández-Pinto AM, Duch M, Vázquez P, Zinoviev K, de la Rosa EJ, Esteve J, Suárez T, Plaza JA. Silicon chips detect intracellular pressure changes in living cells. Nat. Nanotechnol. (2013) 8(7):517-21.

Gómez-Martínez R, Vázquez P, Duch M, Muriano A, Pinacho D, Sanvicens N, Sánchez-Baeza F, Boya P, de la Rosa EJ, Esteve J, Suárez T, Plaza JA. Intracellular silicon chips in living cells. Small. (2010) 6(4):499-502.

Gonzalez C, Armijo E, Bravo-Alegria J, Becerra-Calixto A, Mays CE, Soto C. Modeling amyloid beta and tau pathology in human cerebral organoids. Mol. Psychiatry. (2018) 23:2363-2374.

Guan A, Hamilton P, Wang Y, Gorbet M, Li Z, Phillips KS. Medical devices on chips. Nat. Biomed. Eng. (2017) 1:0045.

Gunda NSK, Singh M, Norman L, Kaur K, Mitra SK. Optimization and characterization of biomolecule immobilization on silicon substrates using (3-aminopropyl)triethoxysilane (APTES) and glutaraldehyde linker. Appl. Surf. Sci. (2014) 305:522–530.

Harnett EM, Alderman J, Wood T. The surface energy of various biomaterials coated with adhesion molecules used in cell culture, Colloids Surfaces B Biointerfaces. (2007) 55:90–97.

Heer F, Franks W, Blau A, Taschini S, Ziegler C, Hierlemann A, Baltes H. CMOS microelectrode array for the monitoring of electrogenic cells. Biosens. Bioelectron. (2004) 20(2):358-66.

Hubert CG, Rivera M, Spangler LC, Wu Q, Mack SC, Prager BC, Couce M, McLendon RE, Sloan AE, Rich JN. A three-dimensional organoid culture system derived from human glioblastomas recapitulates the hypoxic gradients and cancer stem cell heterogeneity of tumors found in vivo. Cancer Res. (2016) 76:2465-2477.

Humpel C. Organotypic brain slice cultures: a review. Neuroscience. (2015) 305:86–98.

Hutter-Schmid B, Kniewallner K, Humpel C. Organotypic brain slice cultures as a model to study angiogenesis of brain vessels. Front. Cell. Dev. Biol. (2015) 3:52.

Ivanov DP, Parker TL, Walker DA, Alexander C, Ashford MB, Gellert PR, Garnett MC. Multiplexing spheroid volume, resazurin and acid phosphatase viability assays for high-throughput screening of tumour spheroids and stem cell neurospheres. PLoS One. (2014) 9(8):e103817.

Jahromi MA, Abdoli A, Rahmanian M, Bardania H, Bayandori M, Basri SMM, Kalbasi A, Aref AR, Karimi M, Hamblin MR. Microfluidic Brain-on-a-Chip: Perspectives for Mimicking Neural System Disorders. Mol. Neurobiol. (2019) 56(12):8489–512.

Jiang B, Zheng W, Zhang W, Jiang X. Organs on microfluidic chips: A mini review. Sci. China Chem. (2014) 57:356–364.

Jo J, Xiao Y, Sun AX, Cukuroglu E, Tran HD, Gö ke J, Tan ZY, Saw TY, Tan CP, Lokman H, Lee Y, Kim D, Ko HS, Kim SO, Park JH, Cho NJ, Hyde TM, Kleinman JE, Shin JH, Weinberger DR, Tan EK, Je HS, Ng HH. Midbrain-like organoids from human pluripotent stem cells contain functional dopaminergic and neuromelanin-producing neurons. Cell Stem Cell. (2016) 19:248-257.

Jorfi M, D'Avanzo C, Kim DY, Irimia D. Three-dimensional models of the human brain development and diseases. Adv. Healthc. Mater. (2018) 7:1–20.

Kadoshima T, Sakaguchi H, Nakano T, Soen M, Ando S, Eiraku M, Sasai Y. Self-organization of axial polarity, inside-out layer pattern, and species-specific progenitor dynamics in human ES cell-derived neocortex. Proc. Natl. Acad. Sci. USA. (2013) 110:20284-20289.

Khan J, Das G, Gupta V, Mohapatra S, Ghosh S, Ghosh S. Neurosphere development from hippocampal and cortical embryonic mixed primary neuron culture: a potential platform for screening neurochemical modulator. ACS Chem. Neurosci. (2018) 9:2870-2878.

Kim YH, Baek NS, Han YH, Chung MA, Jung SD. Enhancement of neuronal cell adhesion by covalent binding of poly-d-lysine. J. Neurosci. Methods. (2011) 202(1):38–44.

Kimura M, Azuma M, Zhang RR, Thompson W, Mayhew CN, Takebe T. Digitalized Human Organoid for Wireless Phenotyping. Iscience. (2018) 4:294-301.

Klaus J, Kanton S, Kyrousi C, Ayo-Martin AC, Di Giaimo R, Riesenberg S, O'Neill AC, Camp JG, Tocco C, Santel M, Rusha E, Drukker M, Schroeder M, Götz M, Robertson SP, Treutlein B, Cappello S. Altered neuronal migratory trajectories in human cerebral organoids derived from individuals with neuronal heterotopia. Nat. Med. (2019) 25(4):561-568.

Koo B, Choi B, Park H, Yoon KJ. Past, present, and future of brain organoid technology. Mol. Cells. (2019) 42(9):617–627.

Kuddannaya S, Bao J, Zhang Y. Enhanced in Vitro Biocompatibility of Chemically Modified Poly(dimethylsiloxane) Surfaces for Stable Adhesion and Long-term Investigation of Brain Cerebral Cortex Cells. ACS Appl. Mater. Interfaces. (2015) 7(45):25529–25538.

Kunze A, Giugliano M, Valero A, Renaud P. Micropatterning neural cell cultures in 3D with a multi-layered scaffold. Biomaterials. (2011) 32(8):2088-98.

Kyrousi C, Cappello S. Using brain organoids to study human neurodevelopment, evolution and disease. Wiley Interdiscip. Rev. Dev. Biol. (2020) 9:e347.

Lancaster MA, Corsini NS, Wolfinger S, Gustafson EH, Phillips AW, Burkard TR, Otani T, Livesey FJ, Knoblich JA. Guided self-organization and cortical plate formation in human brain organoids. Nat. Biotechnol. (2017) 35:659-666.

Lancaster MA and Knoblich JA. Generation of cerebral organoids from human pluripotent stem cells. Nat. Protoc. (2014) 9:2329-2340.

Lancaster MA, Renner M, Martin CA, Wenzel D, Bicknell LS, Hurles ME, Homfray T, Penninger JM, Jackson AP, Knoblich JA. Cerebral organoids model human brain development and microcephaly. Nature. (2013) 501:373-379.

LaPlaca MC, Vernekar VN, Shoemaker JT, Cullen DK. in Methods in Bioengineering: 3D Tissue Engineering. eds F. Berthiaume & J. Morgan. Norwood: Artech House. (2010) 187–204.

Linkous A, Balamatsias D, Snuderl M, Pisapia D, Liston C, Correspondence HAF. Modeling patient-derived glioblastoma with cerebral organoids. Cell Rep. (2019) 26:3203-3211.

Logan S, Arzua T, Yan Y, Jiang C, Liu X, Yu LK, Liu QS, Bai X. Dynamic Characterization of Structural, Molecular, and Electrophysiological Phenotypes of Human-Induced Pluripotent Stem Cell-Derived Cerebral Organoids, and Comparison with Fetal and Adult Gene Profiles. Cells. (2020) 9(5).

Mansour AAF, Gonçalves JT, Bloyd CW, Li H, Fernandes S, Quang D, Johnston S, Parylak SL, Jin X, Gage FH. An in vivo model of functional and vascularized human brain organoids. Nat. Biotechnol. (2018) 36:432-441.

Marton RM, Miura Y, Sloan SA, Li Q, Revah O, Levy RJ, Huguenard JR, Pașca SP. Differentiation and maturation of oligodendrocytes in human three-dimensional neural cultures. Nat. Neurosci. (2019) 22:484-491.

Marton RM, Pașca SP. Organoid and Assembloid Technologies for Investigating Cellular Crosstalk in Human Brain Development and Disease. Trends in Cell Biology. (2020) 30:133-143.

McDonald M, Sebinger D, Brauns L, Gonzalez-Cano L, Menuchin-Lasowski Y, Psathaki O-E, Stumpf A, Rauen T, Schöler H, Jones PD. A mesh microelectrode array for non-invasive electrophysiology within neural organoids. bioRxiv. (2020).

Meseke M, Förster E. A 3D-matrigel/microbead assay for the visualization of mechanical tractive forces at the neurite-substrate interface of cultured neurons. J. Biomed. Mater. Res. A. (2013) 101(6):1726-33.

Miccoli B, Braeken D, Li YE. Brain-on-a-chip devices for drug screening and disease modeling applications. Curr. Pharm. Des. (2018) 24(45):5419-5436.

Muguruma K, Nishiyama A, Kawakami H, Hashimoto K, Sasai Y. Self-organization of polarized cerebellar tissue in 3D culture of human pluripotent stem cells. Cell Rep. (2015) 10:537-550.

Neely RM, Piech DK, Santacruz SR, Maharbiz MM, Carmena JM. Recent advances in neural dust: towards a neural interface platform. Curr. Opin. Neurobiol. (2018) 50:64-71.

Nikolakopoulou P, Rauti R, Voulgaris D, Shlomy I, Maoz MB, Herland A. Recent progress in translational engineered in vitro models of the central nervous system. Brain. (2020).

Pamies D, Hartung T, Hogberg HT. Biological and medical applications of a brain-on-a-chip. Exp Biol Med (Maywood). (2014) 239(9):1096–1107.

Pasca AM, Sloan SA, Clarke LE, Tian Y, Makinson CD, Huber N, Kim CH, Park JY, O'Rourke NA, Nguyen KD, Smith SJ, Huguenard JR, Geschwind DH, Barres BA, Pasca SP. Functional cortical neurons and astrocytes from human pluripotent stem cells in 3D culture. Nat. Methods. (2015) 12:671-678.

Pașca SP. The rise of three-dimensional human brain cultures. Nature. (2018) 553:437-445.

Qian X, Nguyen HN, Song MM, Hadiono C, Ogden SC, Hammack C, Yao B, Hamersky GR, Jacob F, Zhong C, Yoon KJ, Jeang W, Lin L, Li Y, Thakor J, Berg DA, Zhang C, Kang E, Chickering M, Nauen D, Ho CY, Wen Z, Christian KM, Shi PY, Maher BJ, Wu H, Jin P, Tang H, Song H, Ming GL. Brain-region-specific organoids using mini-bioreactors for modeling ZIKV exposure. Cell. (2016) 165:1238-1254.

Qian X, Song H, Ming GL. Brain organoids: advances, applications and challenges. Development. (2019) 146:dev166074.

Qian X, Su Y, Adam CD, Deutschmann AU, Pather SR, Goldberg EM, Su K, Li S, Lu L, Jacob F, Nguyen PTT, Huh S, Hoke A, Swinford-Jackson SE, Wen Z, Gu X, Pierce RC, Wu H, Briand LA, Chen HI, Wolf JA, Song H, Ming GI. Sliced Human Cortical Organoids for Modeling Distinct Cortical Layer Formation. Cell Stem Cell. (2020) 26(5):766-781.

Quadrato G, Arlotta P. Present and future of modeling human brain development in 3D organoids. Curr. Opin. Cell Biol. (2017) 49:47–52.

Quadrato G, Nguyen T, Macosko EZ, Sherwood JL, Min Yang S, Berger DR, Maria N, Scholvin J, Goldman M, Kinney JP, Boyden ES, Lichtman JW, Williams ZM, McCarroll SA, Arlotta P. Cell diversity and network dynamics in photosensitive human brain organoids. Nature. (2017) 545(7652):48-53.

Rambani K, Vukasinovic J, Glezer A, Potter SM. Culturing thick brain slices: an interstitial 3D microperfusion system for enhanced viability. J. Neurosci. Methods. (2009) 180:243-254.

Sakaguchi H, Kadoshima T, Soen M, Narii N, Ishida Y, Ohgushi M, Takahashi J, Eiraku M, Sasai Y. Generation of functional hippocampal neurons from self-organizing human embryonic stem cell-derived dorsomedial telencephalic tissue. Nat. Commun. (2015) 6:8896.

Sakai Y and Nakazawa K. Technique for the control of spheroid diameter using microfabricated chips. Acta Biomater. (2007) 3:1033–1040.

Schneider CA, Rasband WS, Eliceiri KW. NIH Image to ImageJ: 25 years of image analysis. Nat. Methods. (2012) 9(7):671-5.

Seo D, Carmena JM, Rabaey JM, Alon E, Maharbiz MM. Neural Dust: An Ultrasonic, Low Power Solutionfor Chronic Brain-Machine Interfaces. (2013).

Seo D, Carmena JM, Rabaey JM, Maharbiz MM, Alon E. Model validation of untethered, ultrasonic neural dust motes for cortical recording. J. Neurosci. Methods. (2015) 244:114-22.

Seo D, Neely RM, Shen K, Singhal U, Alon E, Rabaey JM, Carmena JM, Maharbiz MM. Wireless Recording in the Peripheral Nervous System with Ultrasonic Neural Dust. Neuron. (2016) 91(3):529-39.

Shamir ER, Ewald AJ. Three-dimensional organotypic culture: experimental models of mammalian biology and disease. Nat. Rev. Mol. Cell. Biol. (2014) 15:647.

Simao D, Pinto C, Piersanti S, Weston A, Peddie CJ, Bastos AE, Licursi V, Schwarz SC, Collinson LM, Salinas S, Serra M, Teixeira AP, Saggio I, Lima PA, Kremer EJ, Schiavo G, Brito C, Alves PM. Modeling human neural functionality in vitro: three-dimensional culture for dopaminergic differentiation. Tissue Eng. Part A. (2015) 21(3e4):654-668.

Sloan SA, Darmanis S, Huber N, Khan TA, Birey F, Caneda C, Reimer R, Quake SR, Barres BA, Pasca SP. Human astrocyte maturation captured in 3D cerebral cortical spheroids derived from pluripotent stem cells. Neuron. (2017) 95:779-790.

Spitz S, Zanetti C, Bolognin S, Muwanigwa MN, Smits L, Berger E, Jordan C, Harasek M, Schwamborn JC, Ertl P. Cultivation and characterization of human midbrain organoids in sensor integrated microfluidic chips. bioRxiv (2019)

Staal JA, Alexander SR, Liu Y, Dickson TD, Vickers JC. Characterization of cortical neuronal and glial alterations during culture of Organotypic whole brain slices from neonatal and mature mice. PLoS One. (2011) 6(7):e22040.

Stoppini L, Buchs PA, Muller D. A simple method for organotypic cultures of nervous tissue. J. Neurosci. Methods. (1991) 37(2):173–82.

Tasciotti E, Liu X, Bhavane R, Plant K, Leonard AD, Price BK, Cheng MM, Decuzzi P, Tour JM, Robertson F, Ferrari M. Mesoporous silicon particles as a multistage delivery system for imaging and therapeutic applications. Nat. Nanotechnol. (2008) 3:151–157.

Terrasso AP, Pinto C, Serra M, Filipe A, Almeida S, Ferreira AL, Pedroso P, Brito C, Alves PM. Novel scalable 3D cell based model for in vitro neurotoxicity testing: combining human differentiated neurospheres with gene expression and functional endpoints. J. Biotechnol. (2015) 205:82-92.

Torisawa Y, Chueh BH, Huh D, Ramamurthy P, Roth TM, Barald KF and Takayama S. Efficient formation of uniform-sized embryoid bodies using a compartmentalized microchannel device. Lab Chip. (2007) 7:770–776.

Torisawa Y, Takagi A, Nahimoto Y, Yasukawa T, Shiku H, Matsue T. A multicellular spheroid array to realize spheroid formation, culture, and viability assay on a chip. Biomaterials. (2007) 28:559–566.

Trujillo CA, Gao R, Negraes PD, Gu J, Buchanan J, Preissl S, Wang A, Wu W, Haddad GG, Chaim IA, Domissy A, Vandenberghe M, Devor A, Yeo GW, Voytek B, Muotri AR. Complex Oscillatory Waves Emerging from Cortical Organoids Model Early Human Brain Network Development. Cell Stem Cell. (2019) 25(4):558-569.

Tung YC, Hsiao AY, Allen SG, Torisawa YS, Ho M, Takayama S. High-throughput 3D spheroid culture and drug testing using a 384 hanging drop array. Analyst. (2011) 136:473-478.

Velasco S, Kedaigle AJ, Simmons SK, Nash A, Rocha M, Quadrato G, Paulsen B, Nguyen L, Adiconis X, Regev A, Leviv JZ, Arlotta P. Individual brain organoids reproducibly form cell diversity of the human cerebral cortex. Nature. (2019) 570:523-527.

Wimmer RA, Leopoldi A, Aichinger M, Wick N, Hantusch B, Novatchkova M, Taubenschmid J, Hämmerle M, Esk C, Bagley JA, Lindenhofer D, Chen G, Boehm M, Agu CA, Yang F, Fu B, Zuber J, Knoblich JA, Kerjaschki D, Penninger JM. Human blood vessel organoids as a model of diabetic vasculopathy. Nature. (2019) 565:505-510.

Wu LY, Di Carlo D, Lee LP. Microfluidic self-assembly of tumor spheroids for anticancer drug discovery. Biomed. Microdevices. (2008) 10:197–202.

Xiang Y, Tanaka Y, Patterson B, Kang YJ, Govindaiah G, Roselaar N, Cakir B, Kim KY, Lombroso AP, Hwang SM, Zhong M, Stanley EG, Elefanty AG, Neagele JR, Lee SH, Weissman SM, Park IH. Fusion of regionally specified hPSC-derived organoids models human brain development and interneuron migration. Cell Stem. Cell. (2017) 21:383-398.

Xu JC, Fan J, Wang X, Eacker SM, Kam TI, Chen L, Yin X, Zhu J, Chi Z, Jiang H, Chen R, Dawson TM, Dawson VL. Cultured networks of excitatory projection neurons and inhibitory interneurons for studying human cortical neurotoxicity. Science Translational Medicine. (2016) 8:333.

Yavin E, Yavin Z. Attachment and culture of dissociated cells from rat embryo cerebral hemispheres on polylysine-coated surface. J. Cell Biol. (1974) 62(2):540-6.

Yoon KJ, Ringeling FR, Vissers C, Jacob F, Pokrass M, Jimenez-Cyrus D, Su Y, Kim NS, Zhu Y, Zheng L, Kim S, Wang X, Dorè LC, Jin P, Regot S, Zhuang X, Canzar S, He C, Ming GL, Song H. Temporal control of mammalian cortical neurogenesis by m(6)A methylation. Cell. (2017) 171:877- 889.

Yoon SJ, Elahi LS, Pasca AM, Marton RM, Gordon A, Revah O, Miura Y, Walczak EM, Holdgate GM, Fan HC, Huguenard JR, Geschwind DH, Pasca SP. Reliability of human cortical organoid generation. Nat. Methods. (2019) 16:75-78.

Zhuang P, Sun AX, An J, Chua CK, Chew SY. 3D neural tissue models: from spheroids to bioprinting. Biomaterials. (2018) 154:113-133.

4. Overall Conclusions

The brain is the most complex and at the same time intriguing human organ. Discovering the molecular and cellular mechanisms that regulate its development, as well as understanding human brain disorders and their possible causes, and developing new therapeutic approach, are just some of the reasons that make the study of the brain so fascinating, attracting the attention of many scientists over the centuries and with enormous implications for our society. Despite the countless studies carried out and technological advances, many diseases are still incurable. A major current limitation is the impossibility of studying the human brain directly across molecular, cellular and brain circuit scales. Therefore, there is the need to advance the development of adapted brain tissue models. Current model systems, however, fail in mimicking the human brain in all its complexity, with the consequence, for instance, of a poor translational relevance of screening results to humans. Developing new technologies and achieving biological models that can faithfully reproduce the complex features of human brain remains a long-standing challenge.

In this PhD thesis, I exploited the opportunity of developing new technologies to advance the development and application of *in vitro* brain-on-chip models that enable to address different biological questions.

In the first part, I focused on a microfluidic device developed in our laboratory to experimentally investigate the synchronization process of clock genes among distant neuronal populations. This original approach allowed to dissect different signaling channels that can not be easily addressed *in vivo* due to the high cellular density and connectivity complexity. Results highlight the presence of at least two pathways for the synchronization of distant and segregated neuronal populations: a neuronal paracrine factors-mediated synchronization and an astrocytes-mediated synchronization. Moreover, results on the study of possible signaling factors suggest that paracrine factors-mediated synchronization occurs through a GABA signaling, while astrocytes-mediated synchronization requires the involvement of both GABA and glutamate.

To date, the role of GABA and glutamate, especially in the circadian field, is still not completely understood, sometimes controversial and often matter of debate. For the direct astrocyte-to-neuron synchronization, for example, Barca-Mayo's study supports a GABA signaling (Barca-Mayo et al., 2017), while Brancaccio's one sustains a glutamatergic signaling (Brancaccio et al., 2017; Brancaccio et al., 2019). My work supports both visions, with an involvement of both GABA and glutamate, but in different contexts. Interestingly, using devices with different lengths of the channel, by means different distances between two neuronal populations, I found

that the capability of paracrine factors released from a synchronous neuronal population to synchronize an asynchronous neuronal population decreases with the increasing of the distance. Differently, astrocytes are able to transmit neuronal clock rhythms also at the maximum distance tested (17 mm), thus revealing the capacity of astrocytes to act as an active communication channel that can synchronize distant neural populations. These results reveal that neural populations can be entrained in synchronization through two pathways that could imply very different potential roles in brain circuits. Neuronal paracrine factors could be involved for local (or short-range) synchronization, while astrocytes can act as active communication channels to transfer circadian information to more distant (long-range) neurons. Overall, these findings not only highlight the synergic regulation of clock genes among neurons and astrocytes, but reinforce the role of astrocytes as active cells in the regulation of clock genes in the brain.

In this direction, during the last period of my PhD I also started to investigate the effects of reactive astrocytes, that are astrocytes responding to CNS injury and other neurological diseases, on the neuronal circadian rhythms synchronization. Interestingly, preliminary results suggest an impairment in the local neuronal synchronization but do not highlight an alteration in the propagation of clock rhythms among distant neuronal populations.

These findings pave the way for the consideration of astrocytes as a new cellular target for neuropharmacology of transient or chronic perturbation of circadian rhythms, although further analysis will be necessary for a better understanding of the possible link among astrocytes, their reactivity, alteration of circadian rhythms and neurodegenerative diseases.

In the second part of this thesis, I investigated the effects of surface functionalization of Si microchips (100 x 100 x 50 μm^3) in driving their 3D assembling with cortical cells and in tuning their 3D incorporation inside neurospheroids. This work is part of a larger project of my laboratory aimed at developing a new generation of "bionic organoids", that are bio-artificial hybrid 3D brain model systems with seamlessly tissue-integrated biosensing microdevices.

Results show that the presence of Si microchips in neurospheroids does not affect the developing 3D morphology, cellular composition and the development of spontaneous neural activity. Originally, by immobilizing various adhesion-promoting proteins on Si microdevices, results reveal the role of the surface-chemical properties of these microchips in driving their assembling with cortical cells and their incorporation inside spheroids.

Together, these findings support the feasibility of a new generation of 3D brain tissue models with tissue integrated biosensing microscale devices. This could provide built-in functionalities for routinely monitoring neural activity at sub-millisecond resolution and from deeply inside

organoids for behind the performances of currently available technologies, or for multiparametric monitoring of other biosignals (e.g. pH, temperature) during 3D model culture or assays. Moreover, these results open the possibility of studying the tuning of the surface chemical properties of Si microchips to control the assembling of 3D bio-artificial neuronal constructs with different levels of in-tissue integrated self-standing microdevices, with the possibility to have more than one device in each organoid. Controlling the microdevice position in the 3D neural aggregate is particularly relevant for brain organoids. For instance, a microdevice with pH sensing capabilities internalized in the center of brain organoid would allow routinely monitoring the diffusion of nutrients and oxygen to detect the formation of a necrotic core, which in turn would provide crucial information to optimize organoid cultures efficiency. Besides, being able to control the placement of microdevices at different locations inside organoids would provide access to different cellular layers to routinely monitor neural activity or the chemical microenvironment, thus overcoming limitations of current imaging techniques for high-throughput read-outs.

This type of bionic organoid will be a promising model system of the human brain. It can be exploit for different applications, such as animal testing replacement for drug discovery and screening, personalized medicine, and for brain development, function and dysfunction studies. Being a middle between 2D systems and *in vivo* models, brain organoids can be used to address biological questions that, due to the dense cellular connectivity and network complexity, are challenging to investigate *in vivo*.

Regarding the molecular clock synchronization of distant neuronal populations, for example, a fascinating and original perspective is to study *in vivo* the pathways proposed in this work and their implication in health and disease. A strategy could be to focus on the optic nerve as the link between the retina and the SCN. If the intercellular communication among optic nerve astrocytes is altered, can "time information" pass from the retina to the SCN?

As it is not easy to use *in vivo* models to address all circadian questions, 3D aggregates, like simple neurospheroids first and more complex brain organoids later, could be a good compromise. In this direction I also started to investigate the expression of clock genes in rat cortical neurospheroids (Figure 30). In this case, spheroids were maintained in culture for 21 days and then pulled at different hours of the day for the analysis. Preliminary results show a circadian expression of some but not all clock genes. It is important to underline that neurons in 2D culture are asynchronous, while astrocytes synchronize by changing medium. This suggests that in 3D aggregates, astrocytes, that are always synchronous, can at least start to entrain neurons. These findings pave the way for the study of circadian rhythms in 3D brain

tissue cultures and might provide a better understanding of mechanisms involved in the regulation of molecular clocks as well as their implication in brain diseases. Such understanding assumes great relevance in an era in which human beings are increasingly subject to dysregulations, mainly caused by the hectic life-style of today's society. Altered rhythms of our daily life can have a negative impact in short and long term. In the short term, altered circadian rhythms interfere with the psycho-physical balance and the consequent efficiency in cognitive performance. In the long term, they constitute an important risk factor for health in terms of various psychosomatic, gastrointestinal, cardiovascular and neoplastic disorders and diseases, which translate into high economic and social costs for individuals and the society. Understanding how to intervene on our habits to keep a good regulation of our rhythms can definetively help us to improve our quality of life and reduce risks associated with aging.

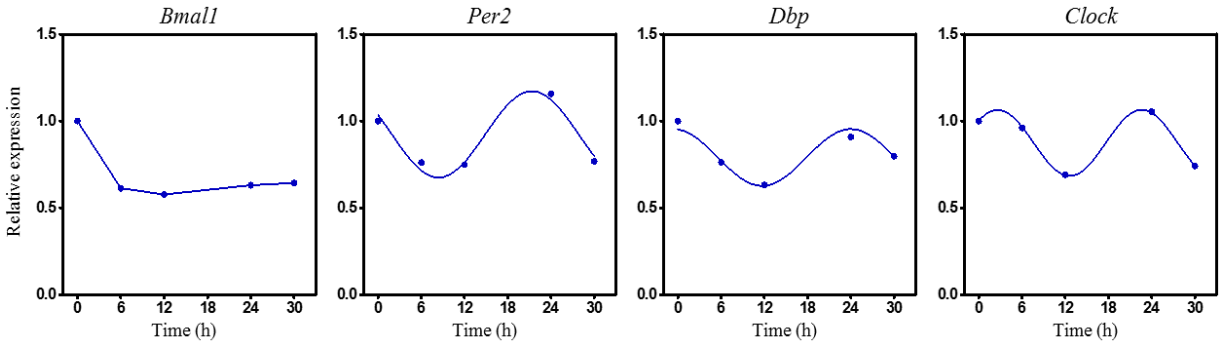

Figure 30: Clock genes expression in cortical neurospheroids. From left to right, *Bmal1*, *Per2*, *Dbp* and *Clock* expression in rat cortical neurospheroids at DIV21. All genes were analyzed at the indicate time points by qPCR. All graphs show the mean ± s.e.m. of the cosine-fitted curves from an experiment.

Annex I

Publications and Conferences

Publications

- Lecomte A*, **Giantomasi L***, Rancati S, Boi F, Angotzi GN, Berdondini L. Surface-Functionalized Self-Standing Microdevices Exhibit Predictive Localization and Seamless Integration in 3D Neural Spheroids. Adv. Biosyst. (2020) 4(11):e2000114. (*These authors contributed equally)

- Angotzi GN, Crepaldi M, Lecomte A, **Giantomasi L**, Rancati S, De Pietri Tonelli D, Berdondini L. A uRadio CMOS device for real-time in-tissue monitoring of human organoids. IEEE Int. Conf. Biomed. Circuits Syst. (2018).

Conference presentations

- **Giantomasi L**, Malerba M, Barca-Mayo O, Miele E, De Pietri Tonelli D, Berdondini L. A microfluidic device to study molecular clocks synchronization among neuronal populations. 41th Annual International Conference of the IEEE Engineering in Medicine and Biology Society – EMBC 2019, Berlin, Germany. (conference paper)

- **Giantomasi L**, Barca-Mayo O, De Pietri Tonelli D, Berdondini L. Astrocytes can synchronize the clock of segregated neuronal populations. XIV European Meeting on Glial Cells in Health and Disease 2019, Porto, Portugal. (poster)

- Riccitelli S, Boi F, Lonardoni D, **Giantomasi L**, Bisti S, Barca-Mayo O, De Pietri Tonelli D, Di Marco S, Berdondini L. Effects of Bmal1 gene deletion in GLAST positive cells on retinal morphology and physiology. Annual Meeting of the Society for Neuroscience 2018. (poster)

Oral presentations

- **Giantomasi L**, Barca-Mayo O, Berdondini L. Circadian rhythms: can astrocytes transmit circadian information among neuronal populations? International Astrocytes School. Bertinoro, Italy, 2018.

Articles in preparation (tentative titles)

- **Giantomasi L**, Ribeiro J, Berdondini L. Astrocytes and neuronal paracrine factors for the molecular clock synchronization of segregated neural populations: a lab-on-chip investigation.

- Riccitelli S, Boi F, Lonardoni D, **Giantomasi L**, Barca-Mayo O, De Pietri Tonelli D, Bisti S, Di Marco S, Berdondini L. Retinal function is altered by clock gene *Bmal1* deletion from adult retinal $GLAST^{+}$ cells.

Annex II

Protocols

Cortical astrocytes from post-natal rat (P2)

Materials:

- **Complete medium**: DMEM/F-12 (Sigma D6421) supplemented with 1% Glutamax (Thermo Fisher Scientific 35050038), 1% Penicillin/Streptomycin (Sigma P4333) and 10% FBS (Sigma F7524).
- **HBSS**: Sigma H6648
- **Digestion solution**: Dispase II 2mg/ml (Roche 04942078001) in Phosphate-Buffered Saline (PBS) (Thermo Fisher Scientific 10010056) + DNAse I 25µg/ml (Sigma D5025) in PBS

Method:

Dissection and trypsinization:

Remove and decapitate pups.

Remove brains from the skulls and put them in cold HBSS: divide the hemispheres, remove the meninges and dissect out the cortex.

Disaggregate cortices by pipetting with P1000 pipette.

Place 10 cortices in 20ml of digestion solution and incubate in water bath at 37°C for 30 minutes.

Centrifuge for 5 min at 900 rpm.

Discard supernatant and add fresh complete medium (10ml per pup).

Dissociate cortex gently by pipetting with 10ml pipette.

Filter the solution with a cell strainer (from BD, 40µm pore size).

Plate 10ml per flask (considering 1 flask per pup).

Changing medium: change completely the medium the day after plating. Then, change completely the medium every 4-5 days in culture.

Cortical neurons from embryonic rat (E18)

Materials:

- **Complete Neurobasal**: Neurobasal medium (Thermo Fisher Scientific 21103049) + 2% B27 (Thermo Fisher Scientific 17504044) + 1% Glutamax (Thermo Fisher Scientific 35050038) + 1% Penicillin/Streptomycin (Sigma P4333)
- **FBS**: Sigma F7524 - heat inactivated for 30 min at 56°C
- **HBSS**: Sigma H6648
- **Poly-D- lysine** in filtered Milli-Q: Sigma P6407 – 0.1 mg/ml
- **Digestion solution**: Trypsin 0.125% (Thermo Fisher Scientific 25050014) in HBSS + DNAse 0.25 mg/ml (Sigma D5025) in HBSS 5mM $CaCl_2$

Method:

Day 1:

Coating plastic substrates or coverglasses: deposit on each surface a suitable volume of Poly-D-lysine diluted in Milli-Q water and incubate overnight at 37°C, 5% CO2.

Day 2:

Setting of substrates: aspirate poly-D-lysine and wash 3 times with filtered Milli-Q water.

Dissection and trypsinization:

Anesthetize and kill pregnant mouse.

Remove and decapitate embryos.

Remove brains from the skulls and put them in cold HBSS: divide the hemispheres, remove the meninges and dissect out the cortex.

Place 4 cortices in 5 ml of digestion solution and incubate in water bath at 37°C for 30 minutes.

After incubation, add to digestion solution few ml of complete Neurobasal + 10% FBS and centrifuge for 5 min at 1200 rpm.

Discard supernatant and add fresh complete Neurobasal + 10% FBS.

Dissociate cortex gently by pipetting for not more than 10 times with P1000 pipette.

Filter the solution with a cell strainer (from BD, 40µm pore size).

Centrifuge for 7 min at 700 rpm, discard supernatant and suspend cells in complete Neurobasal.

Count cells and plate at the desired density.

Changing medium: add 50% of medium after 5 days in culture. Then, change 50% of the medium every 4-5 days in culture.

RNA extraction

Add 300µl Trizol per sample.

Place the tube containing the homogenate on the benchtop at room temperature (15–25°C) for 5 min.

Add 60µl chloroform. Shake it vigorously for 15 s.

Incubate at room temperature for 2–3 min.

Centrifuge at 12000 g for 15 min at 4°C

Transfer the aqueous phase to a new tube. Add 150µl isopropanol. Mix gently.

Incubate at room temperature for 10 min.

Centrifuge at 12000 g for 20 min at 4°C.

Carefully aspirate and discard the supernatant.

Add at least 0.5 ml of 75% ethanol.

Centrifuge at 7500 g for 7 min at 4°C.

Remove the supernatant completely and briefly air-dry the RNA pellet (5-7 minutes).

Resuspend the RNA in 18µl RNase-free water.

Treatment with DNase I (Sigma AMPD1):

Add to an RNase-free PCR tube:

- 8µl sample containing RNA
- 1µl 10X Reaction Buffer
- 1µl DNase I, Amplification Grade

Mix gently and incubate for 15 minutes at room temperature.

Add 1µl Stop Solution.

Heat at 70 °C for 10 minutes.

Place tubes in ice and proceed with quantification of RNA.

Reverse transcription

Depending on the quantification of RNA, calculate: i) how many µl it is necessary to use in order to have a reverse transcription of 300ng of RNA; ii) how many µl of RNase-free water it is necessary to add in order to have a final volume of 9µl.

Material:

M-MuLV-RH First Strand cDNA Synthesis Kit (Experteam R01-500)

Method:

1° step (on ice):

Add RNase-free water in PCR micro strip 8-tubes.

Add RNA Sample.

Add 2µl Random Primers.

Add 1µl OligodT.

Place the tubes in the PCR thermal cycler and use the following program:

- 70 °C 3 min
- 4 °C 5 min

In the meantime, prepare the mix for the 2° step:

- 4µl/sample Buffer 5x
- 2µl/sample DTT 0.1M
- 1µl/sample dNTPs 10mM
- 1µl/ RT enzyme

2° step (on ice):

Add 8µl of the mix.

Place the tubes in the PCR thermal cycler and use the following program:

- 25 °C 10 min
- 42 °C 60 min
- 70 °C 10 min

Real-time quantitative PCR

Materials:

- iTaq Universal SYBR Green Supermix (Biorad 172-5124)
- Primers: prepare a mix of forward and reverse primers (final concentration 10µM)

Method:

Prepare a mix containing 5µl/sample SYBR Green + 0.4µl/sample Primers + 1.6µl/sample RNase-free water.

Add 7µl of the mix in the PCR plate.

Add 3µl of cDNA sample, previously concentrated 3ng/µl.

Centrifuge the plate at 1000g 2min.

Place the plate in the 7900HT Fast Real-Time PCR System and use the following program:

- 95 °C 30 s
- 95 °C 15 s
- 60 °C 60 min } 40 cycles
- dissociation stage

Immunostaining spheroids

Fixing:

Wash 2x with PBS.

Add 2% PFA + 2% GA for 2h at room temperature.

Wash 3x with PBS.

Immunostaining:

Perform all the following steps on a shaker at 4°C.

Day1:

Permeabilize and block with Triton X-100 1% + NGS 10% + BSA 4% in PBS (B-PBT) for 2h.

Incubate with AbI (diluted in B-PBT) overnight.

Day2:

Wash 2x (2h) with PBS + Triton X-100 0.2% (PBT).

Wash 1x (2h) with B-PBT.

Incubate with AbII (diluted in B-PBT) overnight.

Day3:

Wash 2x (2h) with PBT.

Incubate with Hoechst (diluted 1:300 in PBT) for 1h.

Wash 2x with PBS and keep in PBS.

Calcium imaging (spheroids)

Materials:

- Extracellular saline solution: HEPES 10mM + D-Glucose 5.5mM + NaCl 145mM + KCl 5mM + $CaCl_2$ 2mM + $MgSO_4$ 1mM pH 7.3-7.4
- Fluo-4 AM (ThermoFisher 14201) reconstituted in DMSO

Method:

Remove medium.

Incubate with Fluo-4 AM (final concentration of 2.5µg/ml in extracellular saline solution) at 37°C for 15min.

Wash 2x with extracellular saline solution.

Transfer in 300µl of extracellular saline solution in the chamber for live imaging.

Spheroids disaggregation

Material:

Papain Dissociation System (Worthington Biochemical, LK003150)

Method:

Pull spheroids in a tube (one tube per condition).

Wash with PBS.

Place in the papain solution (20 units/ml papain, 0.005% DNase).

Incubate at 37°C in constant agitation (550 rpm).

Every 10 min, triturate by pipetting with P200 pipette and re-equilibrate the solution with 95% O_2:5% CO_2.

After 1h, transfer the single cell suspension to a new tube (skip if do not use µdevices).

Centrifuge at 300g for 5 min at room temperature (RT).

Resuspend the pelleted cells in albumin-inhibitor solution with DNase.

Centrifuge at 1200 rpm for 5 min at RT to obtain final dissociated cells.

Fluorescence-Activated Cell Sorting (FACS)

Material:

FACS buffer: 0.05% Triton X-100 + 0.5% BSA in PBS

Method:

Fix pelleted cells with PFA 4% for 20 min at room temperature (RT).

Centrifuge at 1200 rpm for 5 min at RT.

Permeabilize with Triton X-100 (0.05%) in PBS for 20 min at RT.

Wash with cold FACS buffer.

Centrifuge at 1200 rpm for 5 min at RT.

Incubate with Ab diluted in FACS buffer for 30 min, on ice, in the dark.

Wash with cold FACS buffer.

Centrifuge at 1200 rpm for 5 min at RT.

Resuspend in 200µl of FACS buffer.

Acknowledgment

"Time flies when you are having fun"! This expression fully represents my years in IIT and my journey toward the degree of Ph.D. It was a period of hard work, but lightened and made unforgettable by the presence of fantastic people.

I would first like to thank my supervisor, Dr. Luca Berdondini. While giving me the opportunity to work freely, he has always been there and by my side to provide guidance and help whenever I needed. Many thanks for his support, patience, constructive criticism and helpfulness.

I would also like to thank my former and current lab mates, especially Dr. Gian Nicola Angotzi, Dr. Fabio Boi and Dr. Joao Ribeiro, for scientific discussions, input, for their advices and support, and for sharing good time. I will be eternally grateful!

Thanks a lot to Dr. Aziliz Lecomte and Silvia Rancati, members with me of the "Spheroids' Angels" team, for their contribution to the technical aspects of part of this work and for all the so nice moments spent together.

Many thanks to Dr. Marina Nanni for her technical support in preparing neuronal cell cultures, and to clean room technicians that, together with Dr. Joao Ribeiro, helped me in the realization of microfluidic devices.

I would also like to thank Dr. Davide De Pietri Tonelli for his constant helpfulness in giving me suggestions and advices.

Thanks to Dr. Stefano Zordan and Dr. Andrea Freschi, members with me of the "trio dei disperati", for sharing with me all the "joys and sorrows" during this journey.

In addition to IIT friends and colleagues, achieving this goal would not have been possible without the presence of all the people dear to me. For this reason, I first would like to thank my parents and my brother Fabio, my biggest supporters, for always believing in me.

Thanks to my boyfriend Fabrizio, just entered my life, for putting up with me, supporting and encouraging me.

Thanks to my homemates, especially Doriana and Anna, for tolerating my moments of "madness" at home, especially while writing this thesis.

Many thanks to Maria Grazia, my journey companion from university, and to Martina, Valentina, Miguel, Simone, Andrea, Giulia, Valeria, Daniel e Giulia, for giving me a wealth of unforgettable moments lived here in Genoa.

Thanks to my best friend Adriana and to all the friends "di giù", constantly cheering for me and always close, albeit physically distant.

Last, but not least, thanks to the new entries Alessia, Ambra, Nico, Angelo and Gianluca for all the good time spent together.

If today I am professionally and personally the person I am, I owe it to all of you!

Infinitely thanks to everyone!